Russian Original Vol. 42, No. 6, June, 1977

December, 1977

SATEAZ 42(6) 503-598 (1977)

SOVIET ATOMIC ENERGY

АТОМНАЯ ЭНЕРГИЯ
(ATOMNAYA ÉNERGIYA)

TRANSLATED FROM RUSSIAN

CONSULTANTS BUREAU, NEW YORK

SOVIET ATOMIC ENERGY

Soviet Atomic Energy is a cover-to-cover translation of *Atomnaya Énergiya*, a publication of the Academy of Sciences of the USSR.

An agreement with the Copyright Agency of the USSR (VAAP) makes available both advance copies of the Russian journal and original glossy photographs and artwork. This serves to decrease the necessary time lag between publication of the original and publication of the translation and helps to improve the quality of the latter. The translation began with the first issue of the Russian journal.

Consultants Bureau journals appear about six months after the publication of the original Russian issue. For bibliographic accuracy, the English issue published by Consultants Bureau carries the same number and date as the original Russian from which it was translated. For example, a Russian issue published in December will appear in a Consultants Bureau English translation about the following June, but the translation issue will carry the December date. When ordering any volume or particular issue of a Consultants Bureau journal, please specify the date and, where applicable, the volume and issue numbers of the original Russian. The material you will receive will be a translation of that Russian volume or issue.

Subscription
$117.50 per volume (6 Issues)
2 volumes per year

Single Issue: $50
Single Article: $7.50

Prices somewhat higher outside the United States.

CONSULTANTS BUREAU, NEW YORK AND LONDON

c/b
227 West 17th Street
New York, New York 10011

Published monthly. Second-class postage paid at Jamaica, New York 11431.

Soviet Atomic Energy is abstracted or indexed in *Applied Mechanics Reviews, Chemical Abstracts, Engineering Index, INSPEC—Physics Abstracts and Electrical and Electronics Abstracts, Current Contents,* and *Nuclear Science Abstracts.*

SOVIET ATOMIC ENERGY

A translation of *Atomnaya Énergiya*

December, 1977

Volume 42, Number 6 June, 1977

CONTENTS

CONTENTS

(continued)

The Russian press date (podpisano k pechati) of this issue was 5/24/1977. Publication therefore did not occur prior to this date, but must be assumed to have taken place reasonably soon thereafter.

ARTICLES

URANIUM ORE SYSTEMS.

EXPERIENCE WITH MORPHOGENETIC GROUPING

D. Ya. Surazhskii

An ore system is a collection of ore manifestations which are regularly connected with one another, have unified structural control, and are enclosed in a space whose boundaries may vary depending on economic factors [1].

Each ore system is usually a component of another, more complicated system and can be divided into a number of subordinate systems. The basis of the hierarchical structure so formed should be taken to be the ore body — a system which consists of ore aggregates and rocks containing no ore and which includes useful components in a quantity that justifies the future costs of ore extraction and processing.

A collection of related ore bodies constitutes an ore bed, a collection of ore beds constitutes an ore deposit, and a collection of deposits constitutes an ore field. It is assumed that the shape, dimensions, and spatial position of the components making up ore systems at a particular level of the hierarchical structure is the result of a certain complex of external-environment factors which are peculiar to this level alone.

If the ore is formed at the same time as the surrounding rocks, then the ore systems are subject to one form of control — stratigraphic control (syngenetic sedimentary systems) or facies control (syngenetic magmatogenic systems). The morphological features of the mineralization are usually determined by two or more factors. Some of them are determined by the boundaries of the region (or zone) of ore genesis, others by the boundaries of ore systems within this region (or zone). The factors of the first group are called ore-controlling factors, while those of the second group are called ore-localizing factors. These terms are conditional and should be used only in connection with the level at which the study of ore elements is being conducted: the same element of geological structure (e.g., a fissure developing into a large fracture) may be a localizing factor with respect to the deposit and a controlling factor with respect to the ore beds making up this deposit.

Types of Uranium Ore Systems. Uranium ore systems can be grouped according to many criteria. In a survey, an important role is played by the morphological criterion determining the method used in the survey and the placement of exploratory units; according to this criterion, we can distinguish:

1) systems with two long dimensions and one short dimension — vein systems and veinlike (tabular) systems, which are connected with faults, and stratum systems and stratumlike systems, which are not related to faults;

2) systems with two short dimensions and one long dimension — columns and pipes, which are related to fractures; ribbons and rolls, which are not related to fractures;

3) systems which are isomeric — stock systems;

4) systems which are transitional between the first and third types — lenticular systems.

Morphological groupings of this kind are useful but insufficient for searches to find the optimal solutions of survey problems, since they are constructed according to a purely geometric principle, not taking account of the genesis of the shape and internal structure of the objects under study. The lack of a differentiated approach to objects which, although belonging to the same morphological group, differ in their morphogenetic properties may lead to serious misunderstandings. Accordingly, uranium ore systems and ore systems in general should evidently be classified first of all on the basis of combination of natural factors

Translated from Atomnaya Énergiya, Vol. 42, No. 6, pp. 443-451, June, 1977. Original article submitted December 1, 1976.

TABLE 1. Uranium Ore Systems

Type of ore fields	Morphological type and spatial position			Literature
	deposits	ore beds	ore bodies	
1. Stratum fields, in troughs of the platform mantle, composed mainly of nonmetamorphic and nondislocated rocks of shelf facies of epicontinental seas	1.1. Stratum deposits, in black shales	1.1.1. Stratum beds, bounded by the erosion lines of the productive stratum	The ore bodies are not individually distinguished	
	1.2. Stratum deposits, in dark clays with bone remnants of fossil fishes	1.1.2. The same		[2-5, 32]
	1.3. Stratum deposits, in phosphorite-bearing sandstones	1.1.3. The same		
2. Stratumlike fields, in erosion basins superimposed on a crystalline base and filled chiefly with terrigenous rocks	2.1. Stratumlike deposits, in unmetamorphosed gray bituminous-carbonate carboniferous layers, contrasting in permeability	2.1.1. Stratumlike beds, in permeable rocks between water-resistant rocks	2.1.1.1. Stratumlike and lenticular bodies connected with local accumulations of organic matter	
		2.1.2. Ribbon-shaped beds, in paleochannels	2.1.2.1. The same	
		2.1.3. Roll-shaped beds, on sandy—argillaceous contacts	2.1.3.1. Roll-shaped and lenticular bodies on the boundaries of stratum-oxidation zones	[3, 8-12, 33, 34]
	2.2. Stratumlike deposits, in metamorphosed conglomerates	2.2.1. Ribbon-shaped beds, in paleochannels	2.2.1.1. Stratumlike and lenticular bodies in deeper parts of channel bottom	
3. Stratumlike fields, in gas—oil cupolas composed of unmetamorphized rocks of marine and continental origin	3.1. Isomeric deposits, in variegated and gray layers (sometimes limestones), crumpled in folds and separated by faults	3.1.1. Stratumlike beds, in permeable rocks between water-resistant rocks	3.1.1.1. Stratumlike and lenticular bodies, spatially connected with local accumulations of bitumens	
			3.1.1.2. Saddle-shaped veins in layering fissures in the crowns of anticlines	[8, 9, 19-22, 35]
		3.1.2. Veinlike beds, in fractures intersecting the productive stratum	3.1.2.1. Column-shaped and pipe-shaped bodies, in cave-in funnels and fissure-intersection structures	

TABLE 1. (Continued)

Type of fields	Morphological type and spatial position			Literature
	deposits	ore beds	ore bodies	
4. Isomeric fields, in volcanotectonic depressions filled with heterogeneous sedimentary-effusive layers	4.1. Isomeric deposits, on the intersections of fractures oriented in different directions	4.1.1. Stratum-like beds, of the stratiform-stockwork type, in brittle rocks separated by interlayers of interformation clays	4.1.1.1. Vein-like bodies, lenticular and irregularly shaped stockworks controlling fissures	
		4.1.2. Veinlike beds, in intersecting fractures	4.1.2.1. Same	
	4.2. Column-shaped deposits, in wedge-shaped blocks between converging fractures	4.2.1. Irregularly shaped blocks bounded by fissures of different orders and different directions	4.2.1.1.Lenticular bodies, in tectonic contacts of rocks with different mechanical properties	[7, 15, 23-28]
	4.3.Veinlike deposits, in dikes of acid rocks	4.3.1.Irregularly shaped stockworks at the bends of dikes	4.3.1.1.Lenticular bodies in load fissures 4.3.1.2.Column-shaped bodies, in tectonic contacts of dikes with surrounding rocks	
5. Lenticular fields, in zones of tectonic contacts of granitoid massifs	5.1.Lenticular deposits, in systems of step faults which intersect granitoids and contact-metamorphosed sedimentary rocks	5.1.1.Veinlike beds, in bundles of branching fissures on the conjugations of interlayer fractures and intersecting fractures	5.1.1.1.Columnar bodies, on the intersections of steep fissures of interlayers of "favorable" rocks, on the conjugations of main and connecting fissures, etc.	[3, 5, 10, 25]
			5.1.1.2.Veinlike and lenticular bodies under shielding surfaces and in "structural traps" on the conjugations of differently oriented fissures, etc.	
6. Isomeric fields, in complex nodes of faulted-folded deformations of sedimentary-metamorphic rocks (with concordant ore systems)	6.1. Tabular deposits, in centroclinal closures or complications of the wings of principal structures	6.1.1.Tabular beds, in interstratum stripping areas and zones of fine fissures on the boundary of rocks subject to brittle and plastic deformation	6.1.1.1.Column-shaped bodies, at the flexural bends of productive strata 6.1.1.2.Stratum bodies and saddle-shaped veins, in layering fissures on the crowns of small folds	[26, 30]

TABLE 1. (Continued)

Type of fields	Morphological type and spatial position			Literature
	deposits	ore beds	ore bodies	
7. Isomeric fields, in complex nodes of fault–fold deformations of sedimentary–metamorphic rocks (with nonconcordant ore systems)	7.1. Isomeric deposits, on uplifted portions of anticlinal crests	7.1.1. Vein beds, in break-off fissures oriented normally to the axial planes	7.1.1.1.Columar and veinlike bodies, under shielding planes and in structural traps formed by conjugation of the fissures	[31]
8. Tabular fields, in extended fractures of the basement of ancient platforms	8.1. Tabular deposits, in distorted faults	8.1.1.Columnar deposits, in detritus zones along the boundaries of faults	8.1.1.1.Columnar and veinlike bodies in alkaline metasomatites	[26, 34, 35]
	8.2. Columnar deposits at conjugations of faults with incipient fractures	8.2.1. Same, in systems of parallel fractures	8.2.1.1. Same	

which are responsible not only for the geometry of ore objects but also for their dimensions, their position in space, and the variability and dispersion of the mineralization.

These combinations are not constant but depend on the nature of the geotectonic units in which the uranium mineralization is situated. The largest uranium ore fields known thus far are situated: in the troughs of the platform mantle, in erosion basins superimposed on a crystalline base, in disintegrating gas–oil structures, in volcanotectonic depressions, in zones of tectonic contacts of granitoid massifs, in complex nodes of fault–fold deformations (two modifications), and in extensive fractures of the basement of old platforms (Table 1).

The types of ore fields (see Table 1) are distinguished by the nature of the ore control. In the first and second types the uranium mineralization is essentially subject to stratification control and lithological-facies control. In the third type, for the first time, a significant role in the ore distribution is also played by fissural structures which are not usually accompanied by any significant displacement of the walls and, as a rule, do not go beyond the limits of the productive bands. In the fourth type there are large fractures in stratified rock masses, which are contrasting in their physical and mechanical properties and therefore react in different ways to tectonic stresses. In the fifth type the position of the ore objects is due to a complicated set of natural factors — systems of step faults, conjugation structures of layered and intersecting fractures of different orders, the composition of the surrounding rocks, etc. In the sixth and seventh types the mineralization is controlled by a combination of folds and fault deformations genetically related to folding. In the eighth types the most important factors of the ore control are regional fractures, within which the localization of the ore object is determined by the combined influence of the structural properties (fissures at bends) and lithological properties (zones of preore metasomatosis) of the rocks surrounding the ores.

Within each ore field the complex of ore-control conditions depends on the position of the ore object in the general hierarchical structure. In the great majority of cases it becomes more complicated as we go from higher to lower levels, and it is by no means always possible to establish which of these conditions are the most important and which are secondary.

For ease of inclusion of ore objects in surveys, in some cases it is desirable to distinguish: a) ore fields in which the ore system at all levels of the hierarchical structure belong to the same morphological group and have approximately the same spatial orientation;

b) ore fields in which the included ore systems belong to different morphological groups and have different spatial orientations. The first will be called "ore fields with concordant ore systems," and the second "ore fields with nonconcordant ore systems."

The successive stages of geological survey work on ore fields of the first group differ from one another chiefly in the density of the observation networks. The survey method and the orientation and geometry of the survey network usually remain unchanged. In ore fields of the second group, each successive stage of geological survey work differs from the preceding one not only in the density of the survey network but also in its geometry and orientation, depending on the country in which the work is done.

Ore Fields in Troughs of the Platform Mantle. The amount of uranium contained in such fields is related to the undislocated or only slightly dislocated strata of sedimentary rocks, which consists primarily of shelf facies of epicontinental marine basins and extend over areas measured in tens of thousands (or sometimes hundreds of thousands) of square kilometers.

The mineralization is usually of the single-stage or two-stage type, lean, very uniform, and practically continuous. The continuity of the ore-bearing horizons is sometimes broken by erosion areas, which determine the boundaries of the individual deposits or ore beds. More often, however, the concepts of deposits coincides with the concepts of ore beds and ore bodies.

The most characteristic representatives of ore systems of this type are uranium-bearing black shales, phosphorites, dark clays with bone remnants of fossil fishes, and similar formations, in which the uranium has been deposited during the process of sedimentogenesis and was not subjected to any substantial redistribution as the sediment developed. These have been described in many studies [2-6].

Survey work in such systems is relatively simple. Drilling at the points of a rectangular network and gamma logging of the boreholes yield completely reliable information concerning the boundaries of the productive band and the amounts of useful component contained in it. The role of main-line intersections is played by lines of boreholes which can be oriented in any direction. The study of the ore fields is completed at the stage of detailed surveying. There is usually no need for operational surveying.

Ore Fields in Erosion Basins Superimposed on a Crystalline Base. This is one of the most widespread types of ore bodies. Its most characteristic features are: localization near input areas of water-pressure systems, confinement to terrigenous rocks, multistage structure, sharply fragmented mineralization, and a multiplicity of factors controlling the position of deposits, ore beds, and ore bodies.

In most cases, the ore systems are represented by stratiform formations extending in the direction of an underground stream. The deposits are arranged either in gray, bituminous-carbonate, coal-bearing and multicolored layers of contrasting permeability (type 2.1) or in ancient metamorphosed conglomerates (type 2.2).

Among the ore beds forming deposits of type 2.1 we may distinguish, depending on the morphogenesis conditions, the following: stratified, in permeable rocks between water-resistant rocks (type 2.1.1); ribbon-shaped, in paleochannels (type 2.1.2); roll-shaped, on sandy—argillaceous contacts (type 2.1.3). The ore bodies in the deposits may be stratified (type 2.1.1.1 and 2.1.2.1) or roll-shaped (type 2.1.3.1). In the first case their position is controlled by local accumulations of organic matter, and in the second case by the boundaries of the zones of stratum oxidation.

The type described above includes ore systems in which the uranium concentration is represented chiefly by the products of the activity of groundwater circulating in the boundary region of artesian basins [1, 3, 5, 7-12]. Their dimensions vary over a wide range. The areas occupied by the deposits sometimes reach several hundred square kilometers, and the areas of the ore beds are often measured in square kilometers. The distance between beds within deposits and between ore bodies within beds are highly diverse. The ore-content coefficient* varies from 0.2 to 0.5 for deposits, from 0.4 to 0.6 for ore beds, and from 0.7 to

*This is the ratio of the areas (or volumes) occupied by all the various systems of one level to the area (or volume) of the higher-level ore system enclosing them.

0.9 for ore bodies. The variability of the mineralization, expressed by the absolute-contrast coefficient proposed by J. Matheron, is usually in the 0.03-0.128 range.

This group of ore systems includes uranium-bearing conglomerates similar to those known in the Republic of South Africa (Witwatersrand) and in Canada (Blind River). Morphologically these are similar to the above-described ore systems, although they differ from them in their mechanism of formation and in the nature of the intrasystem relationships [3, 5, 10, 13-17].

Survey work is carried on chiefly by means of boreholes, with lines oriented across the direction of an underground stream. Complications in the surveying process sometimes arise as a result of a breakdown of the radioactive equilibrium and the consequent need for special investigations to determine the correction coefficients to be applied to the metal-content values calculated on the basis of the gamma logging of the boreholes.

Ore fields with disintegrating gas—oil structures are spatially related to eroded anticlines and gas-and-oil-bearing cupolas composed of terrigenous red and gray layers (sometimes limestones), which served in the past as foci for relieving the stresses on ancient water-pressure systems.

The ore fields consist of a set of deposits made up of ore beds of two morphological types: stratified, chief metasomatic deposits, controlled by certain horizons or interlayers of "favorable" rocks (type 3.1.1), and veinlike beds confined to fractures intersecting the productive layers but not going beyond the limits of the productive bands (type 3.1.2). In the stratified beds, individual ore bodies of stratified or lenticular form are confined to local accumulations of bitumens and oriented according to the layering (type 3.1.1.1), while in the veinlike beds they often have the shape of pipes or columns filling cave-in funnels or inclined along the curves of intersection of two fissures (type 3.1.2.1). In the structure of stratified beds we sometimes also find saddle-shaped veins (type 3.1.1.2), whose shapes are determined either by exfoliation fissures in the crowns of small anticlines or by combination of these fissures with intersecting faults.

This group includes ore fields within whose limits the uranium concentration consists chiefly of products of the activity of rising solutions circulating in a region of attenuated destressing of artesian basins [8, 9, 18-19].

Similar to these ore fields in their morphological properties are some ore systems of disputed genesis in black shales [20-22].

The ore-content coefficient is 0.01 for deposits, 0.3-0.5 for ore beds, and 0.7-0.8 for ore bodies. The absolute-contrast coefficient for various ore bodies ranges from 0.18 to 0.54.

The discovery of evaluation of such ore objects is a rather complicated process. In most cases the drilling of vertical boreholes from the surface makes it possible to obtain the information necessary and sufficient for drawing the contours of the deposits and clarifying the general picture of the distribution of ore beds in them, i.e., for solving the problems of evaluation at the preliminary-survey stage. The system of detailed surveying depends on the morphological properties of the mineralization. For stratified beds this means a combination of horizontal and ascending operations; in the case of veinlike deposits it means drifts in combination with cross drifts and ascending operations. Operational surveying, as a rule, consists in the drilling of chamber boreholes arranged in a fan pattern, at various angles to the horizon.

Ore Fields in Volcanotectonic Depressions. The mineralization develops in heterogeneous sedimentary-effusive layers, rocks of funnel-type and subeffusive facies, sometimes in the crystalline basement. The deposits are largely controlled by fault conjugation or intersection structures. Some of them — the isomeric deposits — are combinations of stratified beds of the stratiform-stockwork type with veinlike beds, sometimes going beyond the boundaries of the productive horizons (type 4.1), those of a second group have the shape of columns or wedges bounded by converging faults and including ore beds of different and usually very complicated configuration (type 4.2), and a third group consists of mineralized dikes of acid rocks of subeffusive facies, at the bends of which there are ore beds having the form of stockworks of irregular shape (type 4.3).

The complexes of geological-structure elements controlling the position of ore beds and ore bodies in deposits of all three varieties are highly diverse.

The boundaries of the stratiform stockworks (type 4.1.1) are chiefly due to the physicomechanical properties of the rocks surrounding the ore, reacting in a certain way to tectonic stresses, and interlayers of interformational clays, which play the role of shields for the mineralization. It is difficult to distinguish the ore bodies within these. Large mineralized segments within the beds are connected to one another by individual fissures or boundles of fissures which are mineralized to different degrees. Under such conditions, it is more correct to speak not of ore bodies but of certain structurally homogeneous blocks which differ from one another in the shape and character of the ore-controlling elements.

For the most part, these are stockworks of lenticular, veinlike, or irregular shape on segments of conjugations of fissures of different orders and different directions (types 4.1.1.1 and 4.1.1.2).

In deposits of columnar form the ore beds are most often in the form of irregular blocks bounded by fissures of second and higher orders (type 4.2.1), while the ore bodies in the beds are stockworks, also of irregular, sometimes veinlike, shape, controlled by intrusive dikes or local areas of granulation at the contacts of rocks with different mechanical properties (type 4.2.1.1).

In deposits connected with dikes of acid rocks, stockwork ore bodies of lenticular and columnar shape are confined, respectively, to systems of horizontal fissures and tectonic contacts of dikes with surrounding rocks (type 4.3.1.1 and 4.3.1.2).

Ore fields in volcanotectonic depressions are characterized in many cases by very impressive dimensions. Their cross-sectional areas may be as high as several hundred square kilometers. Individual deposits stretch out over many kilometers, and the areas of ore bodies are measured in thousands of square meters, with the depth of mineralization reaching 1500-2000 m. The ore-content coefficients vary from 0.1 to 0.2 for deposits, from 0.3 to 0.5 for ore beds, and from 0.6 to 0.8 for ore bodies. The absolute-contrast coefficient is usually in the 0.2-0.3 range.

For ore fields in volcanotectonic depressions the most characteristic deposits are those of uranium—molybdenum formation, a description of which may be found in many published studies [7, 20-29]. An evaluation of these requires the use of highly diversified methods. The boundaries of the ore field and the position of individual deposits in it are usually established by drilling boreholes in the surrounding complexes at several levels. The subsequent stages of the survey work consist chiefly in carrying out mining operations — drifts — in combination with cross drifts intersecting the entire thickness of the ore-bearing formation. The resulting system of horizontal and vertical cross sections makes it possible to establish fairly easily the boundaries of the mineralized areas or to draw roughly the contours of the ore deposits. The problem of evaluating individual ore bodies is usually solved by means of chamber drilling, in fans inclined at various angles to the horizon.

Ore Fields in Zones of Tectonic Contacts of Granitoid Massifs. The deposits (type 5.1) are confined to systems of step faults intersecting a sedimentary—metamorphic layer and granitoid massifs. The ore beds (type 5.1.4) consist of bundles of branching veins oriented parallel to these faults. As a rule, they are localized in areas of conjugation of layer-by-layer and intersecting faults. In surveys and operations involving such deposits, the term "ore body" is taken to mean the set of plane ore lenses found in one vein and controlled by a large number of higher diverse factors. An important role is played by lithological control, under the influence of which the ore bodies often take the shape of columns inclined along the dip of a stratum or interlayer of "favorable" rocks (type 5.1.1.1). In addition, the geometry of the ore bodies and their position in space are substantially affected by various kinds of screening surfaces formed by a combination of fractures following the veins in various directions, tectonic contacts of rocks with contrasting physicomechanical properties, intrusive dikes, etc.

Ore fields of this type are particularly characteristic of five-metal formations (uranium—nickel—cobalt—bismuth—silver), which have been described many times in many investigations [3, 5, 10, 22]. In some cases they extend over tens of kilometers, with a width of several hundred meters. In these narrow bands the deposits are arranged in segments measurable in kilometers. The length of individual deposits does not exceed 200 or 300 m, reaching 1-2 km only in isolated cases. The depth of mineralization sometimes reaches 2 km, and the "critical horizon" is usually a surface of granite massifs underlying the productive sedimentary—metamorphic layer.

Because of the high degree of fragmentation and variability of the mineralization, an evaluation of all the ore systems is possible only on the basis of data obtained by carrying out, testing, and mapping mining operations. At the preliminary-survey stage these consist of major cross-cuts oriented along the contact, i.e., normal to the predominant course of the ore veins; in detailed surveying it consists of drifts in combination with ascending cleaving veins on rectangular blocks; at the operational-survey stage it consists of undercut operations and chamber-drilled boreholes used for the fixation of vein apophyses.

Ore Fields at Complex Nodes of Fault—Fold Deformations of Sedimentary—Metamorphic Rocks. Among these it is expedient to distinguish two types: those with concordant ore systems (type 6) and those with nonconcordant ore systems (type 7).

In ore fields of the sixth type the deposits are confined either to centroclinal closures or to complications of the wings of the main structures (type 6.1); the ore beds in them, usually stratified or veinlike in shape, show a clear connection with interstratum breakoffs and zones of fine fissures at the contacts between rocks with different mechanical properties (type 6.1.1). The ore bodies have the shape of columns (type 6.1.1.1), stratified or saddle-shaped veins (type 6.1.1.2). The columns are most often connected with flexural bend and the veins with folds of higher orders. The ore-controlling structures are systems of fine fissures arising at the boundary of rocks which have undergone brittle and plastic deformation.

The folded structures of ore fields are often complicated by series of preore fractures, but in the process of ore formation the predominant role is played not by the filling of open cavities but by the selective displacement of the material of the surrounding medium.

The most characteristic representatives of ore fields of the above-described type are those in iron-ore formations of the Precambrian [26, 30]. The largest of these stretch out over 10-12 km, with a width of 3-4 km and a depth of 1.0-1.5 km.

The deposits themselves, however, occupy no more than 10-15% of this space. They are represented chiefly by collections of ore beds oriented along the stratification of the surrounding rocks, parallel to one another. The distances between the deposits are usually measured in a few tens of meters, while the ore bodies in the beds are arranged fairly compactly, separated from one another by segments of practically ore-free rocks no more than a few meters wide.

The area ore-content coefficient is 0.4-0.6 for deposits, 0.8-0.9 for ore zones, and 0.9-1.0 for ore bodies. The absolute-contrast coefficient is 0.06-0.08.

For a general evaluation of such deposits at the preliminary-survey stage, boreholes along curves oriented across the folded structures have been successfully used. The evaluation of individual beds in detailed surveying is carried out exclusively by mining operations—drifts in combination with cross drifts intersecting the entire thickness of the ore-bearing formation. At the stage of operational surveying, ascending operations and chamber-drilled boreholes are also used.

The seventh type includes ore fields which are also confined to folded structures but differ in the fact that the deposits in them are represented by bundles of subparallel veins which exhibit a clear connection with areas of uplift of fold crests (type 7.1). In such situations these veins can be regarded as ore beds (type 7.1.1). Usually they fill fissures oriented normally to the axial planes of the anticlines and apparently arise primarily as breakoff fissures. The term "ore body" in such beds means vein areas containing uranium minerals in a quantity justifying the expense of extraction and processing of the vein mass. Their position is determined by the curves of conjugation with incipient fissures or by the shielding influence of rocks superimposed on the productive formation (type 7.1.1.1).

The length of one such ore field [31] is 10 km, with the distances between individual deposits measured in kilometers and the distances between individual ore beds measured in hundreds of meters. The productive veins extend for many hundreds of meters horizontally and vertically. The ore bodies in the beds are separated from one another by ore-free masses tens of meters thick. The areas of the ore bodies vary from several tens to several hundreds of square meters.

Underground mining operations constitute the only source of the information required for evaluating the parameters of such ore systems. At the preliminary-survey stage these are chiefly major cross-cuts oriented along the axis of an anticline; at the

detailed-survey stage they are multiple-level drifts with ascending and cleaving ore beds on rectangular blocks; at the operational-survey stage they are undercut drifts and chamber boreholes arranged in a fan, at various angles to the horizon.

Ore Fields in Zones of Regional Faults of the Old Basement. The deposits in these are represented by mineralized blocks of rocks included in the composition of tectonic zones and confined either to distortions of a fracture or to the curves of conjugation of this fracture with incipient fractures of second and higher orders. In the first case they are tabular in form (type 8.1); in the second case they take the form of columns inclined along the line of intersection of two planes (type 8.2). In tabular deposits the ore beds extend along a limited fracture as chains of flat lenses arranged in coulisse form and exhibiting a clear connection with alkaline metasomatites (type 8.1.1). In columnar deposits the concept of ore bed is most closely met by bundles of veinlike ore bodies or collections of lenticular ore bodies parallel to the main structure (type 8.2.1). Ore fields of this type are most characteristic of areas of activation of Precambrian shields and platforms [4, 14, 15].

The length of the ore-bearing faults measures many kilometers, sometimes tens of kilometers; the deposits extend for several kilometers, the ore beds for hundreds of meters, and the ore bodies in the beds for tens of meters. The depth of mineralization amounts to 2-2.5 km. The ore-content coefficient is 0.4-0.5 for deposits, 0.7-0.9 for ore beds, and nearly unity for ore bodies. The absolute-contrast coefficient is 0.08-0.10.

CONCLUSIONS

A systematic approach to the analysis of the natural phenomena involved in the genesis of forms of uranium ore objects enables us to distinguish among them eight fundamental types of ore fields, in which we find at least 14 morphogenetic types of deposits, 18 types of ore beds, and 20 types of ore bodies. Each types arises as a result of a completely definite combination of external-environment conditions which are characteristic of this type alone.

The proposed grouping does not reflect all of the diverse forms of uranium ore systems. It should be regarded only as a first step on the difficult path of establishing a morphogenetic classification of natural geological objects which is necessary for solving a number of methodological problems arising in the process of discovering and surveying deposits of minerals.

The author wishes to express his gratitude to A. N. Eremeev, V. A. Petrov, and S. A. Deinege for their valuable comments.

LITERATURE CITED

1. D. Ya. Surazhskii, Sov. Geol., No. 2, 3 (1974).
2. M. N. Althausen, in: Metals in Sedimentary Rocks [Russian translation], Vol. 3, Moscow (1966), p. 102.
3. M. M. Konstantinov and E. Ya. Kulikova, Uranium Provinces [in Russian], Atomizdat, Moscow (1960).
4. V. McKelvey, D. Everhart, and R. Garrels, in: Problems of Ore Deposits [Russian translation], Izd. Inostr. Lit., Moscow (1959), p. 428.
5. E. Heinrich, Mineralogy and Geology of Radioactive Mineral Raw Materials [Russian translation], Izd. Inostr. Lit., Moscow (1962).
6. V. McKelvey and S. Nelson, Econ. Geol., 45, No. 1, 35 (1950).
7. F. I. Vol'fson (editor), Geology and Problems of the Genesis of Endogenous Uranium Deposits [in Russian], Nauka, Moscow (1968).
8. L. S. Evseeva et al., in: Problems of Applied Radiogeology [in Russian], Atomizdat, Moscow (1967), p. 326.
9. L. S. Evseeva et al., Geochemistry of Uranium in the Zone of Hypergenesis [in Russian], Atomizdat, Moscow (1974).
10. D. Ya. Surazhskii, Methods of Discovering and Surveying Uranium Deposits [in Russian], Atomizdat, Moscow (1960).
11. W. Finch and S. Warren, Geol. Sur. Prof. Papers, No. 538 (1967).
12. D. Shaw and H. Granger, Econ. Geol., 60, No. 2, 240 (1965).
13. U. Libenberg, in: Proceedings of the Second Geneva Conference, 1958. Reports by Foreign Scientists [Russian translation], Vol. 8, Atomizdat, Moscow (1959), p. 377.

14. C. Davidson, Mines Mag., 88, 73 (1953).
15. C. Davidson, Econ. Geol., 52, No. 6, 668 (1957).
16. S. Holmes, Econ. Geol., 50, No. 1, 751 (1955).
17. P. Roscoe and H. Steacy, First International Conference, Geneva (1955), Rep. 224.
18. A. I. Zubov, Geol. Rudn. Mestorozh., No. 5, 6 (1960).
19. R. Russel, in: Proceedings of the First Geneva Conference. Reports of Foreign Scientists [Russian translation], Vol. 8, Atomizdat, Moscow (1959), p. 81.
20. R. V. Getseva, in: Problems of Uranium Geology [in Russian], Atomizdat, Moscow (1957), p. 20.
21. V. A. Krupennikov, Geol. Rudn. Mestorozhd., No. 4, 74 (1969).
22. B. L. Rybalov, ibid., No. 2, 3 (1965).
23. V. P. Vlasov et al., Geology of Deposits of Uranium-Molybdenum Formation [in Russian], Atomizdat, Moscow (1966).
24. F. I. Vol'fson et al., Izv. Akad. Nauk SSSR. Ser. Geol., No. 11, 114 (1967).
25. D. I. Shcherbakov (editor), Geology of Hydrothermal Uranium Deposits [in Russian], Nauka, Moscow (1966).
26. V. I. Kazanskii and N. P. Laverov, in: Ore Deposits of the USSR [in Russian], Vol. 2, Nedra, Moscow (1974), p. 319.
27. A. B. Kazhdan et al., in: Problems of Applied Radiogeology [in Russian], No. 2, Atomizdat, Moscow (1967), p. 287.
28. N. P. Laverov et al., Tr. IGEM, No. 2, Izd. Akad. Nauk SSSR, Moscow (1962), p. 116.
29. N. P. Laverov et al., Geol. Rudn. Mestorozhd., No. 6, 38 (1964).
30. R. P. Petrov et al., Uranium Deposits in Iron-Ore Formations of the Precambrian [in Russian], Atomizdat, Moscow (1969).
31. A. V. Zavarzin et al., in: Uranium Deposits: Zonality and Parageneses [in Russian], Atomizdat, Moscow (1970), p. 93.
32. I. U. Aizeksen, in: Proceedings of the First Geneva Conference [in Russian], Vol. 6, Gosgeoltekhizdat, Moscow (1956), p. 413.
33. S. T. Batulin et al., Exogenous Epigenetic Uranium Deposits [in Russian], Atomizdat, Moscow (1965).
34. T. V. Balibina et al., Geol. Rudn. Mestorozhd., No. 5, 67 (1963).
35. V. I. Kazanskii et al., ibid., No. 1, 3 (1968).

LOW-ADDITIVE URANIUM ALLOYS FOR THE FUEL ELEMENTS OF THE KS-150 REACTOR

V. F. Zelenskii, A. I. Stukalov,
V. P. Ashikhmin, and A. V. Azarenko

UDC 669.822'5:621.785.784/786

The cores of the fuel elements used today in the KS-150 reactor are made of uranium of reactor purity with small admixtures of iron and silicon [$(1-2)\cdot10^{-2}$ and $(2-3)\cdot10^{-2}$% by mass, respectively]. Earlier, it was shown [1, 2] that the use of these admixtures in such a proportion promotes the formation, under β hardening, of uranium rods with a weak axial texture of the [100] type. Loop radiation tests showed that such a texture ensures minimal change of shape in the fuel elements as a result of radiation growth in the 200-350°C temperature range. In fuel-element segments operating at higher temperatures (350-500°C) the radiation deformation develops chiefly as a result of swelling of the uranium, under loop-test conditions close to the design conditions of the KS-150 reactor (gas-coolant pressure 607.95 kPa, temperature 400-500°C, specific thermal stress 55 kW/kg) it reaches 15-20% by volume for a burnup of ∿10,000 MW·day/ton. Local variation in the geometric dimensions of the cores, resulting from this amount of swelling, may lead to rupture of the jacket and breakdown of the fuel element. Therefore, the limitation of fuel swelling is one of the effective methods of increasing fuel lifetime at high burnup values.

A method widely used for reducing the swelling of uranium is alloying it with metallic and nonmetallic admixtures [3, 4]. In the present case the admixtures most acceptable from the standpoint of minimal parasitic capture of neutrons were found to be aluminum and chromium.

In the present paper we discuss the main results of a metal-physics investigation of alloys with admixtures of aluminum and chromium (0.1 and 0.2% by mass, respectively) and radiation tests of fuel elements of the KS type of cores made of these alloys.

Material. The alloys were prepared by the method of vacuum remelting of compact uranium with aluminum, and also with aluminum and chromium in powdered or shaving form. The amount of the additives in the base material corresponded to the chemical composition of KS-type fuel-element cores. Cylindrical castings 40 mm in diameter and having a mass of 2.5 kg were machined on a lathe and were subsequently used for pressing 6.5-mm diameter rods at 950°C; the rods were chilled in a vacuum.

Hot Working. The hardening of the pressed rods from the γ phase included inductive heating to 900-950°C, maintenance at this temperature for 10-15 sec, and transverse hardening in a water shower; these operations were carried out in air, with translational motion of the rod in the inductor of a high-frequency generator and in a cooler. The hardened rods were annealed at 550°C for various lengths of time and then subjected to hardening from the β phase. This kind of hot working ensured uniform separation of the finely dispersed inclusions of the second phase of the uranium matrix (UAl_2, U_3Si, U_6Fe), and also promoted the formation of a fine-grained structure (when the time of intermediate annealing in the α phase was 3-5 h) [5, 6].

Results of the Metal-Physics Investigation

Structure. The macrostructure of the γ-pressed alloys is essentially large-grained, with the diameter of the largest grains reaching 1 mm (Fig. 1a). The intermetallic compounds and carbides form a granular substructure with discrete (discontinuous) boundaries (Fig. 1b). Such a substructure is typical of low-additive uranium alloys cooled slowly from the γ phase. The density of separation of the second phase from the intermetallic and carbide inclusions measuring 0.5-1 μ was calculated by the well-known method of [7] and found to be $6\cdot10^9$ particles/cm³. Such a structure is unacceptable for fuel-element cores because of the large

Translated from Atomnaya Énergiya, Vol. 42, No. 6, pp. 452-456, June, 1977. Original article submitted December 22, 1975; revision submitted July 5, 1976.

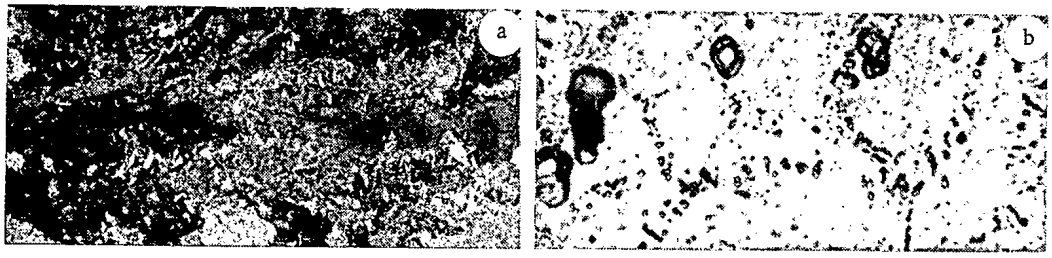

Fig. 1. Macrostructure (a) and granular substructure (b) of γ pressed rods (×8 and ×1000, respectively).

grain size and the coagulated separations of the second phase. Hardening of the pressed rods from the β phase does not lead to any substantial refining of the structure or finer dispersion of the intermetallides. Therefore, we used hardening of the alloys from the γ phase. The structure of the γ-hardened alloys is very fine-grained (Fig. 2a), and the substructure is characterized by a clearly formed dislocation-admixture network (Fig. 2b). The boundaries of the network cells are continuous lines which, as assumed by the authors of [8, 9], are the boundaries of subgrains of the β phase formed during rapid conversion from γ to β and decorated with admixture atoms in the preseparation state.

The above-described structure is substantially different from the structure of γ-pressed alloys and is acceptable in principle for fuel-element cores. However, further investigations showed that the distribution of the texture along the γ-hardened rods was not uniform. This leads to warping of the fuel elements under irradiation and thereby increases the danger of breakdown.

A further improvement of the alloy structure can be obtained by using intermediate annealing in the high-temperature region of the α phase and subsequent β hardening. Annealing of γ-hardened alloys leads to dissociation of the supersaturated solid solution and more uniform separation of the UAl_2 intermetallides, both in the matrix and along the subgrain boundaries [10]. Figure 3 shows the structure of uranium–aluminium alloys annealed after γ hardening. It can be seen that the cells of the subgrains are formed by particles of uranium intermetallides and by admixtures which were present in the γ-hardened alloy in the preseparation state; within the cells we also noticed a large number of second-phase separations. The density of 0.5-1 μ separations is $6 \cdot 10^{11}$ particles/cm^3. Thus, γ hardening and subsequent annealing leads to a refining of the structure of the γ-pressed metal, increases by a factor of 100 the density of second-phase separations, and promotes a more uniform distribution of the intermetallide particles. However, the annealing does not eliminate the nonuniformity of the texture that arises in γ hardening. The formation of the desired texture in the rods and the uniformization of its distribution along the length, as well as the formation of a uniform fine-grained structure, are promoted by the concluding operation of the β hardening. In macrostructure and granular substructure the β-hardened alloys differ little from those shown in Fig. 3.

The separation of the admixtures from the solid solution during intermediate α annealing and their subsequent coagulation apparently have a substantial effect on the formation of the structure during the process of β-to-α conversion, especially when the material is kept in the β phase only for a short time. Some of the intermetallides which grew larger during annealing apparently cannot dissolve in the β phase during the short time the alloy is kept in that phase before hardening, and they limit the growth of the β-uranium grains, which in turn affect the formation of the α structure. The effect of intermediate α annealing on grain size in the hardened alloy of uranium with aluminium and chromium is shown in Fig. 4. The decrease in grain size as the annealing time increases to ∿3 h is easily explained by the above considerations. The increase in the grain size of the β-hardened uranium for longer times of annealing in the α phase before β hardening is due to the coagulation of the intermetallides and the decrease of the separation density.

Texture. The texture of the β-hardened rods was determined by calculating the orientation parameters — the growth indices G_x and $G_{\alpha\rho}$ — on the basis of roentgenographic investigations and also measurements of the coefficients of linear expansion α and electrical resistivity ρ [11, 12].

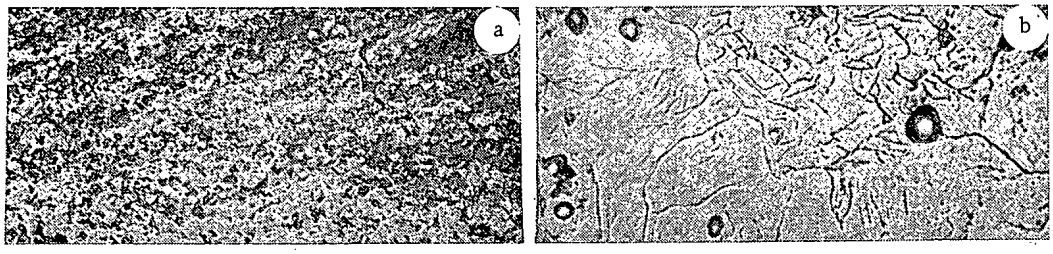

Fig. 2. Macrostructure (a) and granular substructure (b) of γ-cooled alloys of uranium (magnification as in Fig. 1).

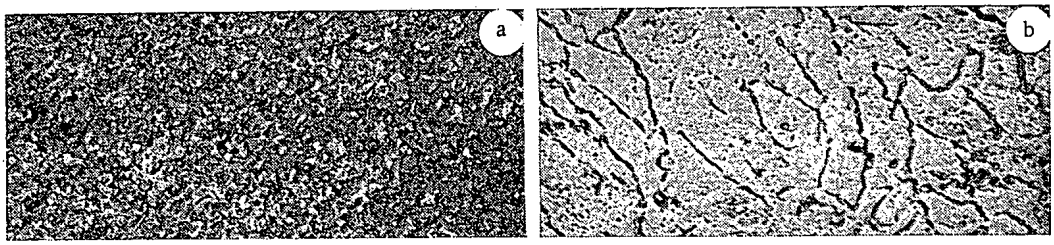

Fig. 3. Macrostructure (a) and granular substructure (b) of annealed alloy (same magnification).

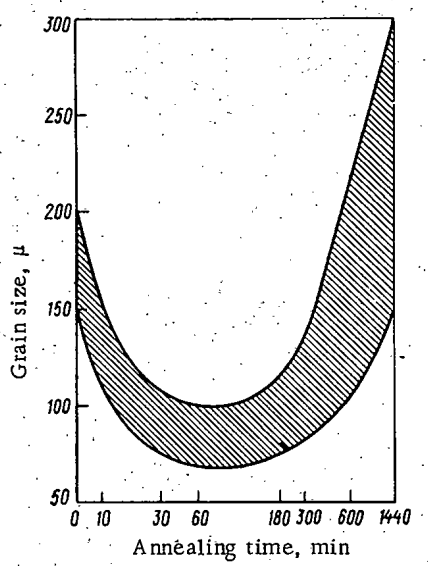

Fig. 4. Grain size in β-hardened uranium alloy as a function of the time of intermediate annealing in the α phase before β-hardening.

It was found that in the β-hardened alloy rods, as in the case of unalloyed uranium rods, a [100]-type texture is formed along the longitudinal axis; how pronounced this texture is for the selected conditions of the β-hardening depends on the duration of the intermediate α annealing (before the β hardening) (Fig. 5). It was noted above that for the formation of a fine-grained structure the optimal length of time for such annealing is 3-5 h. In this case, during the β hardening the alloy forms a texture with a value of 10-12% expressed in terms of the growth indices. It should be noted that the quantitative estimate of the texture in uranium alloys may be inaccurate, since the methods used were designed for determining the texture of unalloyed uranium. Nevertheless, the use of these methods in the present case is completely justified, since it enables us to investigate the nature of the variation in the hardening texture during the hot working of the alloys.

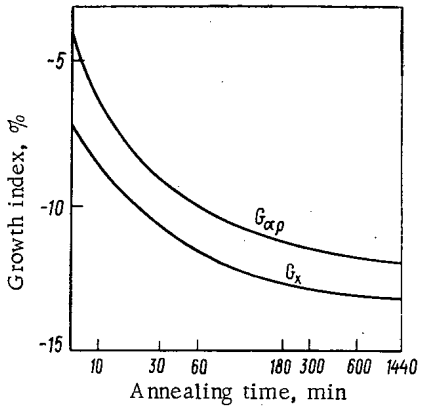

Fig. 5. Texture of hardened alloys of uranium with aluminum and chromium as a function of time of annealing at 550°C.

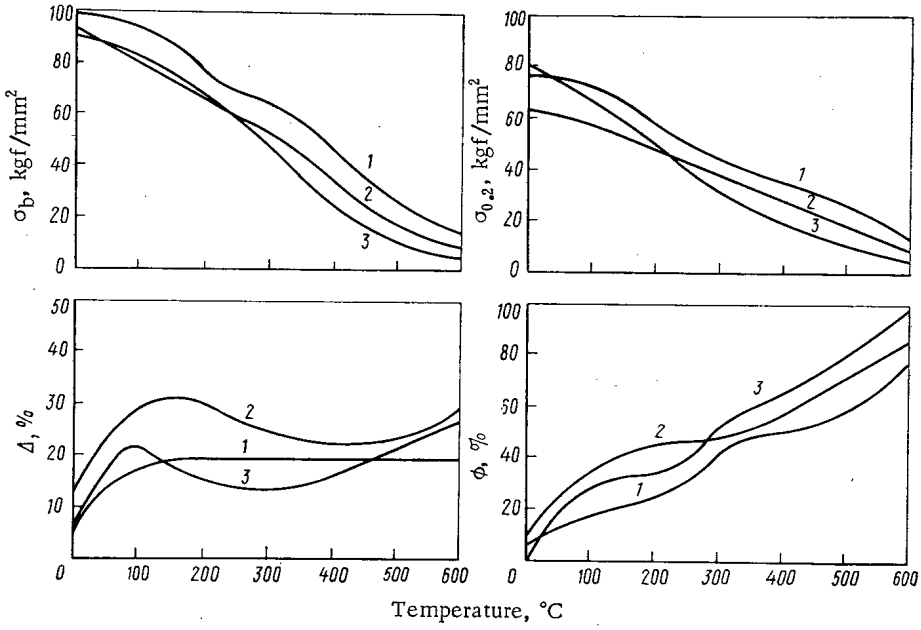

Fig. 6. Mechanical characteristics of alloys of uranium with aluminum and chromium (1), uranium with aluminum (3), and the original uranium (2).

Mechanical Properties. The mechanical tests were conducted on a tensile testing machine over a temperature range of 20-600°C. It follows from Fig. 6 that the alloy with aluminum and chromium admixtures has better strength characteristics than other materials over the entire range of investigated temperatures. The strength of the uranium–aluminum alloy can be compared with that of the original uranium up to a temperature of 200°C; at higher temperatures it is somewhat lower.

For all the materials, we observe a considerable growth in plastic characteristics as the temperature increases to 100°C. At higher temperatures the plasticity of the uranium–aluminum–chromium alloy remains unchanged, while for the uranium–aluminum alloy and the original uranium we observe a decrease in the relative elongation. This type of variation in the plastic properties of materials in this range can be explained [13] by the effect of the temperature on the number of systems in which twinning takes place during the defomation process; as the temperature increases (above 100°C), this number decreases for some alloys.

The minimum relative elongation, linked to the transition to grain-boundary deformation, for the original uranium is found at a higher temperature than for the uranium–aluminium alloy

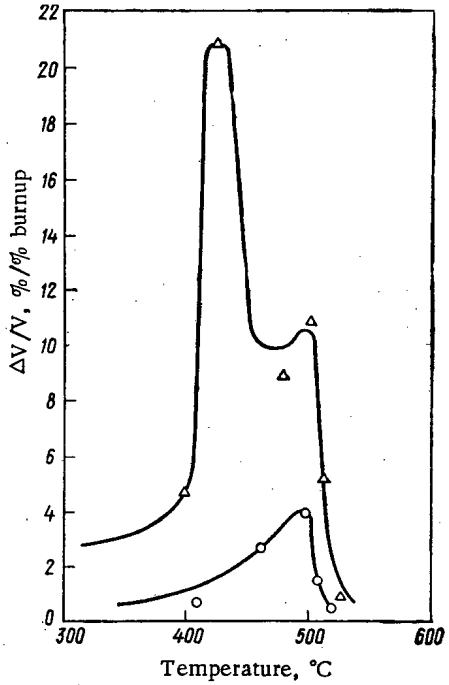

Fig. 7. Swelling of uranium (Δ) and uranium–aluminum–chromium alloy (○) as functions of temperature.

and is practically absent in the case of the uranium–aluminium–chromium alloy. The minimum plasticity in the unalloyed uranium is caused [14] by the formation of cracks around the inclusions and cavities along the grain boundaries. The absence of this minimum in the uranium–aluminum–chromium alloy may be explained by the high density of the UAl_2 and chromium separations which apparently strengthen the grain boundaries. An analogous phenomenon has been observed for an alloy of uranium with beryllium oxide [14].

Radiation Tests. Fuel elements with cores made of the alloys investigated, together with fuel elements whose cores had a chemical composition matching those used in the KS-150 reactor, were tested to a maximum burnup value of 8040 MW·day/ton in the KS-60 loop under conditions close to reactor conditions. The only significant difference found in the loop tests was the large number of shutdowns (∿120), 5-6 times the number found in reactor tests of fuel elements at the same burnup value.

Evaluation of the Results. Figure 7 shows how the swelling of the uranium and the uranium–aluminum–chromium alloy varies with temperature; the swelling was calculated from measurements of the elongation and change in diameter in various segments of the fuel elements. It follows from Fig. 7 that the temperature–swelling curve for unalloyed uranium has two clearly marked maxima: the first at 430°C and the second at 500°C. According to the cavitation-swelling model proposed in [15], we may assume that the low-temperature peak in the swelling is due to the appearance and development of voids (cavitation) along the boundaries of the uranium matrix (grain boundaries, twins), and the appearance of the high-temperature peak is due to the homogeneously degenerating pores of vacancy origin. It can be seen that the contribution of the low-temperature part to the total swelling constitutes the largest portion, while the maximum swelling value at a temperature of 430°C is ∿20% in this case (a diameter increase of ∿8%) and at 500°C the value is 10% (with 3% core thickening). In fuel elements tested to the same burnup value in the KS-150 reactor under similar conditions, a single swelling maximum was found at 500°C (∿9%) [16].

As noted above, the reactor tests differ from the loop tests chiefly in the small number of shutdowns (20-30 shutdowns during the tests up to burnup values of ∿8000 MW·day/ton). Thus, a comparison of these data enables us to conclude that the development of the low-temperature peak in the swelling under the loop-test conditions is due in large measure to the presence of a large number of thermal cycles. The effect of the thermal cycles on the increase in the low-temperature swelling may be attributed to the accelerated development of cracks along the boundaries of the uranium matrix which result from sharp changes in the stressed state of the fuel-element core. The agreement in temperature and magnitude between

the high-temperature maxima indicates that sharp changes in temperature, within the investigated ranges, do not have any substantial effect on the vacancy-swelling process.

It follows from Fig. 7 that the addition of aluminum and chromium to uranium will eliminate the low-temperature swelling almost completely; this can be attributed to strengthening of the grain boundaries by the second-phase separations. The reduction in the amount of swelling in the high-temperature range may be due, as assumed in [15], to the strengthening of the process of recombination of vacancies and displaced atoms through limiting of the finely dispersed separations in the migration of displaced atoms to dislocations and of vacancies to voids.

CONCLUSION

The investigations showed a high resistance to swelling in an alloy of uranium with small amounts of aluminium and chromium at a burnup value of ∿1 at.%. The hot-working scheme for the alloy, including γ hardening of the solid solution, α annealing (aging), and β hardening, ensured the formation of a fine-grained isotropic structure with a finely dispersed distribution of second-phase particles, which facilitated the effective utilization of the alloying additives in limiting the cavitation and vacancy swelling of the uranium.

The results obtained showed that an alloy of uranium with aluminum and chromium will make it possible to obtain high burnup values in the KS-150 reactor.

LITERATURE CITED

1. V. F. Zelenskii et al., At. Energ., 39, No. 1, 24 (1975).
2. V. E. Ivanov et al., in: Start of Operation of the A-1 Power Station. Part I [in Russian], Czechoslovak Atomic Energy Commission Press, Bratislava (1974), p. 224.
3. W. McDonell and E. Sturcken, Nucl. Technol., 26, No. 4, 420 (1975).
4. J. Lehman et al., in: Proceedings of the IAEA Symposium "Investigation of the Swelling and Growth of Uranium Alloys under Irradiation," Vienna, June 2-6, 1969 p. 413.
of Uranium Alloys under Irradiation," Vienna, June 2-6, 1969 p. 413.
5. A. I. Stukalov et al., Byull. Izobret., No. 2, 131 (1975).*
6. A. I. Stukalov et al., Byull. Izobret., No. 2, 131 (1975).
7. D. Kramer, J. Nucl. Mater., 27, No. 3, 281 (1962).
8. C. Angerman and R. Huntoon, J. Less-Common Met., 9, No. 5, 338 (1965).
9. A. A. Bochvar et al., At. Energ., 27, 193 (1965).
10. A. Smith, J. Nucl. Mater., 27, No. 2, 194 (1968).
11. E. Sturcken and W. McDonell, J. Nucl. Mater., 7, No. 1, 85 (1962).
12. J. Stobo and B. Pawelski, J. Nucl. Mater., 4, No. 1, 109 (1961).
13. T. Khan, I. Brun, and I. Decours, J. Nucl., Mater., 37, No. 1, 27 (1970).
14. A. I. Voloshchuk et al., At. Energ., 29, No. 6, 416 (1970).
15. W. McDonell, "Model of cavitational swelling of uranium," International Conference on Physical Metallurgy of Reactor Fuel Elements, Berkeley, England, Sept. 2-7, 1973, p. 266.
16. I. Novak, F. Slancar, and K. Splichal, Jad. Energ., 21, No. 5, 172 (1975).

*References 6 and 6 are identical as in the Russian original — Publisher.

CRITICAL ENERGY IN HEAT-TRANSFER CHANNELS OF COMPLEX SHAPE

L. N. Polyanin

UDC 621.039.524.44:621.039.51

The theoretical analysis of the sharp deterioration of heat transfer as a local phenomenon depends upon estimates of the detailed velocity and temperature fields for the heat carrier over the total channel volume. The critical situation in the establishment of steady flow should then arise out of a phenomenological consideration of the general combined problem of the hydrodynamic and thermal stabilization of flow in specific flow conditions (channel shape, characteristics of the heated surface, initial flow conditions). In practice, however, empirical correlations based on calculations of the mean or local parameters are used for the estimates of the critical heat fluxes in heated channels.

Because there are no sufficiently rigorous equations of heterogeneous two-phase flow, the local heat-carrier parameters in complex channels and, in particular, in bundles of rods [1, 2] cannot be determined with sufficient accuracy, which in a number of cases leads to pronounced lack of agreement between the experimental and calculated values of the critical energy [2, 3]. However, this lack of agreement is not simply the consequence of the inadequate rigor of the expressions of the determination of the local flow parameters. Other factors — the effect of low-frequency pulsations on the thermocouple readings, systematic and random errors of the measuring instruments, and deviations of the geometric characteristics of the channel from the nominal values — mean that the maximum possible accuracy of the empirical correlation should be assumed to correspond to a mean square error of ∿5-6% [4].

As a result of the indeterminacy that exists at present in calculations of the distribution of the heat-carrier parameters over the channel volume, the local approach to the calculation of the critical heat fluxes has no advantage, in terms of accuracy, over the so-called global approach. Moreover, global estimates of critical channel energy in terms of the inlet parameters of the heat carrier, taking into account the real energy distribution and the channel geometry, are more convenient for practical engineering calculations.

The present article outlines a method of calculating the critical channel energy; the method rests on the generalization of experimental material in a sufficiently wide range of flow and geometry parameters, so that it can be used to estimate the critical power in various conditions of forced and natural circulation of heat carrier.

As an example, consider an assembly of fuel-element rods (Fig. 1). The channel is divided into arbitrary hydraulic cells and the thermohydraulic diameter is introduced

$$d_{\text{th}j} = 4f_j/\pi_{0j}, \tag{1}$$

where f_j is the through cross section of the j-th cell; also

$$\pi_{0j} = \frac{1}{K_{rj}^{\max}} \sum_{l} K_{rj}^{l} \pi_{0j}^{l}; \tag{2}$$

π_{0j}^{l} is the part of the perimeter of the l-th heat-transfer surface belonging to the j-th cell; K_{rj}^{l} is the heat liberated in the l-th rod; $K_{rj}^{\max} = \max_{l} K_{rj}^{l}$.

The cell which corresponds to the minimum thermohydraulic diameter is called the maximally heat-stressed cell.

The equation for the critical heat flux can be written in the form

$$q_{\text{cr}} = a - bx, \tag{3}$$

Translated from Atomnaya Énergiya, Vol. 42, No. 6, pp. 457-460, June 1977. Original article submitted August 30, 1976.

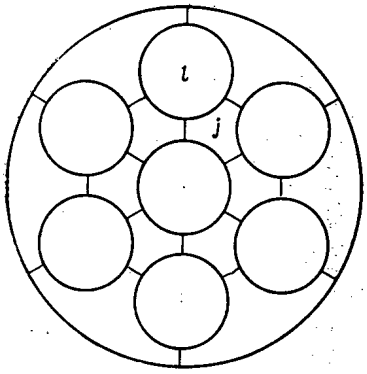

Fig. 1. Cross section of channel arbitrarily divided into hydraulic cells.

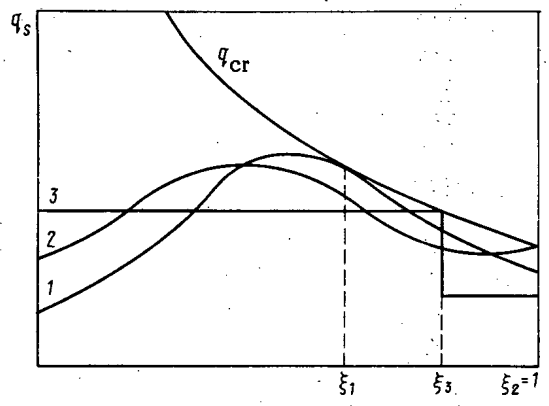

Fig. 2. Cases in which Eq. (11) is and is not satisfied for various energy distributions.

where the parameters a and b are functions of the coordinates of the point of heat-transfer crisis $\xi_0 = Z_0/H$ and, in particular, the shape of the energy distribution $K_z(\xi) = q_s(\xi)/\bar{q}_s$ ($\bar{q}_s$ is the mean over the channel height of the specific heat flux).

The mass vapor content x for the maximally heat-stressed cell is written in the form

$$x(\xi_0) = (\tilde{N}_{cr}/Q)\int_0^{\xi_0} K_z(\xi)\,d\xi - (\Delta i_{in}/r), \tag{4}$$

where $\tilde{N}_{cr}$ is the critical energy of a channel with a nonuniform energy distribution over the height; also

$$Q = rW_\rho \Pi_0 \delta; \tag{5}$$

$$\delta = \min_j \frac{f_j}{\pi_{0j}} = \frac{d_{th}}{4}. \tag{6}$$

Here W_ρ is the mean mass velocity of heat carrier in the channel; Π_0 is the total heated perimeter; r is the latent heat of vaporization.

At the critical point

$$q_{cr}(\xi_0) = q_s(\xi_0). \tag{7}$$

Since

$$q_{cr}(\xi_0) = (\tilde{N}_{cr}/\Pi_0 H)\,K_r^{max} K_z(\xi_0), \tag{8}$$

it follows from Eqs. (3), (4) and (8) that

$$\tilde{N}_{cr} = \frac{\Pi_0 H [a + b(\Delta i_{in}/r)]}{K_r^{max} K_z(\xi_0) + \varkappa \int_0^{\xi_0} K_z(\xi)\, d\xi}, \tag{9}$$

where

$$\varkappa = b\Pi_0 H/Q. \tag{10}$$

Also, when the curve of $K_z(\xi)$ has a continuous derivative for $0 \leqslant \xi \leqslant 1$:

$$\frac{dq_{cr}(\xi_0)}{d\xi} = \frac{dq_s(\xi_0)}{d\xi}. \tag{11}$$

Then Eqs. (3), (4), and (11) give

$$\frac{dK_z(\xi_0)}{d\xi} + \frac{\varkappa}{K_r^{max}} K_z(\xi_0) = 0. \tag{12}$$

In Fig. 2, curve 1 corresponds to a case when Eq. (11) is satisfied and curves 2 and 3 to cases where it is not.

Consider the example of the linear field

$$K_z(\xi) = (1 + \theta/2) - \theta\xi \tag{13}$$

and assume that Eq. (11) is satisfied at the channel outlet ($\xi_0 = 1$); neglecting the dependence of the parameters a and b on the shape of the energy distribution, the result obtained is

$$\theta = 2\varkappa/(2K_r^{max} + \varkappa), \tag{14}$$

i.e., the gradient of the vertical field may be fairly significant ($\varkappa \approx 1$), and the crisis will nevertheless occur at the channel outlet.

Experiment confirms this result and indicates that when the vertical energy distribution is only slightly nonuniform, the critical energy is largely independent of its shape. The critical energy of a channel with a nonuniform energy distribution over the height is determined in terms of the corresponding value of the critical energy for a channel with a constant energy distribution as follows

$$\tilde{N}_{cr} = \frac{\bar{N}_{cr}(i_{in}^0)\, \xi_0^{1/4}}{(\bar{K}_{z0}/K_{z0}) \int_0^{\xi_0} K_z(\xi)\, d\xi}, \tag{15}$$

the inlet enthalpy i_{in} in the calculation of $\bar{N}_{cr}$ being reduced by an amount corresponding to the excess heating of the heat carrier over the length ξ_0 for the maximally heat-stressed cell when the real energy distribution is replaced by a constant distribution with relative parameter $K_z(\xi_0)$. To compensate the excess energy leading to an overestimate of the heating $\bar{K}_{z0}/K_{z0}$ is included in the denominator of Eq. (15); $K_{z0} = K_z(\xi_0)$; $\bar{K}_{z0} = (1/\xi_0) \int_0^{\xi_0} K_z(\xi)\, d\xi$. The presence of the integral up to the limit ξ_0 in the denominator means that the upper part of the assembly ($\xi > \xi_0$) has no effect on the critical energy of the lower part.

The expression for the critical energy of the channel with constant energy distribution over the height is written in a form corresponding to Eq. (3)

$$\bar{N}_{cr} = R(\beta - x), \tag{16}$$

where $\beta = a/b$; x is the outlet equilibrium vapor content; and

$$R = \varepsilon Q/(1 - \varepsilon). \tag{17}$$

As a result of this analysis and treatment of a large quantity of experimental data (in particular, [5-9]), the parameters β and ε may be written as follows

$$\beta = (A + C)/B; \tag{18}$$

$$\varepsilon = (\xi_H^{1/4}/K_r^{max})\, B. \tag{19}$$

Here $\xi_H = H/H^*$, and hence $H^* = 5$ m.

The expressions for $A(\mu)$, $B(\lambda)$, and $C(\lambda)$, where

$$\lambda = P/P_{cr}; \tag{20}$$

$$\mu = W_\rho \delta/(W_\rho \delta)^*; \tag{21}$$

$P_{cr} = 225.6$ kgf/cm^2; $(W_\rho \delta)^* = 0.707$ kgf/m·sec, are independent of the type of channel and are universal functions of the heat-carrier flow parameters, as follows

$$A = \begin{cases} 1/\mu, & \mu \geqslant 1; \\ 2-\mu, & \mu < 1; \end{cases} \tag{22}$$

$$B = \sqrt{3} - \lambda; \tag{23}$$

$$C = \frac{1}{6} \operatorname{ch}(\sqrt{3} - 4\lambda). \tag{24}$$

As well as Eq. (16), the following expression may be used for the critical channel energy

$$\overline{N}_{cr} = \varepsilon Q (\beta - x_{in}). \tag{25}$$

where

$$x_{in} = (i_{in} - i')/r.$$

Note that the parameter μ, like the Reynolds number, characterizes the intensity and transport properties of the turbulent flow. With increase in the flow velocity W_ρ and (or) the characteristic dimension δ, the effect of the flow nucleus on the cooling of the heat-transfer surface is weakened, and hence the expression for A should contain an appropriate correction factor, in the form of a monotonically decreasing function of the Reynolds number. However, in reactor practice, such a situation rarely arises, and Eq. (22) can be used without any correction.

Substituting into Eq. (15) the following expression for i^0_{in}

$$i^0_{in} = i_{in} - \frac{N_{cr}(i^0_{in})\,\xi_0^{1/4}}{Q} r \left(\frac{\overline{K}_{z0}}{K_{z0}} - 1 \right), \tag{26}$$

leads to an expression for $\nu = \overline{N}_{cr}/\tilde{N}_{cr}$

$$\nu = \xi_0 (\overline{K}_{z0}/K_{z0})^2 [K_{z0} \xi_0^{-1/4} + \varepsilon (K_{z0} - \overline{K}_{z0})]. \tag{27}$$

The maximum of ν corresponds to the required energy $\tilde{N}_{cr}$ and the coordinate of the point of heat-transfer crisis $\xi = \xi_0$.

It is found that Eq. (27) satisfactorily describes the experimental data for a channel with cosinusoidal energy distribution in the presence of a maximum shifted to the inlet, and also with falling (in particular, stepped) forms of $K_z(\xi)$.

Note that skewing of the energy distribution q_v will lead to a maximum heat flux in each cylindrical fuel element exceeding the average by [10]

$$\frac{q_s^{max}}{\bar{q}_s} = 1 + \frac{\omega}{2} \frac{Bi}{1+Bi}, \tag{28}$$

where $\omega = (q_v^{max} - \bar{q}_v)/\bar{q}_v$: Bi is the Biot number for the fuel element. The effect of skewing of the energy distribution over the fuel elements on the critical channel energy may be approximately taken into account by reducing the calculated energy value by a factor $[1 + \omega/2 + Bi/(1 + Bi)]$.

The use of this method of calculating the critical energy is confirmed by experimental data for the following approximate ranges of the flow and geometry parameters: $0.2 < \lambda < 0.9$; $0.2 < \mu < 10$; $0.01 < |x_{in}| < 0.4$; $0.04 < \xi_H < 1.0$; $K_r^{max} < 1.5$; $K_z^{max} < 1.5$.

In the majority of cases, the scattering of the experimental results with respect to the calculated dependence does not exceed 7-8% and the mean value of the ratio of the calculated

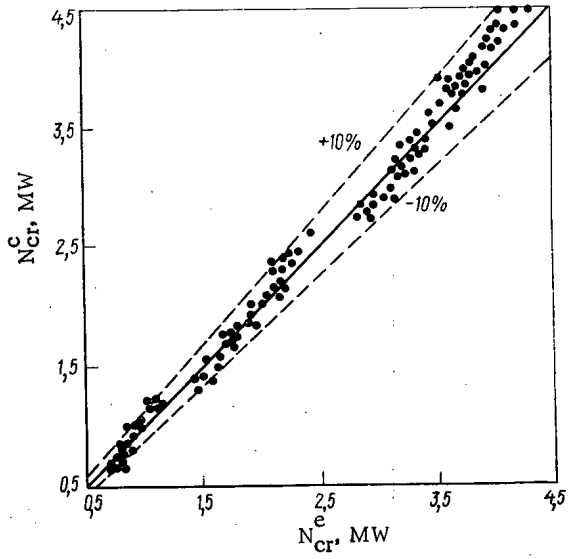

Fig. 3. Comparison of calculated and experimental results for the crisis of heat transfer in bundles of rods (the points in the energy ranges 0.7-1.4, 1.9-2.5, and 2.8-4.5 MW, satisfying the conditions $\mu < 10$ and $|x_{in}| < 0.4$, correspond to assemblies of 7, 19, and 37 rods, respectively [5]).

and experimental energies is close to unity. In particular, sufficiently reliable results may be obtained for the critical energy of channels of VVÉR-440 reactors. An experimental investigation of this reactor carried out on the KS test bed of the I. V. Kurchatov Institute of Atomic Energy can be described by the method proposed with a mean square error of ∿6.5% (Fig. 3).

LITERATURE CITED

1. M. Lakhi and R. Shiralkar, Teploperedacha, No. 2, 64 (1971).
2. Izrael', Kasterlain, and Matsner, Teploperedacha, No. 3, 64 (1969).
3. L. Maroti et al., in: Papers of a Thermophysical Seminar of the COMECON Standing Committee on the Use of Atomic Energy [Russian translation], Moscow (1974), p. 79.
4. S. P. Kaznovskii, V. V. Pashichev, and R. S. Pomet'ko, in: Papers of a Thermophysical Seminar of the COMECON Standing Committee on the Use of Atomic Energy [Russian translation], Moscow (1974), p. 335.
5. V. A. Kapustin et al., in: Papers of a Thermophysical Seminar of the COMECON Standing Committee on the Use of Atomic Energy [Russian translation], Moscow (1974), p. 99.
6. A. Companile et al., EUR-4468e, Part VI (1970).
7. A. Campanile et al., EUR-4514e, Part VII (1970).
8. B. Le Tourneau and S. Green, Nucl. Sci. Eng., 43, No. 1, 90 (1971).
9. V. N. Smolin and V. K. Polyakov, Teploenergetika, No. 4, 54 (1967).
10. L. N. Polyanin, Inzh.-Fiz. Zh., 24, No. 6, 1118 (1973).

RADIATION TESTING OF MATERIALS IN REACTORS

B. A. Briskman and E. A. Kramer-Ageev

UDC 621.039.51

Through radiation testing a relationship is established between a change in the characteristics of an object and a certain measure of radiation effect (MRE). The selection of one or another MRE can determine the reliability of the results obtained. One can use as MRE such quantities as the fluence of fast neutrons with a given threshold energy, the fluence of thermal neutrons, the total radiation absorbed dose (its γ and neutron components).*

Material Classes and MRE

The type of correlation for the results of irradiation depends on the class of material to which the irradiated object belongs and on the type of radiation responsible for the effect produced.

As is well known, radiation effects in the irradiation of metals are associated mainly with atomic displacements which are accompanied by the formation of clusters of defects and gas-filled microcavities [1]. Where neutrons with energies of several tens of kiloelectron volts are responsible for the formation of point displacements and clusters, thermal or ultrafast neutrons are responsible for nuclear reactions. The MRE used here is the fluence of fast neutrons with energies above some threshold value.

In the irradiation of semiconductors and semiconductor instruments, structural defects are produced within their volume which lead to a decrease in electrical conductivity and in the lifetime of excess carriers [2]. In semiconductor instruments, structural breakdowns produce deterioration of the parameters and primarily a decrease in the gain of bipolar transistors. At the present time, the fluence of fast neutrons with energies above 0.1 MeV is taken as the MRE.

In testing instruments of the metal—insulator—semiconductor type, it was established that the effect of γ rays produces a shift in the operating characteristics because of the buildup of charge in insulator layers. Neutron irradiation changes the form of the characteristics and gradually makes the instrument inoperable so that it is difficult to say immediately which factor is predominant: the formation of defect clusters within the volume of the semiconductor or in the insulator layer although the effect of γ rays is apparently a controlling factor [3].

In the irradiation of electron tubes, their longevity is mainly determined by loss of envelope integrity because of the interaction of thermal neutrons with the boron in the bulb [4]. Consequently, it is necessary to consider the fluence not only of fast neutrons but also of thermal neutrons when performing studies.

The irradiation of polymer materials causes breaking of existing bonds and the formation of new interatomic and intermolecular bonds. Radiation effects are associated with the transfer of radiation energy to an object because of ionization and excitation of atoms and molecules. For such interactions, it is customary to use the total absorbed radiation energy as the MRE. However, since the effect of various kinds of radiation on this class of objects can be significantly different in the general case, the use of the total absorbed energy leads to incorrect analysis of testing results in certain cases. An evaluation including the effect of the components in the absorbed energy presupposes a preliminary experimental determination of the radiation effect for neutrons and γ rays.

*Neutron flux density, absorbed dose rate, and irradiation temperature should also be included in this group. These parameters are not considered in this paper.

Translated from Atomnaya Énergiya, Vol. 42, No. 6, pp. 461-464, June, 1977. Original article submitted July 26, 1976.

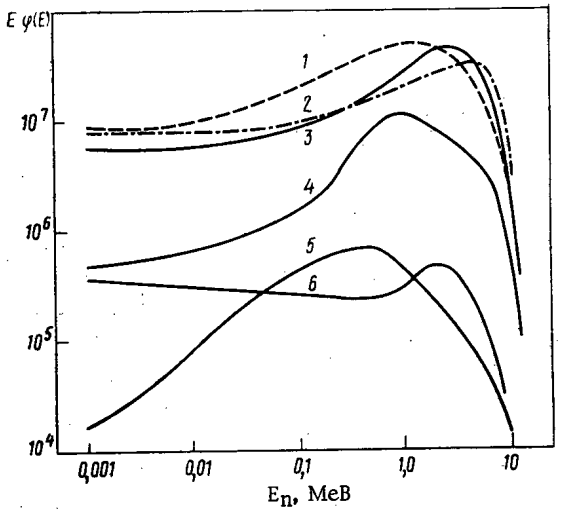

Fig. 1. Some reactor spectra: 1) VEC-6, $\overline{E}$ = 0.98 MeV; 2) VEC-12, $\overline{E}$ = 1.7 MeV; 3) HEC-2, $\overline{E}$ = 1.7 MeV; 4) HEC-2, lead filter, $\overline{E}$ = 1.4 MeV (IRT reactor); 5) TVR critical assembly, $\overline{E}$ = 0.83 [17]; 6) Enrico Fermi reactor, $\overline{E}$ = 0.59 MeV [7]. VEC) Vertical experimental channel; HEC) horizontal experimental channel.

Deficiencies of Accepted Methods for Correlation of Radiation Test Results

Considering the actual irradiation conditions in modern nuclear reactors where the ratios between the neutron and γ-ray fluxes vary over wide limits with simultaneous variation in the spectra of these radiations, one can conclude that the use of the fluence of fast neutrons with energies greater than E_{th} as the MRE for all classes of irradiated objects can and will lead to a lack of comparability for the test results from different reactors (and even from different experimental arrangements in the same reactor). We consider the reasons for such a situation.

Variation of Neutron Spectrum. A difference in the type of reactor used is responsible for a marked difference in neutron spectra. More than that, neutron spectra depend on the point of measurement within a given reactor. Some typical spectra are shown in Fig. 1. For an extensive group of spectra, the number of atomic displacements (or Frenkel' pairs) produced by the identical neutron fluence can vary by factors of 1.5-4 depending on the material in the object [5]. The international recommendations [6] on the use of the fluence of neutrons with energies above 0.1 MeV as a spectrum-independent measure of neutron flux are not in agreement with calculations of the number of defects produced within crystals by neutron irradiation [7].

γ-Ray Contribution to Radiation Damage. A widely accepted idea is that neutrons are the main cause of the production of radiation defects in metals and semiconductors and that the effect of γ rays can be neglected because the atomic displacements in the core produced by fast neutrons and knock-on electrons differ by two to three orders of magnitude for materials which are of practical interest. In a reflector, however, where a large number of experimental channels are located in modern research reactors, the ratio between the γ-ray and fast-neturon fluxes changes rapidly in favor of the γ rays; the γ-ray flux density exceeds the fast-neutron flux density by factors of 100-1000 at separations of 40-60 cm from the edge of the core. It then follows that the γ-ray contribution to the formation of radiation defects becomes comparable to the neutron contribution. Neglect of the γ-ray contribution can lead to serious errors amounting to 100%.

Irradiation of Objects with Comparable Sensitivity to Neutrons and γ Rays. Among such objects are organic materials, glass, etc. In this case, the correlation of radiation effects on the basis of absorbed dose is most logical. However, the fluence of neutrons with energies greater than E_{th} is often used also, particularly if such materials are part of composite systems.

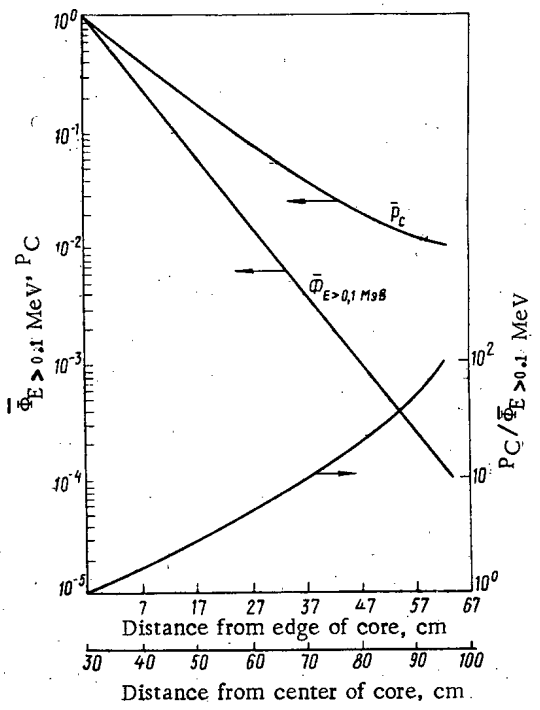

Fig. 2. Variation of the relative values of the neutron flux density $\Phi_{E > 0.1\ MeV}$, of the absorbed dose rate P_C, and of their ratio as a function of separation from the edge of the core of a VVR-Ts reactor.

Using the VVR-Ts reactor as an example, Fig. 2 shows the variation of the neutron flux density $\bar{\Phi}_{E > 0.1\ MeV}$ and of the absorbed dose rate in graphite P_C as a function of the separation from the center or edge of the core. We assume that irradiation of some object, the sensitivity of which is roughly the same for neutrons and γ rays, is performed in the core at 63 cm from the edge of the core until identical fluences are reached, i.e., the identical radiation effect. Figure 2 indicates that the absorbed dose will be 100 times less in the first case than in the second. Therefore extrapolation of the results obtained in the first case to the irradiation conditions in an actual situation corresponding to the second case will lead to an overestimate of the radiation resistance of the object.

Thermal Neutron Contribution to Radiation Effect. Formal addition to dosimetric information of the values of thermal-neutron influence does not always clear up the situation in radiation tests. It is well known that the addition of boron reduces the radiation resistance of materials during irradiation in thermal reactors [8]. For example, the addition of 5 wt.% of boron to natural rubber decreased its radiation resistance by a factor of 25. Without additional tests under other irradiation conditions, it remains unclear whether the indicated addition of boron sharply increased the absorbed energy or whether the specific effect of α particles played a decisive part.

Review of Existing Proposals

Because of the complexity of the situation during intrareactor irradiation, it is hardly possible to find a single universal criterion connecting radiation effect and irradiation conditions for any material. We consider the following proposals.

1. Optimal Value of Neutron Threshold Energy. The minimum effect of a neutron spectrum on irradiation results is achieved by using a fluence of neutrons with a threshold of 300-400 keV [7]. This conclusion is confirmed by more recent calculations which include the effect of the disorder regions (clusters) produced by the neutrons and by direct experiments on irradiation of alloy transistors [9]. For all groups of transistors, the use of ^{237}Np as a threshold detector is an acceptable compromise. In that case, the effect of neutron spectrum on the change in gain is no more than 20%.

2. For materials where atomic displacement is the controlling mechanism, the "number

of atomic displacements per atom of stopping medium" is used as the MRE [10]. In principle, such an MRE is universal for neutron, electron, and γ irradiation but is limited to certain materials in which the change in properties is produced by a breakdown in the regularity of the relative locations of atoms.

3. The various irradiated objects are subdivided into classes, e.g., metals, semiconductors, organic materials, etc., and each class has its own MRE. Such an approach is widely accepted but it does not eliminate uncertainties in the interpretation of irradiation results.

4. It was proposed [11, 12] and analytically demonstrated [13] that one can use the neutron component of the absorbed dose as the MRE for irradiation of metals and semiconductor materials with the dependence of the number of defects on the neutron spectrum being sharply reduced in this case. An experimental confirmation of this proposal would make it possible to unify the analysis of test results for practically all classes of materials from the standpoint of absorbed dose.

There are a number of other very interesting proposals with reference to methods for describing irradiation conditions but they all reduce to one of those enumerated above.

Design of Radiation Tests for Materials

To discover the cause for the production of radiation breakdowns and to ensure the comparability of test results from different reactors, it is necessary to perform irradiation with several markedly different neutron spectra with and without thermal-neutron filtration and also with different ratios of neutron and γ-ray fluxes.

Thus, considering the present level of development of dosimetric methods and the degree to which reactors are supplied with the appropriate detectors and instruments, one can recommend as a minimum program the following procedures for the irradiation of materials with provision of dosimetric information.

For Metals and Alloys: reactor irradiation in three different neutron spectra with and without filtration of thermal neutrons.

For Semiconductors and Semiconductor Instruments: irradiation with isotopic γ irradiators to a dose of several tens of megarad and reactor irradiation in two different neutron spectra with and without filtration of thermal neutrons.

For Organic Materials: irradiation with isotopic γ irradiators and reactor irradiation in channels with a significant fast-neutron contribution to the absorbed dose (not less than 40-50%) with and without filtration of thermal neutrons.

Dosimetric Information: for irradiation of γ irradiators — absorbed dose in water or exposure dose; for reactor irradiation — integral fast-neutron spectrum measured with threshold detectors [14], thermal-neutron fluence, absorbed dose and its γ and neutron components in a hydrogenous material (in polyethylene, for example). Additional information is the γ-ray spectrum or the γ-ray absorbed dose in the material. Indirect information about the γ-ray spectrum can be obtained by means of the spectral parameter [15]. It is recommended that the absorbed dose rate for intrareactor conditions be measured by means of a calorimeter with polyethylene and graphite absorbers which provides an opportunity not only to determine the dose components in hydrogen and carbon, but also to calculate their contribution to the dose in any material [16], the relative number of displaced atoms [13], and the fluence of neutrons with a threshold of 0.3 MeV.

It is to be hoped that the accumulation of such information and the comparison of the results of radiation testing under various irradiation conditions will lead, in the final analysis, to the use of a more universal criterion for any object — the effective value of the absorbed dose

$$\text{MRE} = aD_{\text{en}} + bD_{\text{th}} + D_{\gamma},$$

where the coefficients a and b take into account the relative effectiveness (in comparison with γ rays) of neutrons for objects of a given class.

LITERATURE CITED

1. M. W. Thompson, Defects and Radiation Damage in Metals, Cambridge Univ. Press (1969).
2. R. F. Konopleva, V. L. Litvinov, and N. A. Ukhin, Features of Radiation Damage in Semiconductors by High-Energy Particles [in Russian], Atomizdat, Moscow (1971).

3. V. A. Girii et al., At. Energ., 35, No. 1, 48 (1973).
4. D. Hamman et al., in: Effects of Radiation on Materials and Components, Reinhold Publ. Corp. New York (1964).
5. V. D. Popov et al., in: Metrology of Neutron Radiation in Reactors and Accelerators [in Russian], Vol. 2, Standartov, Moscow (1972), p. 163.
6. J. Mottef, in: Proceedings of the IAEA Symposium "Neutron Fluence Measurements," Vienna (1970), Rep. N 107.
7. N. A. Ukhin and A. V. Khrustalev, Preprint IAE 18-80, Moscow (1969).
8. R. W. King et al., in: Effects of Radiation on Materials and Components, Reinhold Publ. Corp., New York (1964).
9. V. A. Knyazev et al., in: Proceedings of the IAEA Symposium "Neutron Monitoring for Radiation Protection Purposes," Vol. 2, Vienna (1973), p. 321.
10. J. Buswell, in: Proceedings of the International Conference "Phys. Met. React. Fuel Elem.," London (1975), p. 170.
11. B. A. Briskman and V. P. Savina, in: Metrology of Neutron Radiation in Reactors and Accelerators [in Russian], Vol. 2, Standartov, Moscow (1972), p. 168.
12. E. A. Kramer-Ageev et al., in: All-Union Symposium on Radiation Defects in Semiconductors [in Russian], BGU, Minsk (1972).
13. E. A. Kramer-Ageev et al., At. Energ., 34, No. 4, 255 (1973).
14. E. A. Kramer-Ageev et al., Izmer. Tekh., No. 1, 61 (1973).
15. Yu. L. Poglin and S. S. Ogorodnik, At. Energ., 38, No. 2, 96 (1975).
16. B. A. Briskman, Components of Absorbed Dose of Reactor Radiation [in Russian], Atomizdat, Moscow (1976).
17. L. Miric and Z. Ubovic, in: Proceedings of the Third IAEA Nucl. Accident Intercomparison Experiment, Beograd, May 14-25, 1973 p. 6.

MODEL STUDIES OF THE STRESSED STATE IN PRESSURE VESSELS

N. N. Zorev, Yu. S. Safarov,
V. K. Tutynin, V. N. Sakhelashvili,
and N. L. Narskaya

UDC 620.171.5

The requirements for quality and reliability of reactor vessels and other equipment at nuclear power stations can be met by using modern methods for evaluation of load capacity and strength. One of the steps is the determination of the stress–strain state of vessels under the action of operating loads. This paper describes the results of a study of the stress state of a reactor vessel by the polarized-optics method of "freezing" strains using models made of optically sensitive materials. The model was made of hardened epoxy resin on a 1:20 scale with the preservation of complete geometric similarity to a prototype (Fig. 1) and consisted of a vessel and a dome joined by 60 studs. The vessel was built up from three regions: a piping region, a support shell, and the bottom. In the simulation of the operation of the flange connections (sealing points), a procedure was followed which essentially involved the selection of a preliminary "tightening" of the studs at room temperature in order to obtain the required tightening at the "freezing" temperature.

We consider the practical application of the procedure. According to similarity theory, the force similarity of model and prototype (subscripts "m" and "p") in the case of uniaxial stress states is determined by the relations

$$\alpha^2 = \beta/\lambda \quad \text{or} \quad \sigma_m/E_m = \sigma_p/E_p, \tag{1}$$

where $\alpha = l_p/l_m$ is the coefficient of geometric similarity; $\beta = p_p/p_m$ is the coefficient of force similarity; $\lambda = E_p/E_m$ is the coefficient of material similarity; σ_m and σ_p are stresses;

Translated from Atomnaya Energiya, Vol. 42, No. 6, pp. 465-472, June, 1977. Original article submitted April 26, 1976; revision submitted February 7, 1977.

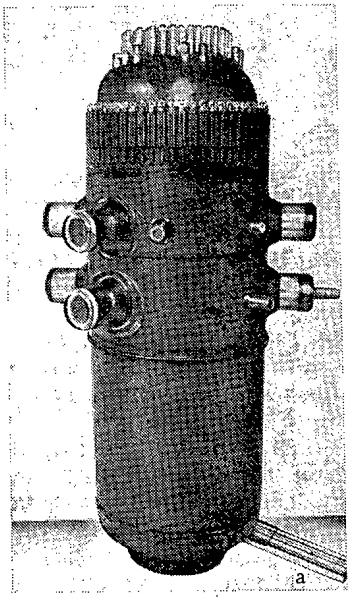

Fig. 1. External view (a) and diagram (b) of a model of a water-cooled–water-moderated reactor: 1) bottom; 2) support shell; 3) support ring; 4) piping region; 5) dome; 6) dome piping; 7) studs; 8) sealing ring; 9) pipe fitting.

l_m and l_p are geometric dimensions; p_m and p_p are loads; E is the modulus of elasticity. Then the force stretching a stud during tightening is

$$p_m = p_p(1/\alpha^2\lambda). \quad (2)$$

An experimental check of the correspondence of the stresses in a stud from tightening at room temperature and after "freezing" was made on models which simulated the region of the flange joint of the reactor. Tensile forces of 0.1, 5, 10, and 15 kg were established by

 necessary preliminary tightening. Uniform tightening was accomplished by means of a torque wrench. The wrench was calibrated in a special device. The gauges on the wrench recorded the forces produced in the studs during loading. Simultaneous recording of the readings of the gauges on the wrench and studs by measurement of static strains provided an opportunity to establish the dependence of the strain in the elastic element of the wrench on the stresses in the studs during tightening. The deviation from the average stress was ±5%.

After assembly and gluing, the model was loaded by an internal pressure in accordance with a standard temperature regime which ensured "freezing" of strains in the model. An analysis of present practice shows that the pressure is usually set arbitrarily based on the possibility of obtaining a larger number of bands in cut sections of the model in order to increase the accuracy of the measurements. Strains produced in the model are more than an order of magnitude greater than the strains in the prototype and thereby geometric similarity breaks down; this can lead in a number of cases to larger errors than those resulting from an inequality in Poisson coefficients. At the same time, an attempt to obtain a unique pressure in the model based on equality of the components of the strain tensor is unsuccessful because of the inequality of the Poisson coefficients of the model and prototype. In loading a cylinder by an internal pressure, the following relations are valid for the components $\varepsilon_{1,2,3}$ of the principal strains:

$$\begin{aligned} \varepsilon_1 &= (pR/Et)(1-\mu/2); \\ \varepsilon_2 &= (pR/Et)(1/2-\mu); \\ \varepsilon_3 &= (-pR/Et)\,3/2\,\mu, \end{aligned} \tag{3}$$

where p is the internal pressure; R is the mean radius of the cylinder; t is the thickness of the cylinder wall; μ is the Poisson coefficient.

If it is assumed that

$$(\varepsilon_1)_m = (\varepsilon_1)_p; \quad (\varepsilon_2)_m = (\varepsilon_2)_p; \quad (\varepsilon_3)_m = (\varepsilon_3)_p,$$

when $\mu_m = 0.5$ and $\mu_p = 0.3$ we obtain, respectively,

$$\begin{aligned} p'_m &= 1.133 p_p (E_m/E_p); \\ p''_m &= \frac{0.2}{0} p_p (E_m/E_p) = \infty; \\ p'''_m &= 0{,}6 p_p (E_m/E_p), \end{aligned}$$

i.e., the pressure in the model is indeterminate. The following method is proposed for determination of stresses in a reactor vessel from measurements in a model in order to eliminate this indeterminacy and to "neutralize" the effect of the Poisson coefficient.

The strain state at a given point is characterized by the strain intensity

$$\varepsilon_i = \frac{\sqrt{2}}{2(1+\mu)} \sqrt{(\varepsilon_1-\varepsilon_2)^2+(\varepsilon_2-\varepsilon_3)^2+(\varepsilon_3-\varepsilon_1)^2}, \tag{4}$$

which does not depend on the Poisson coefficient.* In a uniaxial stress state, the relations between strains will be $\varepsilon_2 = -\mu\varepsilon_1$; $\varepsilon_3 = -\mu\varepsilon_1$; $\varepsilon_1 - \varepsilon_2 = \varepsilon_1(1+\mu)$ and the strain intensity $\varepsilon_i = \varepsilon_1$. In the case of a thin-walled cylinder under an internal pressure producing strains whose values are given by Eqs. (3), the intensity is

$$\varepsilon_i = (\sqrt{3}/2)(pR/Et).$$

Thus, in order to obtain an identical strain state in model and prototype (eliminating the effect of the difference in Poisson coefficients in this way), it is necessary that the

*When μ = 0.5, Eq. (4) reduces to the more customary expression in the mechanics of deformable media

$$\varepsilon_i = \sqrt{2}/3 \quad \sqrt{(\varepsilon_1-\varepsilon_2)^2+(\varepsilon_2-\varepsilon_3)^2+(\varepsilon_3-\varepsilon_1)^2}.$$

strain intensities be equal, i.e.,

$$(\varepsilon_i)_m = (\varepsilon_i)_p. \tag{5}$$

Since in the elastic load region

$$\varepsilon_i = \sigma_i/E, \tag{6}$$

where the stress intensity is

$$\sigma_i = \sqrt{2}/2\sqrt{(\sigma_1-\sigma_2)^2+(\sigma_2-\sigma_3)^2+(\sigma_3-\sigma_1)^2}, \tag{7}$$

we then have from Eqs. (5) and (6)

$$(\sigma_i/E)_m = (\sigma_i/E)_p. \tag{8}$$

At the same time, the stress intensity at each point of model and prototype (since the elastic problem is being considered) is directly proportional to the load (pressure), i.e.,

$$\sigma_i = kp. \tag{9}$$

Equations (8) and (9) show that the pressure determined by the equality of strain intensities (5) is

$$p_m = (E_m/E_p)\, p_p. \tag{10}$$

The condition (10) guarantees equal strain intensities and identical order of magnitude for the strain components in the model and reactor vessel although the disparity of the components of the strain tensor remains.

With a pressure in the model realized by means of Eq. (10), the components of the stress tensor, or their differences, can be determined; from them, using Eqs. (7) and (8), the stress intensity is found to be

$$(\sigma_i)_p = \{\sqrt{2}/2\sqrt{(\sigma_1-\sigma_2)^2+(\sigma_2-\sigma_3)^2+(\sigma_3-\sigma_1)^2}\}_p = (E_p/E_m)\,(\sigma_i)_m. \tag{11}$$

Direct transition from the stress tensor in the model to its components in the reactor vessel, as is done at the present time in similar studies using the relation

$$(\sigma_{ij})_p = p_p/p_m(\sigma_{ij})_m \tag{12}$$

is not rigorous and introduces an indeterminate error in the calculation. In fact, from the equations of the theory of elasticity

$$\sigma_{ij} = \lambda\delta_{ij}\varepsilon_{kk} + 2G\varepsilon_{ij}, \tag{13}$$

where

$$\lambda = \mu E/(1+\mu)(1-2\mu);\quad G = E/2(1+\mu); \tag{14}$$

$$\varepsilon_{kk} = \varepsilon_1+\varepsilon_2+\varepsilon_3;\quad \delta_{ij} = \begin{cases} 1, & i=j, \\ 0, & i\neq j, \end{cases} \tag{15}$$

which are brought to the form

$$\sigma_1/E = \varepsilon_1/(1+\mu) + \frac{\mu(\varepsilon_1+\varepsilon_2+\varepsilon_3)}{(1+\mu)(1-2\mu)}, \tag{16}$$

. . . . . .

it follows that

$$(\sigma_{ij}/E)_m = (\sigma_{ij}/E)_p \text{ or } (\sigma_{ij}/p)_m = (\sigma_{ij}/p)_p,$$

which are sufficient when Eq. (10) is taken into consideration, can be satisfied only when the right-hand sides of Eq. (16) are equal for model and prototype. However, equality is not satisfied since

$$\varepsilon_1+\varepsilon_2+\varepsilon_3 = 0 \text{ and } \mu = 0.5$$

in the model and the right-hand side takes on an indeterminate value, while in the prototype

$$\varepsilon_1+\varepsilon_2+\varepsilon_3 \neq 0 \text{ and } \mu = 0.3.$$

Consequently, we have for the components of the stress tensor the inequalities

$$(\sigma_{ij}/E)_m \neq (\sigma_{ij}/E)_p \quad \text{or} \quad (\sigma_{ij}/p)_m \neq (\sigma_{ij}/p)_p. \tag{17}$$

As follows from Eq. (4), the strain intensity at corresponding points of model and reactor vessel will be equal in the case where we have the relations

$$[(\varepsilon_1-\varepsilon_2)/(1+\mu)]_m = [(\varepsilon_1-\varepsilon_2)/(1+\mu)]_p. \tag{18}$$

. . . . . .

Returning to Eq. (16), we obtain

$$(\varepsilon_1-\varepsilon_2)/1+\mu = (\sigma_1-\sigma_2)/E. \tag{19}$$

Thus, there follow from Eqs. (18) and (19) relations for the differences of the components of the principal stresses in the model and reactor vessel,

$$[(\sigma_1-\sigma_2)/E]_m = [(\sigma_1-\sigma_2)/E]_p. \tag{20}$$

. . . . .

To determine contour stresses, it is sufficient to use the value of the third principal stress in the reactor vessel, which is equal to the internal pressure, i.e.,

$$\sigma_3 = -p \tag{21}$$

on the internal surface and zero on the external surface. The other two stresses are determined from Eqs. (20) with Eq. (21) taken into account:

$$(\sigma_1)_p = (\sigma_3)_p + (\sigma_1-\sigma_3)_m(E_p/E_m); \tag{22}$$
$$(\sigma_2)_p = (\sigma_3)_p + (\sigma_2-\sigma_3)_m(E_p/E_m).$$

In the general case of a stress–strain state based on calculated values for the principal stress differences in accordance with Eq. (20), it is necessary to consider the equilibrium equations in addition when making separate determinations of σ_1, σ_2, and σ_3. Having found the stress components, one can determine the components of the strain tensor from Eq. (19); they will be different for model and reactor vessel. Thus, the actual stress–strain state of the vessel is determined by the approach given.

When the pressure in the model is set higher than follows from conditions (10), this means that

$$(\varepsilon_i)_m = (\varepsilon_i)_p n, \tag{23}$$

where n is the number by which the pressure in the model calculated from Eq. (10) is multiplied. Such an arbitrary increase in pressure is permissible where the strain has no effect on the distribution of the effective external forces in the body. If in each specific case the increase in pressure above the calculated value is sufficiently justified, stress calculations for the reactor vessel are performed by determination of the differences in the principal stresses from the condition

$$[(\sigma_1-\sigma_2)/E]_m = [(\sigma_1-\sigma_2)/E]_p n \tag{24}$$

using the equilibrium equations in the general case. The coefficient n for a given pressure p_m in the model is given by [see Eqs. (8) and (10)]

$$n = p_m E_p / p_p E_m. \tag{25}$$

After loading and "freezing" of the strains, the model is cut up into thin sections 2-3 mm thick and the optical path difference determined at required points by the method of band compensation. The measurement error was 0.02 bands.

One of the factors which is extremely difficult to take into consideration when using the "freezing" method is the fringe effect which is produced by the instability of the properties of optically sensitive materials. The creation of a pressure in the model in accordance with Eq. (10) for simulation using Eq. (5) leads to a situation where the fringe effect becomes commensurable with the optical path difference in the "frozen" sections and introduces a significant error in the measurements.

Studies showed that repeated annealing of the sections has no influence on the fringe effect (Fig. 2). Thus, in order to determine the actual stresses in three-dimensional models, it is necessary to measure them in two stages. First the stresses are determined in flat "frozen" sections. Then the sections are annealed in a constant-temperature bath. Annealing

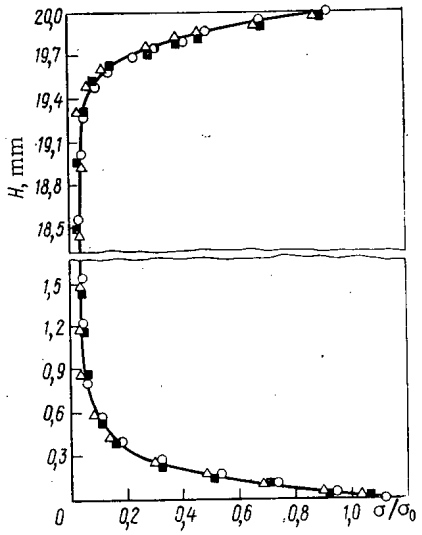

Fig. 2. Measurements of stresses produced by fringe effect in a flat sample after the first (○), second (■), and third (△) annealing.

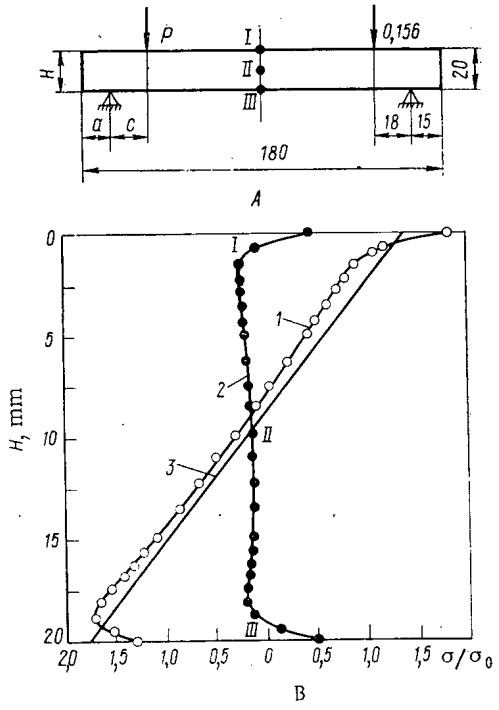

Fig. 3. Experimental verification of the technique for consideration of fringe effect in flat samples: A) loading scheme; B) stress curves over height of sample: 1) total stresses from effective load and fringe effect; 2) stress distribution in sample after annealing (stress curve created by fringe effect); 3) stress distribution over sample height produced by load.

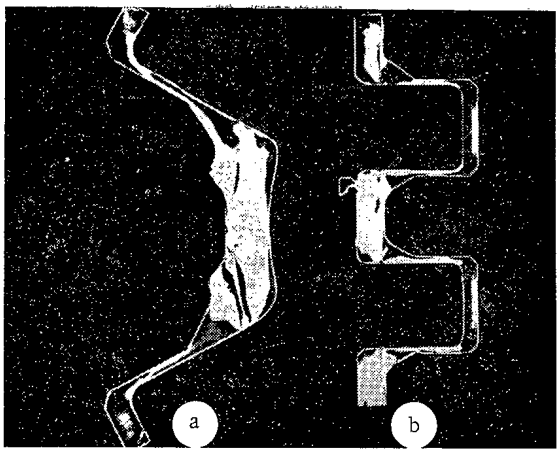

Fig. 4. Cross sections of the piping region in "frozen" sections of the model in the transverse (a) and longitudinal (b) directions.

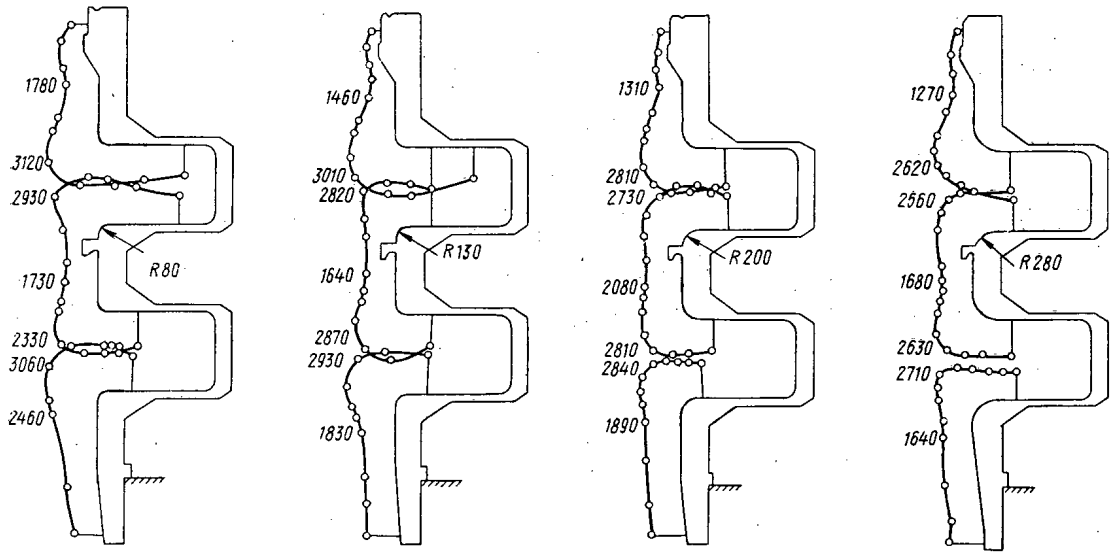

Fig. 5. Curves of contour stresses in a plane normal to a piping-region section.

removes the stress produced by a load, but the "stress" from the fringe effect remains. The difference of the two measurements (with the sign of the fringe effect taken into account) is the true stress at a given point of the model. A check of this technique was performed with flat samples loaded in accordance with a pure bending scheme over the rectangular section I, II, III (Fig. 3).

The maximum stress in the central section including the intrinsic mass of the model is found from the expression

$$\sigma_{\max} = M/W = 6/bH^2\,[ql^2\,(0.5 - a/l) + pc], \tag{26}$$

where q is the distributed load from the intrinsic mass of a beam (the other notation is shown in Fig. 3). On the other hand, $\sigma_{\max}$ is associated with the optical constant of the material by the relation

$$\sigma_{\max} = \sigma_0^{1,0}\,(m/b), \tag{27}$$

where $\sigma^{1,0}$ is the optical constant of the material in the model; m is the order of the band on the sample contour; b is the thickness of the model.

From these expressions one can obtain the order of the band on the contour:

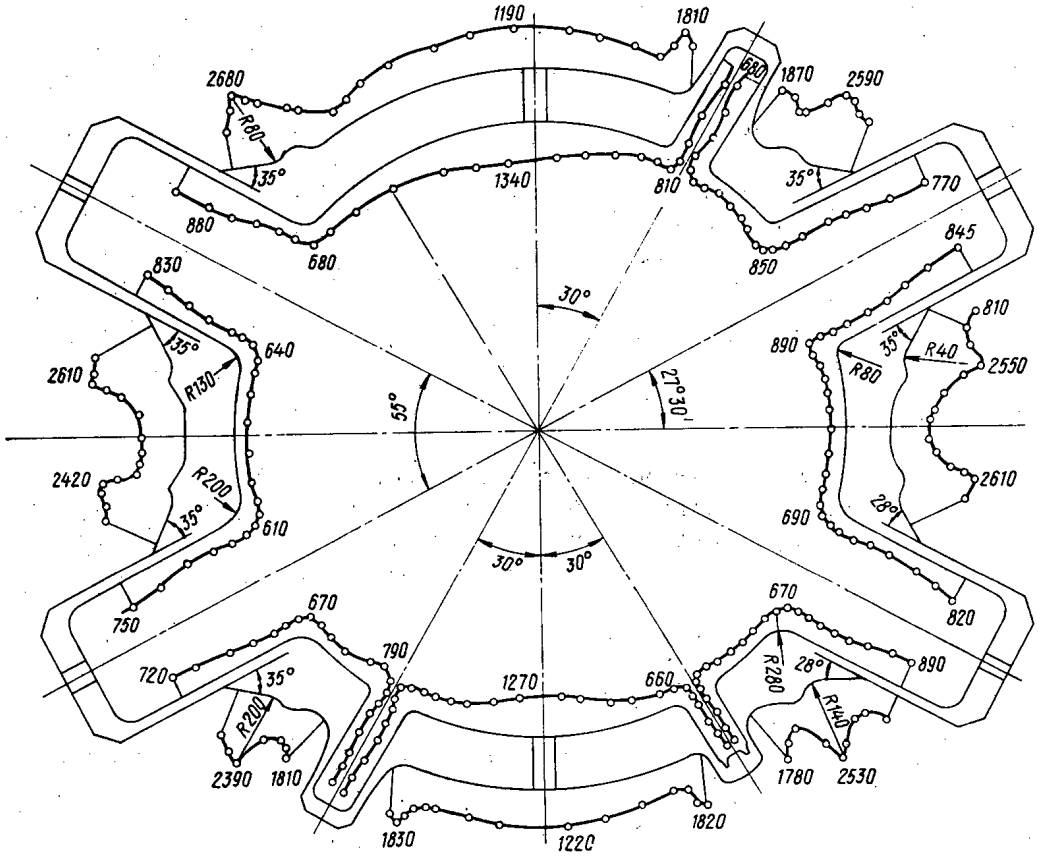

Fig. 6. Curves for contour stresses in the plane of a section through the upper set of piping.

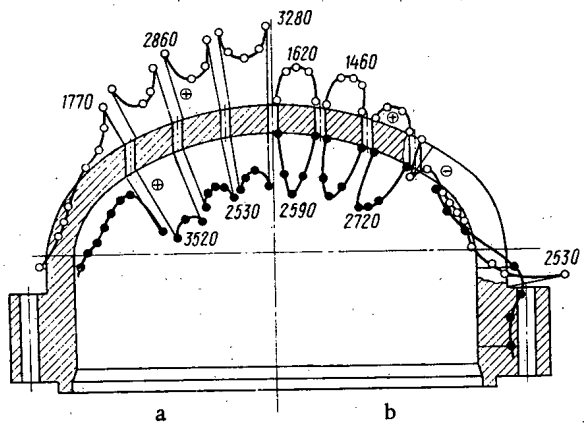

Fig. 7. Distribution of circumferential (a) and meridional (b) stress in reactor dome (P = 180 kgf/cm^2).

$$m = \frac{6}{\sigma_0^{1,0} H^2} [ql^2 (0.5 - a/l) + pc]. \tag{28}$$

Figure 3 also shows the results of stress measurements in the central section of the sample. The deviation between calculated and experimental data is 1.2%. These studies confirm the correctness of the method developed for including the influence of the fringe effect in the determination of stresses on the contour of three-dimensional "frozen" models.

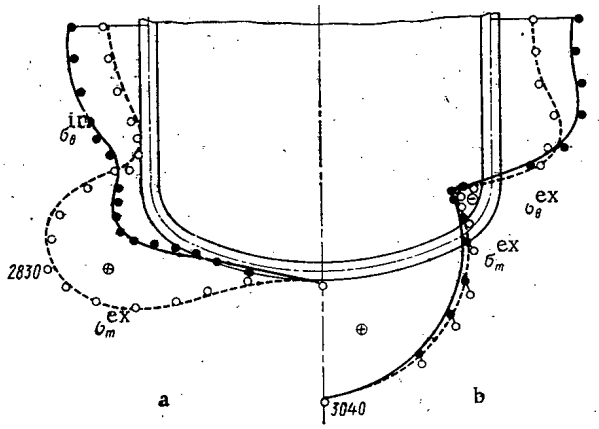

Fig. 8. Distribution of circumferential and meridional stresses in reactor bottom along internal (a) and external (b) surfaces.

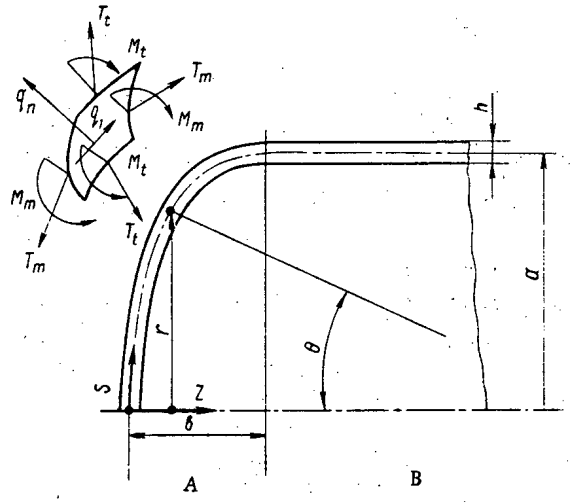

Fig. 9. Computational scheme for bottom of reactor vessel: A) bottom; B) cylindrical shell.

Using the method described, the circumferential and meridional contour stresses were determined. We denote the circumferential, meridional, and radial stresses by σ_1, σ_2, and σ_3. By transillumination of longitudinal and transverse sections of the model, the data required for stress calculations were obtained in the form

$$\begin{aligned}\sigma_1-\sigma_3&=n\sigma_0^t;\\ \sigma_2-\sigma_3&=n\sigma_0^t;\end{aligned} \tag{29}$$

where n is the order of an isochromatic band (see the sections in Fig. 4); σ_0^t, kgf/cm^2-band, is the optical constant of the material in the section.

The results of stress determinations (in kgf/cm^2) for the prototype are shown in Figs. 5-8. The curves (solid and dashed) correspond to calculated data and the points to experimental data. The stresses for the bottom portion of the reactor, which can be considered axisymmetric in view of the separation from piping, were also calculated from the moment theory of shells.

The complete system of differential equations describing the stress–strain state of a shell of rotation with an arbitrary meridional form is written in the matrix form

$$\bar{y}'=\bar{F}\bar{y}+\bar{g}, \tag{30}$$

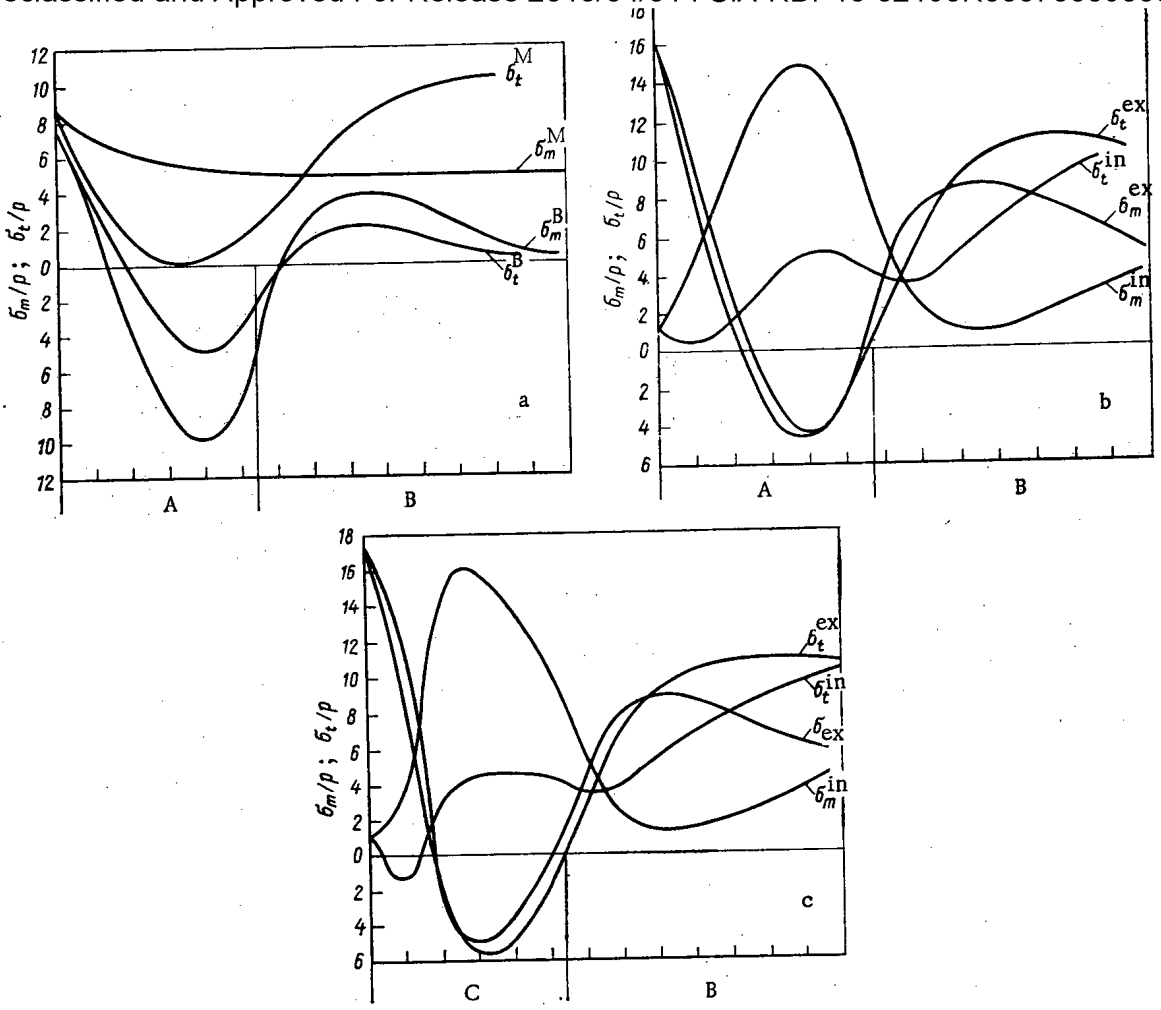

Figure 10. Calculated stress curves: a) membrane and bending stresses in elliptical bottom A; b, c) total stresses in ellipical bottom A and torospherical bottom C; B is the cylindrical shell.

where the state vector $\bar{y} = \begin{pmatrix} \rho \\ \vartheta \\ rH \\ rM_m \end{pmatrix}$, ρ is the radial displacement; ϑ is the angle of rotation of the normal to the meridian; H is the thrust; M_m is the meridional bending moment (Fig. 9).

The numerical matrix $F = \begin{bmatrix} -\mu\frac{\cos\Theta}{r} & -\sin\Theta & \frac{(1-\mu^2)\cos^2\Theta}{Ehr} & 0 \\ 0 & -\mu\frac{\cos\Theta}{r} & 0 & \frac{12(1-\mu^2)}{Eh^3r} \\ \frac{Eh}{r} & 0 & \mu\frac{\cos\Theta}{r} & 0 \\ 0 & \frac{Eh^3}{12}\frac{\cos^2\Theta}{r} & \sin\Theta & \mu\frac{\cos\Theta}{r} \end{bmatrix}$.

The load vector $\bar{g} = \begin{pmatrix} \frac{1-\mu^2}{Eh} \frac{\sin\Theta\cos\Theta}{r} f(s) \\ 0 \\ \mu \frac{\sin\Theta}{r} f(s) - q_2 r \\ -\cos\Theta f(s), \end{pmatrix}$, where $f(s) = \int_0^s (q_n \cos\Theta - q_1 \sin\Theta)\, r ds$; $q_r = q_1 \cos\Theta + q_n \sin\Theta$; q_1, q_n are intensities of the distributed load tangential and normal to the meridian; r, h, and Θ are geometrical parameters (see Fig. 9).

Solution of the problem was carried out numerically by orthogonal stepping* for the boundary conditions $M_m = M_t$ and $T_m = T_t$ in a band and damping of the moment solution in a long cylinder. Force factors were determined from the resultant vector which described the stress state of the shell:

$$T_m = H\cos\Theta + \frac{f(s)}{r}\sin\Theta;$$
$$T_t = \mu T_m + \frac{Eh}{r}\rho; \qquad (31)$$
$$M_t = \mu M_m + \frac{Eh^3}{12}\frac{\cos\Theta}{r}\vartheta.$$

Then the membrane stresses

$$\sigma^{M}_{m(t)} = \frac{T_{m(t)}}{h}$$

and the bending stresses

$$\sigma^{B}_{m(t)} = \frac{6M_{m(t)}}{h^2}$$

were found. Here, $T_{m(t)}$ is the meridional (circumferential) membrane force; $M_{m(t)}$ is the meridional (circumferential) bending moment.

To evaluate the effect of bottom shape on its stress state, calculations were made for two types of model (Fig. 10): an elliptical bottom ($a/b = 2$) and a torospherical bottom ($R1/a = 1.9$, $R2/a = 0.4$, where R1 and R2 are the radii of the circles forming the meridian of the torospherical bottom). The bending stresses are of the same order of magnitude as the membrane stresses (see Fig. 10a) and this points to the necessity of including them, i.e., to the correctness of the choice of moment theory. The curves in Figs. 10b and 10c illustrate the total effect of bending and of membrane tension where the stresses at points of the external surfaces were calculated from the expressions

$$\sigma^{ex}_{m(t)} = \sigma^{M}_{m(t)} + \sigma^{B}_{m(t)};$$
$$\sigma^{in}_{m(t)} = \sigma^{M}_{m(t)} - \sigma^{B}_{m(t)}. \qquad (32)$$

From a comparison of the curves for the two types of bottom, it is clear that they are almost indistinguishable with respect to stress state and are equivalent from this standpoint. The good agreement between calculation and experiment should be noted.

These studies show that for an internal pressure set at 180 kgf/cm² the stresses in elements of the reactor vessel do not exceed the yield point, which is 55 kgf/cm². The piping region of the reactor vessel shows the greatest stress. Furthermore, the maximum stress is concentrated in the transition region between pipe fitting and reactor vessel. The insignificant effect of transition radius on the stress level in the transition region was shown for four transition radii.

Stress distributions in plane sections passing through the upper and lower sets of pipe fitting were practically identical and this is evidence of the significant effect of the support ring located between the upper and lower sets of fittings.

*S. K. Godunov, Usp. Mat. Nauk, 16, No. 3(99), 171 (1961).

The agreement of experimental and calculated results indicates the appropriateness of the use of the "freezing" method for studies of objects of complex geometry since in such a case the use of computational methods is associated with tremendous difficulty and complexity.

SOME PROBLEMS ON THE MECHANISM OF BREAKUP AND MASS TRANSFER IN PULSE EXTRACTION COLUMNS

E. I. Akharov and S. M. Karpacheva

UDC 66.063.3.023.3

The droplet size d_D* in column extractors enables one to determine the principal technological indices of the equipment: the specific throughput ($W \sim \nu_0 \sim \bar{d}_D$), efficiency (HTU $\sim \Omega/d_D$), and rate of phase separation in settling tanks ($\nu_i \sim d_D$, h_e).

Breakup of a droplet into two equal parts requires the energy

$$E_D = C\pi\sigma d_D^2. \quad (1)$$

This energy can be supplied by rotating disks, agitators (columns with a mechanical energy supply), and reciprocating motion of plates (vibration columns) or of a continuous phase (pulse columns).

Breakup of the dispersed phase in extraction columns can occur in the center of the flow of the continuous phase as a result of turbulent pulsations in the flow rate of the continuous reagent (the change in velocity at opposite ends of the droplet is ΔU), induced by reciprocating motion of the continuous phase, by change in the dynamic pressure at the holes, channels in the packing, the column walls, and the packing surface (rings, plates) when the flow rate changes and when the droplet strikes the packing surface.

To elucidate the breakup mechanism of the dispersed phase in pulse columns, we carried out still and motion picture photography of various sections of a model column (cross section 176 × 176 mm; H_D = 1.2 m), using the most common types of packing (Table 1).

We employed a system of 20% tributyl phosphate (TBP) in kerosene (fraction boiling at 170-240°C) with 0.1-0.2 M HNO_3 in water (σ = 12 dyn/cm, ρ_c = 1 g/cm^3, $\Delta\rho$ = 0.21 g/cm^3, μ_d = 1.65 cP).

We found that in pulse columns with sieve plates and KRIMZ packing breakup of the dispersed phase occurs in the center of the flow of the continuous phase at the entrance and exit of the holes. When the KRIMZ packing is used, the droplet size becomes essentially constant at the point along the column at which the dispersed reagent has passed three plates.

The droplet size is determined by the type of packing, the pulse intensity, and the properties of the liquid system (Fig. 1). Variation of $I = f\alpha$ will provide a specified d_D in almost any system [1, 2]. Since theory [3] gives the energy required for breakup of a droplet as

$$E_D = C\rho_c \Delta U^2 d_D^3, \quad (2)$$

then when the change in velocity ΔU is due, respectively, to inertial or viscous forces [3, 4]

$$\Delta U^2 = C_1^{\dagger}\, \varepsilon^{2/3} d_D^{2/3}; \quad (3)$$

$$\Delta U^2 = C_2 \varepsilon \rho_c d_D^2/\mu. \quad (4)$$

*Conventional symbols are listed at the end of the paper.
†In all cases C_{1-6} is the constriction coefficient of the flow [5].

Translated from Atomnaya Énergiya, Vol. 42, No. 6, pp. 473-477, June 1977. Original article submitted May 19, 1976.

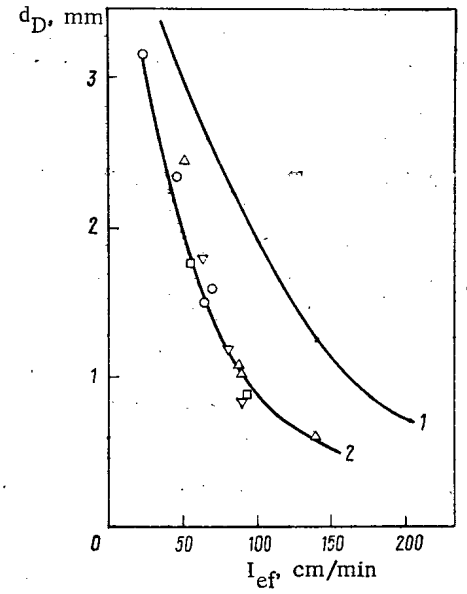

Fig. 1. Dependence of droplet diameter on the pulse intensity; 1) Raschig rings (10 × 10 × 0.4 and 25 × 25 × 0.8 mm) (data from [7]); 2) KRIMZ packing, pulse frequency 100 (○); 176 (△); 310 (▽), 360 min^{-1} (□).

TABLE 1. Properties of the Stainless Steel Packings

Type of packing	Geometry of the packing	Method of filling
Raschig rings	10×10×0,4 mm; ε_p=0,82 25×25×0,8 mm; ε_p=0,866	Continuous, sectional with gaps 0,05—0,2 mm
Sieve plates KRIMZ*	d_o=3,2 mm, F=20—25% Holes 10×20 mm α=10—45°; F=20—43%	h_p=50 mm h_p=50 — 200 mm

*Inventor's Certificate No. 175489; Byull. Izobret., No. 20, 18 (1965); KRIMZ comes from the initials of the inventors' family names.

These expressions for the breakup of the dispersed phase in pulse columns with sieve plates and KRIMZ give

$$\bar{d}_D = \text{const}\,(\sigma/\rho_c)^{0.6}\varepsilon^{-0.4}; \tag{5}$$

$$\bar{d}_D = \text{const}\,(\sigma\mu/\rho_c^2\varepsilon)^{0.33}. \tag{6}$$

For sieve-plate columns ε is [5]

$$\varepsilon = \pi^2(1-F)(fa)^3/2C_0^{2*}F^2h_p \tag{7}$$

$$\bar{d}_D = C_3(\sigma/\rho_c)^{0.6}[F^{0.8}h_p^{0.4}/(1-F)^{0.4}](fa)^{-1/2}, \tag{8}$$

or

$$\bar{d}_D/d_o = C_3\mathrm{We}_I^{-0.6}[F^2/(1-F)]^{0.4}(h_p/d_o)^{0.4}; \tag{9}$$

$$\bar{d}_D = C_4(\sigma^{0.33}\mu_c^{0.33}/\rho_c^{0.66}) \times [F^{0.66}h_p^{0.33}/(1-F)^{0.33}](fa)^{-1.0}, \tag{10}$$

or

$$\bar{d}_D/d_o = C_4\mathrm{We}_I^{-0.33}\mathrm{Re}_I^{-0.33}[F^2/(1-F)]^{0.33}(h_p/d_o)^{0.33}. \tag{11}$$

*C_o = 0.6 is the constriction coefficient of the flow [5].

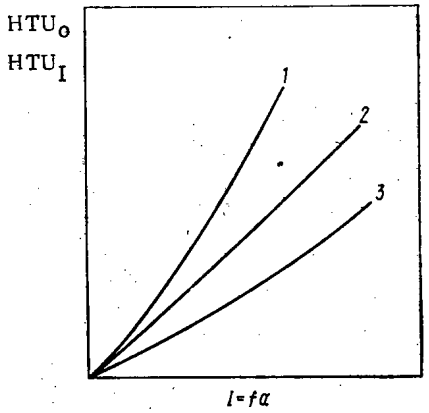

Fig. 2. Effect of pulse intensity ($I = fa$) on the operating efficiency of the pulse column in various operating regimes of the equipment: 1, 2, 3) at $I_1 > I_2 > I_3$.

TABLE 2. Correlation Equations for d_D (experiment)

Property of the system	Property of the packings	Experimental relation
	Packed column	
$\sigma = 5{,}8-50$; $\rho_c = 0{,}998-1{,}084$; $\rho_d = 0{,}67-0{,}81$; $\mu_c = 1-2{,}9$; $\mu_d = 0{,}4-4{,}2$	Rasching ring (ceramic) 7,76×25 mm $\varepsilon_p = 0{,}54-0{,}77$	$d_D \rho_c (fa)/\mu_c = 2{,}21 \cdot 10^{-2} \varepsilon_p^2 \times (\sigma \rho_c d_p/\mu_c^2)^{0{,}526} (\Delta\rho g d_p^2/\sigma)^{0{,}177} (\mu_d/\mu_c)^{0{,}17}$ [8]
$\sigma = 12$, $\rho_c = 1{,}02$; $\rho_d = 0{,}796$; $\rho_c = 1{,}02$; $\mu_d = 1{,}65$	Rasching ring (stainless steel) 10×10×0,5 mm 25×25×0,8 mm	$\bar{d}_D = C\,(\sigma/\rho_c)^{0{,}5} (fa)^{-1{,}4}$ [9]
	Sieve-plate column	
$\sigma = 1{,}08-37$; $\rho_c = 0{,}99-1{,}0$; $\rho_d = 0{,}8-0{,}958$; $\mu_c = 1-1{,}2$	$d_o = 5-10$ mm $h_p = 0{,}25$ mm $F = 0{,}14-0{,}61$	$\bar{d}_D = 0{,}439 d_o [\sigma F^{0{,}5}/(5{,}1fa + W_c)^2 \rho_c d_o]^{0{,}6}$ [10]
Methyl isobutyl ketone–water	—	$\bar{d}_D = 0{,}81\,(af/h_p^{0{,}33})^{-1{,}2}$ [11]
	Column with KRIMZ packing	
$\sigma = 6-24$; $\rho_c = 1-1{,}25$; $\rho_d = 0{,}6-1{,}0$; $\mu_c = 1-1{,}2$; $\mu_d = 1{,}2-6$	$h_p = 50-250$ mm $\alpha = 10-45°$; holes 10×20–70×140 mm	$\bar{d}_D = 0{,}135 F\,(\sigma/\rho_c)^{0{,}6}\,(fa)^{-1{,}0}$; $F = 4a^2 \sin\alpha\,(2+\cos\alpha)\,N_{hol}/\pi D_p^3$ [12]

In pulse columns with Raschig rings, the breakup of the dispersed phase depends on the pulse intensity and the state of the packing surface – its wettability by the dispersed phase, which is characterized by the contact angle θ.

For a packing that is not wetted by the dispersed phase at low intensities (100-200 mm/min), breakup of the dispersed phase occurs when the droplet strikes the surface of the ring. At high intensities breakup takes place close to the surface of the ring. In this case theory [6, 7] has

$$d_D \sim (\sigma v/\rho_c v_t^3)^{0{,}5}, \tag{12}$$

where v_t is the rate of turbulent pulsations.

Assuming $v_t \approx fa$, we get

$$\bar{d}_D = C_5\,(\sigma/\rho_c)^{0{,}5} \mu_c^{0{,}5}\,(fa)^{-1{,}43} \tag{13}$$

or

$$\bar{d}_D/d_p = C_5 \mathrm{We}_I^{-0{,}5} \mathrm{Re}_I^{-0{,}5}. \tag{14}$$

TABLE 3. Effect of Pulse Intensity of the Parameters of a Pulse Column with Distributive Packing

Index	I, cm/sec						
	0	0,33	0,66	1,0	1,73	2,0	2,33
Experiment							
$\bar{d}_D$	0,46	0,32	0,25	0,145	0,10	0,08	0,06
a_D/b_D	0,8	1,3	1,1	1,0	1,0	1,0	1,0
D_c	1,02*	1,02*	1,0	1,0	1,5	2,0	2,5
D_d	65*	65	65	60	24	12	6
Ω, %	4,6	5,5	9,0	10,0	23	30	24
HTU_l	92	82	66	48	45	21	22,5
Calculation							
S	60	100	180	452	1390	1800	2400
W_c*	10,5	10,6	11	11,2	13,0	14,3	9,9
W_d*	218	181	111	100	43	33	21
HTU_{add}	12	16,4	22	24,8	24,1	17,8	19,3
HTU_m	80	65,6	44	23,2	20,9	3,2	3,5
K_e	1,0	1,22	1,81	3,43	3,8	25,0	22,9
K_m	1	1,66	3,00	7,53	23,1	30	40
K_m	1,0	0,735	0,6	0,465†	0,165†	0,83	0,57

*Assumed for I = 0.66 cm/sec.
†The substantial change in K_m on going from I = 1 cm/sec to I = 1.73 cm/sec is plainly due to the error in measuring HTU_l in this pulsation regime.

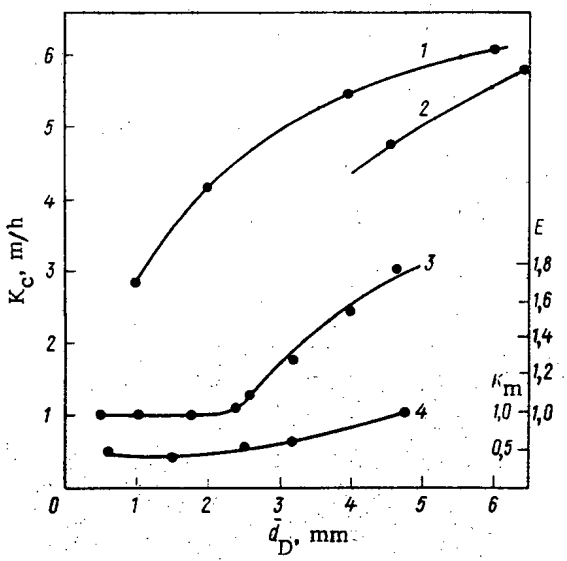

Fig. 3. Dependence of the mass-transfer coefficient K_o, the shape factor of the droplet E, and the mass-transfer factor K_m on $\bar{d}_D$: 1, 2) change in K_o for a packed pulse column with Raschig ring [6] and a single droplet moving in a space in the column, respectively; 3, 4) change in E ($E = a_D/b_D$) and K_m in a pulse column with KRIMZ packing, respectively.

For packings that are wetted by the dispersed phase, the nature of the motion of the breakup of the dispersed phase are rather different. The dispersed phase moves over the rings as a film; droplets are formed only in the spaces in the rings or in gaps in the packing. At low intensities, breakup occurs when the dispersed phase flow off the rings, and at high intensities in the flow. In the latter case, the droplet size can obviously be described by:

$$\bar{d}_D/d_p = C_6 \mathrm{We}_I^{-0,6} [\varepsilon_p^2/(1-\varepsilon_p)]^{0,4} (d_{\mathrm{eqv.P}}/d_p)^{0,4}, \quad (15)$$

or

$$\bar{d}_D/d_p = C_6 \mathrm{We}_I^{-0.33} \mathrm{Re}_I^{-0,33} [\varepsilon_p^2/(1-\varepsilon_p)]^{0,33} \times (d_{\mathrm{eqv.P}}/d_p)^{0\,33}. \quad (16)$$

Thus, to calculate $\bar{d}_D$ we have:

for sieve-plate pulse columns

$$\bar{d}_D \sim (\sigma/\rho_c)^{0.33-0,6} \mu_c^{0.33} (fa)^{-(1,0-1.2)}; \quad (17)$$

for packed pulse columns

$$\bar{d}_D \sim (\sigma/\rho_c)^{0,33-0,6} \mu_c^{0-0,5} (fa)^{-(1,0-1,43)}. \quad (18)$$

Table 2 summarizes the experimental relations (from published data) used to calculate the droplet diameter in pulse columns. The theoretical expressions for d_D [Eq. (17) and (18)] derived from analysis of the mechanism of breakup plainly give adequately reliable agreement with the experimental relations.

Reciprocating vibration of the reagent (pulsation) is known [12] to increase the operating efficiency of a column extractor by a factor of 5-10 (Fig. 2). Information regarding the mechanism of intensification of the process in pulse extractors is conflicting. This we attribute to the increase in the mass-transfer coefficient when the surface of the droplet becomes turbulent [13-16] or to increase in the interfacial area [12, 17]. Analysis of the mass-transfer process in pulse columns requires information regarding the breakup (shape and size of droplets), the distribution and structure of the flows in the equipment (uniformity of phase distribution, longitudinal mixing), and the efficiency. This requirement has not in general been met in previous studies.

We have examined this problem in an analysis of the hydrodynamic and technological parameters of a model pulse column with KRIMZ packing using the system TBP in kerosene + 30-35 g/liter U + 0.1 M HNO_3, characterized by $\alpha_m n \approx 1$.

We used our experimental results on the longitudinal mixing and the efficiency to calculate the HTU due only to mass transfer (HTU_m) for different pulsation regimes:

$$\mathrm{HTU_m} = \mathrm{HTU}_l - \mathrm{HTU_{add}} \quad (19)$$

where

$$\mathrm{HTU_{add}} = \lambda (D_c/W_c^* + D_d/W_d^*). \quad (20)$$

For this system with $\alpha_m n \approx 1$, we assumed $\lambda = 1$. We calculated W* from

$$W_c^* = W_c/(1-\Omega); \; W_d^* = W_d/\Omega. \quad (21)$$

Then data on the size and shape of the droplets and the holdup of the dispersed phase gave the mass-transfer factor, $K_m = K_e/K_s$ [17, 18]:

$$K_m = (\mathrm{HTU\,m}/\mathrm{HTU_{mI}})(S_0/S_I) = K_e/K_s. \quad (22)$$

The results of our analysis appear in Table 3, while the effect of droplet size (pulse intensity) on K_m is shown in Fig. 3.

Table 3 shows that the mass-transfer coefficient diminishes with increased pulse intensity, i.e., intensification of the process in pulse extraction columns is due only to increase in the interfacial area.

The intensification coefficient is $(0.45-0.5)K_0$, which indicates substantial reduction in the mass transfer coefficient during pulsation (Fig. 3, curves 1 and 4). This change in the mass-transfer coefficient arises from change in the shape of the droplet (curves 3 and 4

in Fig. 3). Indeed when the pulse intensity is increased the droplet size is reduced; the droplet becomes spherical. In large nonspherical droplets when $d_D > d_{D.sphr}$

$$d_{D.sphr} \leqslant (\sigma/\Delta\rho g)^{0.5}. \quad (23)$$

The extractable substance circulates internally; this is responsible for the high values of K (curve 2 in Fig. 2). The substance penetrates into the centers of the spherical droplet only as the result of molecular diffusion. The reciprocating vibration of the continuous phase promotes diffusion of the substance (turbulent diffusion, but does not affect diffusion in spherical droplets, in which only circulation of the substance in the boundary layer occurs.

NOTATION

HTU_l, height of transfer unit, derived with the laboratory column, cm; $HTU_{m,add}$, height of transfer unit due to mass transfer; additional component resulting from longitudinal mixing, cm; a, pulse amplitude, width of hole in KRIMZ packing, cm; a_D, b_D, major and minor axes of nonspherical droplet, cm; D, coefficient of longtidinal mixing, cm^2/sec; D_p, plate diameter, cm; d_D, droplet diameter, cm; $\bar{d}_D$, mean hydraulic diameter of droplet, cm; d_P, diameter of packing (Raschig ring), cm; d_o, diameter of hole in plate, cm; $d_{eqv.P}$, equivalent diameter of channel in packing, cm; $d_{D.sphr}$, diameter of the droplet at which it assumes spherical form, cm; E_D, energy required for breakup of droplet, erg; F, relative open area of plate, %; f, pulse frequency, sec^{-1}; H_D, column height, m; h_p, plate separation, cm; h_e, height of emulsion layer at the interface, cm; I, pulse intensity, cm/sec; I_{ef}, effective pulse intensity, cm/sec; K, mass-transfer coefficient; N_{hol}, number of holes in the packing; K_{es}, coefficient characterizing the effect of pulsation on the efficiency and interfacial area, respectively; n, ratio of flow rates; S, interfacial area, m^2/m^3; v_o, flow rate of the droplet, cm/sec; v_p, rate of coalescence of droplets at the interface, cm/sec; W, unit load, $m^3/m^2 \cdot h$; α, angle of inclination of vanes; α_m, distribution coefficient; ΔU, difference between flow rates in a section of length d_D, cm/sec; ε, energy dispersed by vortexes in unit volume of continuous phase (dissipation energy), erg/cm^3; ε_p, free volume of packing, m^3/m; μ, viscosity cP; ν, kinematic viscosity; ρ, density, g/cm; $\Delta\rho$, difference in densities of the phases, g/cm^3; σ, interfacial surface tension, dyn/cm; Ω, holdup of dispersed phase, %; $We_I = \rho_c I^2 d_o/\sigma$, Weber number; $Re_I = I d_o \rho_c/\mu_c$, Reynolds number.

INDICES

c, d, continuous and dispersed phases; I, 0, value of the parameter in the presence or absence of pulsation.

LITERATURE CITED

1. S. M. Karpacheva and E. I. Zakharov, in: Development and Use of Pulse Equipment [in Russian], Atomizdat, Moscow (1973), p. 131.
2. E. I. Zakharov and S. M. Karpacheva, Tsvetn. Met. No. 2, 53 (1973).
3. A. N. Kolmogorov, Dokl. Akad. Nauk SSSR, 32, No. 1, 19 (1941).
4. A. Fischer, Chem. Rundschau, 26, No. 19, 1 (1973).
5. J. Thornton, L. Smith, and H. Pratt, Trans. Inst. Chem. Eng., 35, No. 4, 292 (1957).
6. V. G. Levin, Physicochemical Hydrodynamics [in Russian], Fizmatgiz, Moscow (1959), p. 453.
7. S. Z. Kagan and Yu. N. Kovalev, in: Liquid Extraction and Chemisorption Processes [in Russian], Khimiya, Leningrad (1966), p. 43.
8. W. Widmer, Chem.-Ingr.-Tech., 39, No. 15, 900 (1967).
9. S. M. Karpacheva, E. I. Zakharov, and L. F. Kiseleva, Zh. Prikl. Khim., 37, 2668 (1964).
10. T. Misek, Coll. Czech. Chem. Commun., 29, No. 8, 1755 (1964).
11. T. Maychi and H. Oya, AIChE J., 11, No. 3, 395 (1965).
12. S. M. Karpacheva et al., Pulse Extractors [in Russian], Atomizdat, Moscow (1964), pp. 129, 144.
13. S. M. Golovko, V. N. Zadorskii, and N. V. Vasin, Izv. Vyssh. Uchebn. Zaved., Khim. Khim. Tekhnol., 15, No. 11, 1737 (1972).
14. A. S. Zheleznyak and B. I. Brounshtein, in: Liquid Extraction and Chemisorption Processes [in Russian], Khimiya, Leningrad (1966), p. 175.
15. A. P. Perovskii and V. G. Kosykh, in: Processes in Chemical Technology [in Russian], Nauka, Moscow–Leningrad (1965), p. 213.
16. A. D. Vasenev, A. F. Galeev, and A. I. Tur'yanov, in: Liquid Extraction [in Russian], Khimiya, Leningrad (1969), p. 181.

17. A. M. Rozen, Nauchn. Dokl. Vyssh. Shkol., Energetika, No. 3, 173 (1958).
18. A. M. Rozen, et al., in: Extraction [in Russian], Vol. 2, Gosatomizdat, Moscow (1962), p. 320.

INVESTIGATION OF THE ADIABATIC EXPANSION OF WATER VAPOR FROM THE SATURATION LINE IN LAVAL NOZZLES

É. K. Karasev, V. V. Vazinger,
G. S. Mingaleeva, and E. I. Trubkin

UDC 621.694

The effectiveness of the operation of a jet thermal pump [1] depends on the perfection of its basic subassemblies, one of which is the nozzle for the expansion of water vapor from the saturation line into the two-phase region. As the investigations of [2] show, when thermal differentials of more than 4 kJ/kg are acting in nozzles, i.e., when a velocity of more than 70-80 m/sec is reached, the greatest acceleration of a flow is possible in Laval nozzles. The absence of systematic data on the operation of Laval nozzles for saturated waver vapor with a pressure of more than 30 bars at the entrance has led to the present investigations. The results of this research can also be employed in the design of equipment to limit the flow in the case of a rupture of the pipes, for motors operating with a two-phase medium, and also in other areas associated with the flow of a two-phase flow at high velocities and pressure gradients.

Preliminary investigations have shown that the effectiveness of nozzles operating with a two-phase mixture is greater for those which have a more elongated shape than for nozzles intended for the expansion of steam. Fundamental investigations have been conducted on nozzles with the dimensions and shape given in Fig. 1. The effect of geometrical parameters (the length of the nozzle entrance, the degree of expansion, and the expansion angle of the expanding part of the nozzle) and the initial and exit pressures on the value of the critical flow rate of boiling water and the pressure distribution along the length of the nozzle (see Table 1) has been studied.

The characteristic picture of the pressure distribution along nozzle 1 for different back pressures is presented in Fig. 2. When the back pressure is higher than the calculated value in the expanding part of the nozzle (as in single-phase Laval nozzles) a discontinuity is established which travels to meet the flow as the back pressure increases. The flow rate of the saturated water vapor remains constant and does not depend on the back pressure until the pressure discontinuity enters the throat of the nozzle.

The pressure variation along the nozzle length (Fig. 3) depends on the initial pressure. Thus as the initial pressure at the end of the cylindrical section of the nozzle entrance decreases, a weak-gradient flow appears, which indicates completion of the phase transition processes, offering the possibility of decreasing the length of the nozzle entrance.

A simultaneous measurement of the pressure and temperature on the nozzle wall (Fig. 4) ascertained a thermodynamic nonuniformity in the initial section. This nonuniformity reaches ~20°C in nozzle 1 with a comparatively short entrance length.

The initial state of the flow has a significant effect on the velocity coefficient of the nozzle φ_n. If $\varphi_n = 0.75$ for a flow expanding from the saturation line or with underheating, then this same nozzle operates with $\varphi_n = 0.9$-0.95 after its initial throttling by 1-2 bar, which indicates the role of the vaporization nuclei in the thermodynamic completion of the process. The actual flow rate exceeds that calculated for an equilibrium expansion. A throttle grid in front of the nozzle decreases the critical flow rate and approximates it to the equilibrium value. The critical flow rate for a given nozzle depends only on the

Translated from Atomnaya Énergiya, Vol. 42, No. 6, pp. 478-481, June, 1977. Original article submitted May 31, 1976.

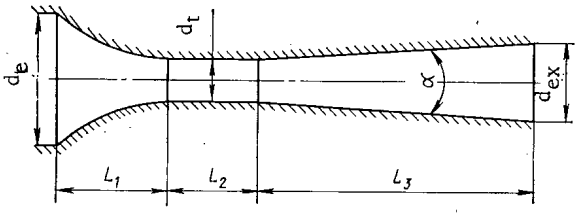

Fig. 1. Geometrical characteristics of nozzles.

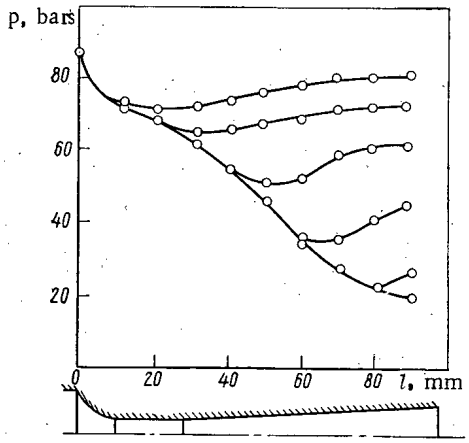

Fig. 2. Pressure distribution along nozzle 1 for different back pressures.

TABLE 1. Geometry of Investigated Nozzles

Nozzle No.	d_e^*	d_t	d_{ex}	L_1	L_2	L_3	α, degrees
1	23	3,84	7,5	10	18	69	3
2	80	19	28	114	65	172	3
3	80	19	28	114	120	86	6
4	80	19	30	114	87	210	3

*The linear dimensions are given in mm.

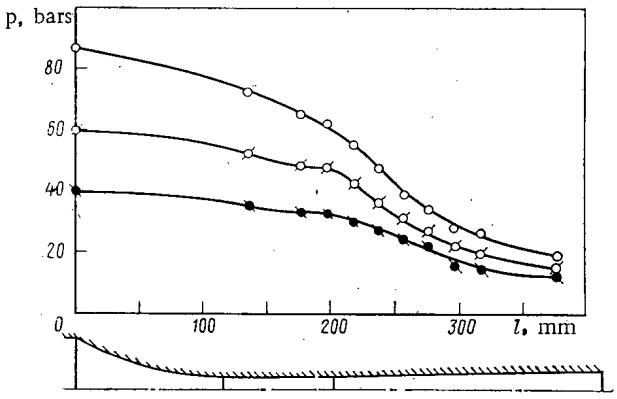

Fig. 3. Pressure distribution along nozzle 4 under calculated flow conditions for different initial pressures (the dots correspond to experimental measurements).

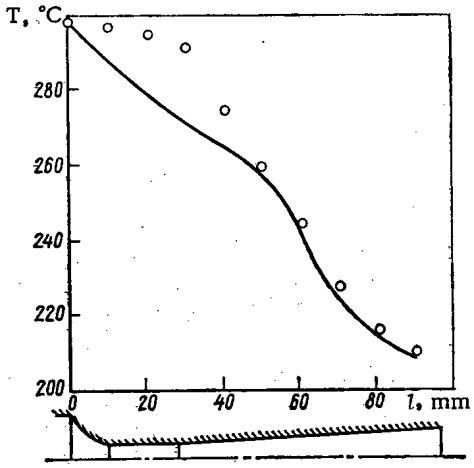

Fig. 4. Temperature distribution of the flow in nozzle 1 under the calculated flow conditions: o) measured wall temperature; ——) saturation temperature.

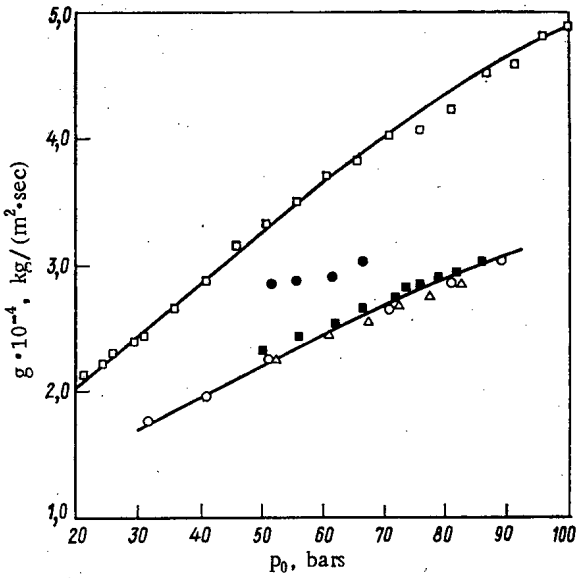

Fig. 5. Flow-rate characteristics of the investigated nozzles: □, ●) nozzles 1 and 2; ■, ▲, and o) nozzles 2, 3, and 4 (a throttle grid is mounted in front of them).

initial conditions in front of the nozzle. The flow-rate characteristics of nozzles are presented in Fig. 5.

The information about the effect of the nozzle entrance diameter on the flow-rate characteristics is often contradictory. For example, it is shown in [3] that the specific flow rate in the case of the discharge of saturated water vapor through cylindrical channels with sharp entrance edges is lowered as the diameter increases from 3 to 6 mm, but no diameter effect is detected in [4] for channels 4-8 mm in diameter with a smooth entrance. In addition, a significant effect of the relative channel length has been emphasized in [3]. In our opinion (Fig. 6) the absolute length of the channel, which determines the thermodynamic nonuniformity of the flow at the end of a cylindrical channel or nozzle, has the main effect on the specific critical flow rate in channels with a round entrance, since the effect of l/d as the hydraulic friction factor is less significant here. No effect of the degree of expansion on the flow-rate characteristic of the nozzle has been established in the case of

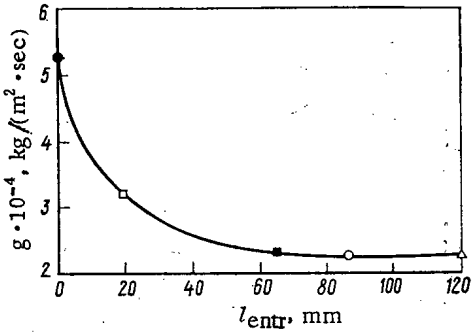

Fig. 6. Dependence of the critical flow rate of saturated vapor on the nozzle entrance length: ●) based on the data of [4]; □, ■, △, and ○) nozzles 1, 2, 3, and 4, respectively.

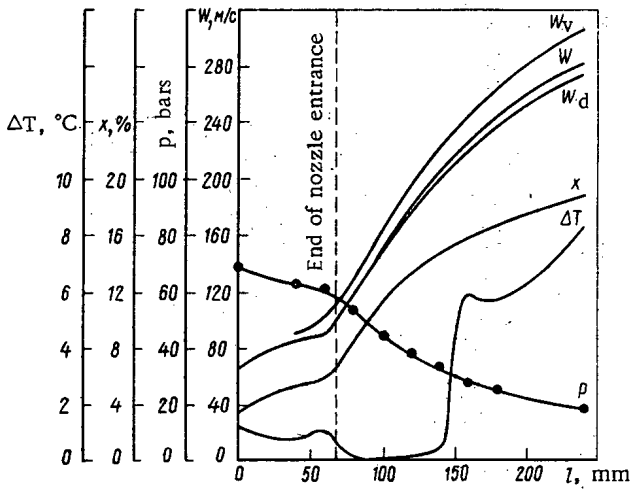

Fig. 7. Variation of the flow parameters calculated for the limiting models.

small expansion angles (within the limits of 3 and 6°).

The size of the pressure head developed by the thermal pump was an indirect estimate of the effectiveness of nozzle operation. Other conditions being the same, the pressure head of the thermal pump was greater for a nozzle with an expansion angle of 3° than for one with an expansion angle of 6°.

The results were elaborated for two simplified models. The first one is based on the following assumptions: the velocities of the phases are equal, the steam is equilibrium, and the water is nonequilibrium; the second one is based on the following assumptions: the temperatures of the steam and the water, which correspond to the saturation temperature at a given pressure, are identical, but the velocities of the two phases may be different. It was assumed in both cases that the flow is one-dimensional and the pressure distribution, temperature, and velocity in each cross section are two-dimensional, and the two-phase medium was arbitrarily treated as continuous. With these assumptions, the three conversion equations permit calculating all the basic parameters in each cross section along the nozzle length:

$$A/Q = [(1-x)\,v_d]/w_d + xv''/w_v;$$
$$i_o = (1-x)\,(i_d + w_d^2/2) + x\,(i'' + w_v^2/2);$$
$$I_1 = Q_d W_d + Q_v W_v + pA + F_{fr} + F_w,$$

where $F_{fr} = \lambda l/d\,(w_i^2/2dv)\,A$; $F_w = (p_i + p_{i+1})/2A$.

The momentum in the first cross section of the nozzle entrance ($I_1 = Qw_1 + p_1A_1$) was determined from the assumption that the expansion process up to the first cross section occurs with $\varphi_n = 0.96$ (found from experiment with a nonboiling flow). Therefore, it follows from the continuity and energy equations that

$$Q = \varphi_n w_{1s} A / [(1-x) v_d + x v''];$$
$$i_0 = (1-x) i_d + x i'' + \varphi_n^2 w_{1s}^2 / 2$$

where $i_d = i'(T_d) + c_s'(T_v - T_d)$; $v_v \approx v'$; $w_1 = \varphi_n w_{1s}$.

Choosing T_d, we find w_{1s} and x for the given i_0, Q, and s_{01}.

The results of a calculation of the velocity, vapor content, and superheating along the nozzle on the basis of an experimental determination of the pressure, which refer to nozzle 2 with an initial saturated vapor pressure of 80 bar, are presented in Fig. 7. The first pressure sampling is taken as the origin of coordinates. The velocity increases to 280 m/sec and the vapor content to 0.187 in the case of the expansion of boiling water in a nozzle from 80 to 18.5 bar. The maximum possible superheating of the liquid phase reaches 9.4°C, and the maximum possible ratio of the velocities of the two-phases ($m = w_v/w_d$) is nearly constant along the length and is equal to 1.12. Calculations carried out in a similar fashion in the initial pressure range from 30 to 100 bars show that the maximum possible value of this velocity ratio varies from 1.08 to 1.15 and the maximum possible superheating of the liquid phase at the end of the nozzle increases from 2 to 12°C as the initial pressure increases, while the coefficient φ_n is within the limits 0.92-96. Comparison of the velocity at the end of the nozzle entrance with the calculated speed of sound based on the equations of [5-7] has shown good agreement within 10% limits with the recommendations of [5], which have been obtained for an equilibrium homogeneous two-phase medium. The flow velocity in the expanding part of the nozzle is greater than the speed of sound, and it is ≈ 1.3 times greater at the nozzle cutoff than the local speed of sound calculated from the formula of [5].

It is possible on the basis of the investigations performed to offer the following recommendations on the design of effective nozzles for the expansion of water vapor from the saturation line: nozzles should have an elongated entrance but no longer than 100 mm; it is desirable to produce vapor formation nuclei in front of the nozzle in the form of fine vapor bubbles; the expansion angle of the expanding part should be no greater than 3°.

CONVENTIONAL NOTATION

Q, mass flow rate, kg/sec; q, specific flow rate, kg/(m²·sec); A, area of the straight-through cross section, m²; p, pressure, N/m²; w, velocity, m/sec; x, mass vapor content; i, specific enthalpy, J/kg; s, specific entropy, J/(kg·deg K); v, specific volume, m³/kg; c_p, specific heat of water vapor on the saturation line at constant pressure, J/(kg·deg K); F, force, N; F_w, reaction of the wall, N; I, momentum, N.

SUBSCRIPTS

0, initial state; 01, at the nozzle entrance; 1, at the first pressure sampling; d, v, drip and vapor media; thr, throttling; fr, friction; s, isoentropic flow (process).

LITERATURE CITED

1. É. K. Karasev, in: Problems of Atomic Science and Engineering. Reactor Construction Series. No. 2, Izd. TsNIIatominform, Moscow (1973), p. 3.
2. Boiling Adiabatic Flows [in Russian], Atomizdat, Moscow (1976).
3. V. D. Keller, V. K. Mal'tsev, and D. A. Khlestkin, in: Digest of Lectures at the Fifth All-Union Conference on Heat Exchange and Hydraulic Drag upon the Motion of a Two-Phase Flow in the Units of Energy Machines and Apparatus [in Russian], Leningrad (1974), p. 235.
4. K. S. Polyakov, in: Transactions of the LPI. Turbomachine Series, No. 247, Mashinostroenie, Moscow–Leningrad (1965), p. 16.
5. V. V. Sychev, Inz.-Fiz. Zh., No. 6, 64 (1961).
6. V. V. Dvornichenko, Teploenergetika, No. 10, 72 (1966).
7. M. E. Deich and G. A. Filippov, Gasdynamics of Two-Phase Media [in Russian], Energiya, Moscow (1968).

THE ORIGIN OF THE TRACKS OF FISSION FRAGMENTS IN WHITLOCKITE FROM THE BJURBÖLE METEORITE

V. P. Perelygin, S. G. Stetsenko,
and N. Bhandari*

UDC 523.165

Searches for the tracks of far transuranic elements in minerals from meteorites and from the surface of the moon can be carried out in two different ways. First of all, there are the searches and the identification of tracks from the stopping of heavy nuclei of the primary cosmic radiation in the region $Z \geq 90$ up to $Z = 110$-114 [1-3]. Such nuclei produce, during their retardation prior to stopping, extended zones of defects in crystals whose length is proportional to their atomic number [2, 3]. However, due to the fact that heavy and superheavy nuclei have relatively short ranges in the material of meteorites [3, 4] and a relatively high probability of nuclear interaction with decelerating medium [5], it is necessary for the conduct of such searches to expose sections situated near the preatmospheric surface of the meteorites at a depth of greater than 5-8 cm [3]. The trend in searches is the detection and identification of the tracks of fragments from the spontaneous fission of heavy transuranic elements synthesized about 4.6 billion years ago during the formation of the solar system [6, 7].

The conditions of outer space have facilitated the preservation of the tracks of spontaneous fission of nuclei in minerals from the time of the cooling of the parent bodies of the meteorites, i.e., for 4-4.5 billion years [6, 7]. Thus, the minerals from meteorites are more suitable objects for the search for the effects of spontaneous fission of relatively short-lived transuranic nuclides than are crystals and glasses of terrestrial origin, whose track age does not exceed 2 billion years [8, 9].

This article was undertaken in connection with investigations [10] on a search for far transuranic elements in samples of terrestrial minerals, ores, rocks, and also in meteorite samples.

The Bjurböle meteorite belongs to the stony meteorite group — the L-chondrites of petrological type IV with spherical olivine-hypersthene chondrules. Its fall occurred in the spring of 1899 in Finland. The mass of the Bjurböle meteorite was about 330 kg [11], and during its fall it broke up into a large number of fragments. The age of this meteorite (8-11 million years) was determined from cosmogenic isotopes in 1960 by Eberhardt and Hess [12].

As follows from the analysis of the preatmospheric masses of the St. Séverin, Keyes, Allegan, and Přibram stony meteorites [13, 14, 15] carried out by the method of dielectric track detectors, the losses of material upon passage through the terrestrial atmosphere amount to from 20 to 70%. The data of Lavrukhina et al. [16] for the Přibram chondrite show that the degree of ablation can exceed 99%.

Taking account of the effects of ablation and crushing during passage through the dense layers of the atmosphere, it is possible to conclude that it is extremely difficult to detect in stony meteorites surface sections which have a track density for nuclei of the iron group of more than 10^6 per 1 cm^2. It has been shown in [17] that the most suitable indicator of the depth of location of samples away from the preatmospheric surface is olivine. Actually, since the uranium content in olivine does not usually exceed 10^{-10}-10^{-11} g/g, it contains practically no background of tracks from spontaneous fission. This permits one to determine

*Laboratory of Physical Research, Ahmedabad, India.

Translated form Atomnaya Energiya, Vol. 42, No. 6, pp. 482-485, June, 1977. Original article submitted August 2, 1976.

with a high degree of reliability the contribution produced by fast cosmic nuclei to the track density in the crystals of feldspars, pyroxenes, phosphates and so on which are adjacent to the olivine.

Samples of the Bjurböle meteorite with a total mass of 15 g selected from one spot were ground into a powder with particle size less than 1 mm. Transparent homogeneous crystals were sorted out from the powder under a stereomicroscope at a magnification of 20-25×. In all, about 200 transparent crystals from 100 to 600 microns in size were selected, which were mounted in an epoxy resin and polished.

Since olivine is one of the principal components making up the composition of the chondrules of this meteorite, the etching of the mounted samples was carried out in a special solution suggested in 1971 by Krishnaswami et al. [18] for revealing tracks in olivine. The crystals along with the etchant were enclosed in a hermetic Teflon container which excluded the possibility of variation of the composition of the solution during the chemical processing. The temperature of the etching solution was 110°C, and the etching time was 6-8 h. The developed samples were examined under the microscope at a magnification of $\approx 1400\times$. It did not prove possible to detect in the olivine crystals tracks from heavy cosmic nuclei or fission fragments. Only the defects of the structure of the olivine were revealed — capillary inclusions, dislocations, and microcracks. The upper limit to the track density of heavy charged particles in the olivine was $\leqslant 5 \cdot 10^3/cm^2$. It is possible to conclude on the basis of the known cosmic age of the Bjurböle meteorite and the limit obtained on the track density that the depth of location of the investigated sample was $\leqslant 20$-25 cm from the preatmospheric surface of this meteorite [4].

However, four transparent crystals containing $(2\text{-}5)\cdot 10^7$ tracks/cm^2 of surface were detected among the samples. The tracks in these crystals represent hollow cylindrical holes with plane-parallel walls. Due to the exceptionally high rate of etching along a track v_{etch} in the volume of the crystal on tracks which start from the surface, small chains of secondary tracks (TINT) were revealed [4]. It is known that the etchant suggested in [18] reveals the tracks of heavy charged particles also in minerals of the phosphate type [6].

The identification of crystals and the measurement of the content of their main components were performed on a JKhA-50 electron beam microanalyzer. It was established that calcium and phosphorus constitute the base of these crystals; an admixture of magnesium (about 5%) was also noted. The analysis permitted concluding that crystals of whitlockite, $Ca_3(PO_4)_2$, which are distinguished by a relatively high magnesium content, are being observed. The high track density on the surface of the whitlockite hindered the scanning. Therefore, an upper layer of the crystals 15-20 μ in thickness was removed for the measurement of the spectra of the track lengths. The tracks were measured at a magnification of $\approx 2200\times$. We determined the length and depth of the track contained in the volume of the crystal. The length distribution of the measured tracks is given in Fig. 1. It is evident that there is a single group of tracks in the spectrum of length having an average length of 16.7 ± 0.8 μ. The length distribution in Fig. 1 has a shape similar to the spectrum of the lengths of fission fragments in augite from the Angra dos Reis meteorite [19]. This result, in combination with the absence of an observable track density in olivine from the same spot in the Bjurböle meteorite, permits us to conclude that the tracks detected in the whitlockite are produced by the spontaneous fission of uranium and of heavier transuranic elements.

The uranium content in the whitlockite crystals was measured. For this purpose, the crystals were placed into close contact with a film of polyterephthalate (Lavsan) and irradiated by a 10^{16} neutrons/cm^2 beam of thermal neutrons. This layer of natural uranium (0.1 μg/cm^2), applied by the method of cathode spraying onto a nickel boat and placed in contact with the Lavsan detector, served as the neutron flux indicator. The uranium content in these crystals amounts to $(0.2\text{-}0.4)\cdot 10^{-6}$ g/g. Thus, spontaneous fission of the uranium could produce no more than 5-10% of the measured track density. It is evident that the main part of the effect is caused by the spontaneous fission of transuranic elements. Four developed crystals were scanned for the determination of an upper limit to the probability of ternary fission of the transuranic nuclei contained in the whitlockite. A search was made for three-pronged events with tracks longer than 2 μ and interangular spacings of $95° \leqslant \varphi \leqslant 170°$, and a count was also made of two-pronged events (individual straight tracks longer than 12 μ). Not one event of fission into three fragments of comparable mass was discovered in 3700 tracks of fission into two fragments. Thus, the upper limit to the probability of ternary fission with respect to binary fission is $P_{3f}/P_{2f} \leqslant 2.7\cdot 10^{-4}$.

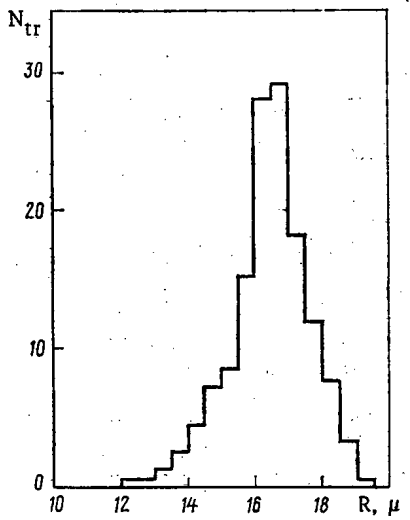

Fig. 1. Length distribution of the tracks of spontaneous fission fragments in whitlockite from the Bjurböle meteorite.

Let us discuss in greater detail the question of the origin of the tracks of fission fragments in the phosphates from the Bjurböle meteorite. A high density of tracks of spontaneous fission fragments which cannot be explained by the spontaneous fission of ^{238}U has been detected in the whitlockite from this meteorite, as in a number of other minerals from meteorites and from the surface of the moon [19-21]. The majority of authors attribute this effect to the spontaneous fission of the most stable known transuranic nucleus, ^{244}Pu, which has a half life of $8.2 \cdot 10^7$ years [22]. However, there are other hypotheses which explain the origin of such tracks. Thus Rao and Gopalan [23] advance the suggestion, based on anomalies in the relative concentration of the heavy isotopes of xenon, that the spontaneous fission of ^{248}Cm makes an appreciable contribution to the observed track density in some samples.

The question of another possible source of the observed effect — the spontaneous fission of a relatively stable transuranic element in the region of Z around 114 (or 126) with a closed neutron shell (N = 186) — has been discussed in detail in a paper of Price and Fleischer [22]. It should be noted that an anomalously high concentration of the heavy isotope ^{136}Xe has been observed in a number of meteorites, e.g., in carbonaceous chondrites. As has been shown in the paper of Anders and Heymann [24] and also Dakowski [25], this anomaly may be caused by the spontaneous fission of nuclei of superheavy elements. However, the analysis of the content of anomalous xenon is usually carried out for the entire meteorite and for the most representative fractions. Such an analysis is often extremely difficult in crystals of phosphates, pyroxenes, and feldspars due to the relatively small amount of these minerals in meteorites.

Therefore, each sample with an excess track density of fission fragments should be analyzed in detail for the origin of these tracks. It has been suggested in [22, 26] that such an analysis should be based on the difference in the ranges of the fission fragments of uranium and plutonium and element 114. This difference should amount to 15-20% in the opinion of the authors of [22]. In addition, it was suggested that the probability of spontaneous fission of a nucleus with Z around 114 into three fragments of comparable mass should be significantly higher than that of the nuclei ^{238}U and ^{252}Cf, for which this probability amounts to about 10^{-6} with respect to binary fission. However, a more detailed comparison carried out in [27] of the track lengths of fragments from the spontaneous fission of ^{244}Cm and composite nuclei with Z = 110 and 112 formed upon the interaction of ^{40}Ar and ^{40}Ca ions with ^{238}U has permitted concluding that the average track lengths of fission fragments of nuclei with Z = 92-96 and Z = 110-112 practically coincide. Actually, the kinetic energies of the spontaneous fission fragments of these two groups of nuclei (MeV/nucleon) agree within 5-10% limits. According to the range—energy relations presented in Northcliffe and Shilling [28], fission fragments of the uranium—plutonium group and the hypothetical superheavy elements having identical energies should have one and the same range in matter.

It is necessary to take into account in a discussion of the question of the probability ratio of ternary fission of far transuranic elements of the fact that this probability falls off rapidly with an increase in the energy of the composite nucleus. As the energy of the bombarding particles decreases from 300 to 230 MeV (the reaction is $^{238}U + ^{40}Ar$), the ratio of the probability of ternary fission to binary fission decreases by a factor of 10 [29]. The simple extrapolation carried out in [27] shows that the probability $P_{3f}/P_{2f} \leq 10^{-4}$ for nuclei with Z = 110-114 which are in the ground state. Thus, both arguments cited in [22] fail to find sufficient experimental foundation, at least for the region Z = 110-114, and the question of the origin of the tracks of spontaneous fission in the minerals from meteorites requires further study. One should note one more possibility for the identification of the tracks of fission fragments which recently appeared in connection with investigations on the annealing of the trails of ions of krypton and xenon in crystals [30]. As has been shown in [3, 30], a selective annealing process takes place in crystals with a relatively high threshold for the appearance of tracks (olivine, diopside, and others), which results in the practically complete elimination of the tracks of krypton ions, while the low-energy part of a xenon track is shortened by 1.5-2 μ in all. This procedure can be applied to crystals containing tracks from the spontaneous fission of transuranic elements. In this case it will be possible, in principle, to distinguish in the spectrum of the track lengths two groups of tracks, which correspond to the fission of nuclei of the uranium–plutonium group (a reduction of the average track lengths by a factor of 2-3) and of the hypothetical transuranic elements (a reduction in length by 20-30%). The procedure requires detailed investigations of the process of the regression of tracks from the ions of krypton and xenon and of the fission fragments of ^{235}U by thermal neutrons. In particular, it is necessary first of all to isolate for the Bjurböle meteorite at least 10-12 whitlockite crystals larger than 100 μ. This procedure can be carried out with samples of minerals from the St. Séverin, Angra dos Reis, Toluca, Odessa, and El Taco meteorites, in which a large excess density of the tracks of spontaneous fission fragments with an age up to 4.5 billion years has been found.

In conclusion, the authors express their deep gratitude to G. N. Flerov for constant attention to the research and useful advice, and also to Kh. B. Viik for representative samples of the Bjurböle meteorite and to V. K. Garanin and T. P. Kudryavtseva for the mineral analyses which they performed.

LITERATURE CITED

1. M. Maurett et al., Meteorite Res., 12, 286 (1968).
2. P. Price, R. Rajan, and E. Shirk, Geochim. Cosmochim. Acta, Suppl., 3, 2625 (1971).
3. O. Otgonsurén and V. P. Perelygin, Communication of the JINR, P7-7406, Dubna (1973); At. Energ., 37, No. 2, 164 (1974).
4. D. Lal, Space Sci. Rev., 14, 3 (1972).
5. R. Daniel and N. Durgaprasad, Nuovo Cimento, Suppl. Ser. 10, 23, 82 (1962).
6. R. Fleischer, P. Price, and R. Walker, Nuclear Tracks in Solids, Univ. of California Press, Berkley (1975).
7. R. Fleischer, P. Price, and R. Walker, Geochim. Cosmochim. Acta, 32, 21 (1968).
8. Kh. Abdullaev et al., Communication of JINR, P7-2961, Dubna (1966).
9. D. Miller, Earth Planetary Sci. Lett., 4, 379 (1968).
10. G. Flërov, in: Proceedings of the International Conference on Reaction between Complex Nuclei Paper N 23, June 10-14, 1974, Nashville, Oak Ridge National Laboratory.
11. M. Hey, Catalogue of Meteorites, London (1966), p. 57.
12. P. Eberhardt and D. Hess, Astrophysical J., 131, 38 (1960).
13. Y. Cantelaube and P. Pellas, in: Origin and Distribution of the Elements, L. Ahrens (editor), Pergamon Press, Oxford (1968), p. 479.
14. Y. Lorin and G. Poupeau, Meteoritics, 8, 410 (1973).
15. P. Pellas, A. Ducater, and Y. Berdot, Meteoritics, 8, 418 (1973).
16. A. Lavrukhina, A. Fisenko, and E. Kolesnikov, Bull. Astronom. Inst. Chechoslov, 25, No. 2, 122 (1974).
17. V. P. Perelygin, Kh. B. Viik, and O. Otgonsurén, Preprint of the JINR, P13-8359, Dubna (1974).
18. S. Krishnaswami et al., Science, 174, 287 (1971).
19. D. Lal, R. Rajan, and A. Tamhane, Nature, 221, 33 (1969).
20. Y. Cantelaube, M. Maurett, and P. Pellas, Radioactive Dating and Low Level Counting, IAEA, Vienna (1967), p. 213.
21. G. Crozaz et al., Geochim. Cosmochim. Acta, Suppl., 2, (1972).
22. P. Price and R. Fleischer, Phys. Lett., 30B, 246 (1969).
23. M. Rao and K. Gopalan, Nature, 245, 304 (1973).

24. E. Anders and D. Heymann, Science, 164, 281 (1969).
25. M. Dakowski, Earth Planetary Sci. Lett., 6, 152 (1969).
26. N. Bhandari et al., Nature, 230, 219 (1971).
27. O. Otgonsurén et al., At. Energ., 32, No. 4, 344 (1972).
28. L. Northcliffe and R. Shilling, Nuclear Data Tables, A7, 233 (1970).
29. V. Perelygin et al., Nucl. Phys., A127, 577 (1969).
30. G. N. Flërov, O. Otgonsurén, and V. P. Perelygin, Izv. Akad. Nauk SSSR, Ser. Fiz., 29, No. 2, 388 (1975).

SPUTTERING AND BLISTERING IN THE BOMBARDMENT OF INCONEL, SiC + C ALLOY, AND CARBON-PYROCERAMIC BY H^+ AND He^+ IONS

N. P. Busharov, V. M. Gusev,
M. I. Guseva, Yu. L. Krasulin,
Yu. V. Martynenko, S. V. Mirnov,
and I. A. Rozina

UDC 539.2:539.12.04

Austenite steels and chrome–nickel alloys, widely used in reactor construction [1], are being considered as possible construction material for the "first wall" of thermonuclear reactors (TNR) in conjunction with shields of a material with a low atomic number [2-4]. It is known that the radiation resistance of steel increases with an increase in the nickel content [1, 5]. The wall of the T-10 chamber is built of an alloy based on nickel: Inconel (Table 1).

The sputtering of different stainless steels by hydrogen and deuterium ions with energies up to several tens of kiloelectron volts has been studied [6, 7]. The law of the formation of blisters in 316 and 304 steels during bombardment by helium ions [8-14] and hydrogen ions [13] have been studied in adequate detail. Experiments on the sputtering of Inconel by mercury ions with energies of 50-500 eV showed [15] the closeness of the sputtering coefficients of this alloy and nickel.

One of the promising materials for the shield of a first wall is graphite [2-4], the use of which is confined to a certain temperature range because of chemical sputtering during bombardment by hydrogen ions [16, 17].

The results of a study of sputtering and blistering during the bombardment of Inconel, SiC + C alloy, and carbon-pyroceramic by H^+ and He^+ ions are presented in the present report.

Sputtering of Inconel. The experiments were conducted on an ILU-3 accelerator [18]. The sputtering coefficient was determined by the weight method with a sensitivity of 1 μg. The integral ion flux comprised from 10^{18} to 10^{20} cm^{-2}. The topography of the irradiated surfaces was studied in a "Stereoscan" scanning electron microscope with a resolution of 150 Å. Before irradiation the specimen surface was mechanically ground and electrochemically polished.

The results of the measurement of the coefficients of sputtering of Inconel by H^+ ions with energies of 10 and 17.5 keV and by He^+ ions with energies of 20 keV at a temperature of 500°C are presented in Fig. 1. In the same graph we present the dependences for H^+, D^+, and He^+ calculated with the help of Sigmund's theory [19] in accordance with the method proposed earlier [4] (the value of $S^{H^+} = 7.8 \cdot 10^{-3}$ atoms/ion measured with E = 10 keV was taken as the reference point). The disagreement between the calculated and experimental values of S^{H^+} and S^{He^+} [20] is 10-20%. All the curves of S = f(E) have a flat maximum in the energy region of 2-3 keV.

Translated from Atomnaya Énergiya, Vol. 42, No. 6, pp. 486-489, June, 1977. Original article submitted October 11, 1976.

TABLE 1. Composition of Inconel

Element	Content, mass %	Element	Content, mass %
Ni	74,69	Mn	0,03
Cr	20,18	C	0,01
Mo	2,25	Ce	0,01
Nb	1,19	Cu	0,01
Al	0,64	S	0,009
Ti	0,55	P	0,009
Si	0,13		

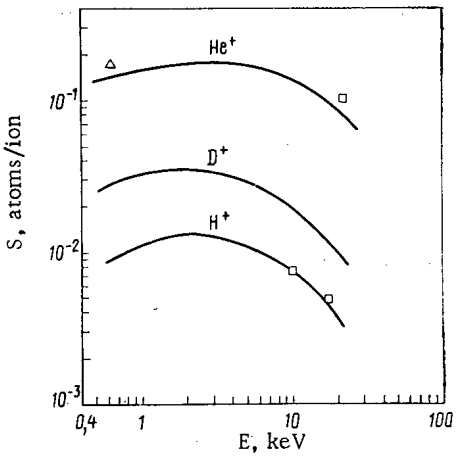

Fig. 1. Dependence of sputtering coefficients of Inconel on energy of H^+, D^+, and He^+ ions: ——) calculation [4, 19]; □) experiment; △) data of [20].

The coefficient of sputtering of Inconel by H^+ ions is ≈ 1.5 times higher than that of 304 steel [7].

To estimate the possible role of sputtering of the wall in experiments on Tokamaks we calculated the amount of heavy impurities of Ni and Cr which can enter the plasma of the T-10 installation in the process of the discharge (t = 0.5 sec) because of sputtering of the wall by fast neutral H^0 atoms.

On the basis of the calculated energy distribution of H^0 and the data of Fig. 1 one can estimate the average sputtering coefficient of the T-10 wall, which comprised 0.5-0.7 atoms/ion with variation of $T_i(0)$ from 500 to 1700 eV. With a flux of fast neutral atoms of $\sim 2 \cdot 10^{15}$ atoms/sec•cm^2 (which is close to the measured flux) heavy impurities in an amount corresponding to their average concentration of ∼0.5% could enter the plasma of the T-10 during the discharge, which would mean an increase in the effective charge Z_{ef} = 4-5 of the plasma for a uniform distribution of the impurities over the cross section.

The sputtering of the first wall in thermonuclear reactors can lead to more serious consequences.

Study of Blistering. The study of the formation of blisters after the implantation of He^+ ions with energies of 20 and 80 keV in the surface layer of Inconel was carried out at room temperature on targets annealed at a temperature of 900°C. The microstructure of an Inconel surface irradiated by He^+ ions with energies of 20 keV until an integral flux of 10^{18} cm^{-2} is reached is shown in Fig. 2a. The size distribution of blisters obtained from photomicrographs of Fig. 2a is given in Fig. 3. Dome-shaped blisters with a diameter from 0.5 to 1.2 μ were formed over the greater part of the irradiated surface (∼70%). The absence of broken blisters of peeling of the shell means that in the indicated mode of irradiation the blistering does not cause erosion of Inconel.

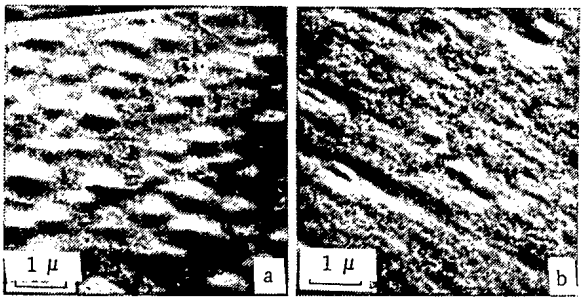

Fig. 2. Microstructure of Inconel surface after irradiation by He^+ ions with energies of 20 keV when D = 10^{18} (a) and 10^{19} cm^{-2} (b).

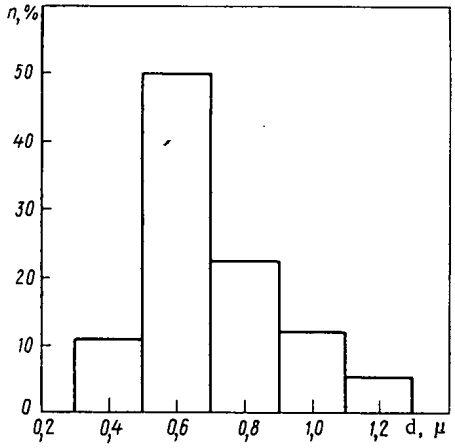

Fig. 3. Size distribution of blisters in Inconel irradiated by He^+ ions with energies of 20 keV when D = 10^{18} cm^{-2}.

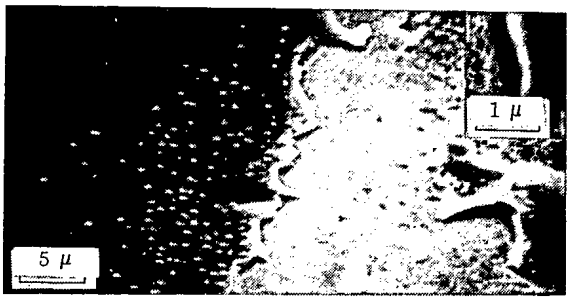

Fig. 4. Photomicrograph of Inconel surface after irradiation by He^+ ions with energies of 20 (left section) and 80 keV (right section) with D = 10^{18} cm^{-2}.

With an increase in the integral flux to 10^{19} cm^{-2}, other conditions being equal, the blisters completely disappear (see Fig. 2b). This effect is due to the sputtering of the blister shell in the process of bombardment of Inconel by He^+ ions. As the thickness of a blister dome decreases owing to the sputtering the energy of the helium ions penetrating into the target surface lying below it gradually changes. Thanks to this the distribution of implanted helium atoms in the surface region of the target coincides with the distribution of defects produced by them. In such a case the formation of gas bubbles proves to be hindered because of the immobilization of interstitial helium atoms at vacancies and because of the diffusion of helium through pores and cracks in the strongly disturbed surface layer of the target [20]. Since the coefficient of sputtering of Inconel by He^+ ions with energies

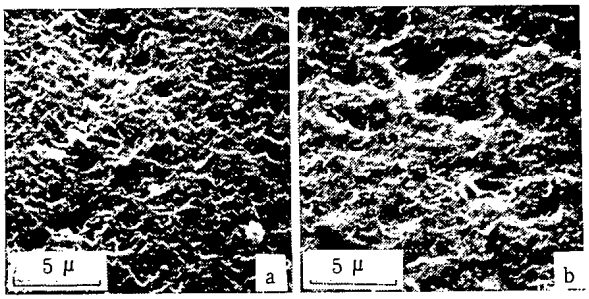

Fig. 5. Photomicrograph of surface of carbon-pyroceramic after irradiation at room temperature by He^+ ions with energies of 20 (a) and 80 keV (b) with D = 10^{18} cm^{-2}.

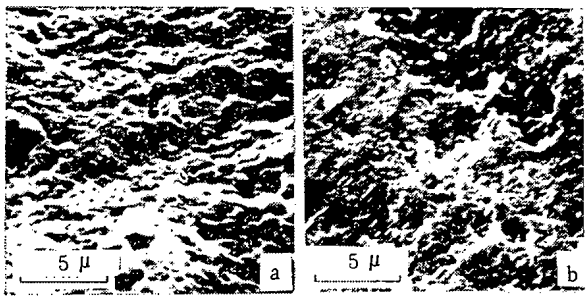

Fig. 6. Photomicrographs of surface of SiC + C after irradiation by He^+ and H^+ ions with D = 10^{19} and 10^{20} cm^{-2} and with energies of 20 (a) and 10 keV (b), respectively.

TABLE 2. Sputtering Coefficients

Target	Ion	E, keV	S, atoms/ion
SiC+C	H^+	10	$(3,7\pm0,5)\cdot10^{-3}$
	He^+	20	$(4,2\pm0,5)\cdot10^{-2}$
Carbon-pyroceramic	H^+	10	$(5\pm0,6)\cdot10^{-3}$
	He^+	20	$(9\pm1)\cdot10^{-2}$

of 20 keV equals 0.11 atoms/ion (see Fig. 1), the integral flux of 10^{19} cm^{-2} causes in sputtering of a layer of ∿1100 Å, which is ≈ 1.5 times greater than the range of He^+ ions with energies of 20 keV in Inconel (R ≈ 750 Å)[21]. With E = 20 keV the thickness of the blister shells is close to R [22]. The effect of the suppression of blistering was first observed [23] in the bombardment of niobium by He^+ ions with E ⩽ 15 keV as well as in the implantation of hydrogen ions with energies of 7.5 keV in 304 steel [20].

An entirely different pattern of Inconel erosion develops upon an increase in the energy of the He^+ ions to 80 keV. As seen from a comparison of the structures in Fig. 4, at this ion energy one observes the intensive peeling of the irradiated layer with a thickness of ∿2000 Å. The erosion rate of the Inconel estimated from the photomicrograph is ∿1 atom/ion.

Thus, with an He^+ ion energy of 80 keV the dominant process of Inconel erosion is blistering, whereas with E ⩽ 20 keV it is sputtering. The total coefficient of erosion of Inconel with an He^+ ion energy of 80 keV is 10 times higher than with E = 20 keV. This must be taken into account in the choice of a material for the first wall of a thermonuclear reactor which will be irradiated by He^+ ions with a wide energy spectrum.

New Materials. Relatively new materials have been discussed as possible construction materials for shields for the first wall: SiC + C alloy [24] and USB-15 carbon-pyroceramic. The sputtering coefficients of these materials were measured at a temperature of 600°C (Table 2). The coefficients of sputtering of SiC + C and carbon-pyroceramic by H^+ ions at 600°C are close in value and ≈ 20 times lower than the sputtering coefficients of graphite [16]. The results obtained indicate that physical rather than chemical sputtering is observed in the bombardment of SiC + C and carbon-pyroceramic by hydrogen ions. The absence of a chemical interaction of hydrogen ions with energies of 300-600 eV with the surface of SiC was noted earlier [17]. The measurement of the sputtering coefficients of these materials in a wide temperature range is of interest.

The values of S^{He^+} indicated in Table 2, determined from the mass loss of the targets, characterize the total coefficient of erosion owing to sputtering and blistering [7]. The coefficient of erosion of carbon-pyroceramic by He^+ ions with energies of 20 keV is approximately the same as that of ordinary graphite [25] and is about two times greater than that of SiC + C. It should be noted that the character of the structure of the carbon-pyroceramic surface irradiated by He^+ ions (Fig. 5) is both the same as that of graphite and is specific for the case of the destruction of a brittle material [25]. On the surface one can see a large number of cracks whose size increases with an increase in the energy of the bombarding ions (Fig. 6a and b). When E = 80 keV (see Fig. 6b) the separate cracks overlap, forming depressions with a length of up to 10-12 μ and a depth of up to 3 μ.

Figure 6 illustrates the microstructure of the surface of SiC + C after irradiation by an integral flux of 10^{19} cm^{-2} of He^+ ions with energies of 20 keV. As in the case of carbon-pyroceramic, one observes a large number of pits and cracks with a size of from 0.15 to 1.5 μ on the irradiated surface of SiC + C. An analogous pattern of erosion of this material is obtained [26] in the implantation of He^+ ions with energies of 100 and 250 keV, with the erosion being proportional to the ion energy in this energy range and increasing from 0.2 to 0.5 atoms/ion.

With the implantation of hydrogen ions (see Fig. 6b) the erosion of the surface is considerably less than with the implantation of He^+ ions of the same energy (see Fig. 6a).

Thus, with bombardment by high-energy hydrogen ions carbon-pyroceramic and SiC + C differ advantageously from graphite by the absence of chemical sputtering at 600°C, whereas with the implantation of He^+ ions the character of the erosion of these materials is the same as for graphite.

The authors thank Dr. H. R. Hopkins for the specimens of SiC + C alloy presented.

LITERATURE CITED

1. N. P. Agapova et al., in: Problems of Atomic Science and Technology, Series on Fuel and Construction Materials [in Russian], Part 1, Izd. Tsent. Nauchn.-Issled. Inst. Atom. Inf., Moscow (1974), p. 14.
2. G. Kulcinsky et al., UWFDM-108, Madison, Wisconsin (1974).
3. G. Kulcinsky et al., UWFDM-127, Madison, Wisconsin (1975).
4. V. M. Gusev et al., Preprint Inst. Atom. Energ. 25445, Moscow (1975).
5. N. P. Agapova et al., Fourth Geneva Conference, Report No. 49/P/453 (1971).
6. M. I. Guseva, Radiotekh. Elektron., 9, 1680 (1962).
7. B. Kadomzev and R. Berisch, in: Proceedings of Fifth International Atomic Energy Conference on Plasma Physics and Controlled Nuclear Fusion Research, Tokyo (1974).
8. S. Das and M. Kaminsky, J. Appl. Phys., 44, 2520 (1973).
9. S. Das and M. Kaminsky, IEEE Trans. Nucl. Sci., NS-21, 31 (1974).
10. M. Kaminsky, in: Proceedings of Fifth International Atomic Energy Conference on Plasma Physics and Controlled Nuclear Fusion Research, Tokyo (1974).
11. W. Bauer and G. Tomas, J. Nucl. Mater., 47, 241 (1973).
12. G. Tomas and W. Bauer, Rad. Effects, 17, 221 (1973).
13. W. Bauer and G. Tomas J. Nucl. Mater., 53, 102 (1974).
14. S. Das and M. Kaminsky, ibid., p. 115.
15. G. Wehner, Phys. Rev. 108, 35 (1957).
16. N. Busharov et al., in: Proceedings of Second International Conference on Surface Effects in Controlled Fusion Devices, San Francisco, Feb. 16-20 (1976).
17. J. Roth et al., ibid.
18. V. M. Gusev et al., Prib. Tekh. Eksp., 4, 19 (1968).

19. R. Behrisch, P. Sigmund, and R. Weissmann, SPP-9/13, München (1973).
20. J. Roth, R. Behrisch, and B. Schezzer, J. Nucl. Mater., 57, 356 (1975).
21. M. A. Kumakhov et al., Deposited Article, Izd. Vsesoyuz. Inst. Nauch. Tekh. Inf., Moscow (1974).
22. J. Martel et al., in: Proceedings of Second International Conference on Surface Effects in Controlled Fusion Devices, San Francisco, Feb. 16-20 (1976).
23. J. Martel et al., J. Nucl. Mater., 53, 142 (1974).
24. General Atomic Project 2100 GA-A13430, USA (1975).
25. V. M. Gusev et al., Fiz. Khim. Obrab. Mater., 1, 15 (1976).
26. M. Kaminsky and S. Das, in: Proceedings of First Topical Meeting on the Technology of Controlled Nuclear Fusion, San Diego, USA (1974), p. 508.

SOME CHARACTERISTICS OF THE IRRADIATION OF SPECIMENS DURING ACTIVATION STUDIES IN A FAST REACTOR

L. N. Yurova, A. V. Bushuev,
V. N. Ozerkov, V. V. Chachin,
G. I. Gadzhiev, and A. V. Inchagov

UDC 621.039.519.621.039.526

The experiments described in the present report were conducted on the "Spektr" fast thermal installation and the BOR-60 reactor. In the experiments on the "Spektr" installation we studied the effect on the experimental information of the irradiation conditions (Fig. 1) and of irregularities of the active zone: packets with different depths of depletion and the control elements (Fig. 2, Table 1).

TABLE 1. Effect of Irregularities of Active Zone on Functions*

Functional	Exp. No.			
	1	2	3	4
$\bar{\sigma}_c^{238}/\bar{\sigma}_f^{235}$	1,02±0,02	1,02±0,02	1,03±0,02	0,96±0,02
$\bar{\sigma}_f^{238}/\bar{\sigma}_f^{235}$	0,84±0,03	0,94±0,04	0,93±0,03	1,06±0,03
$\bar{\sigma}_f^{239}/\bar{\sigma}_f^{235}$	0,97±0,04	0,98±0,04	1,02±0,04	1,00±0,04

*The value of the functional at the center of the installation comprised only of cassettes of 90% enrichment is taken as the unit.

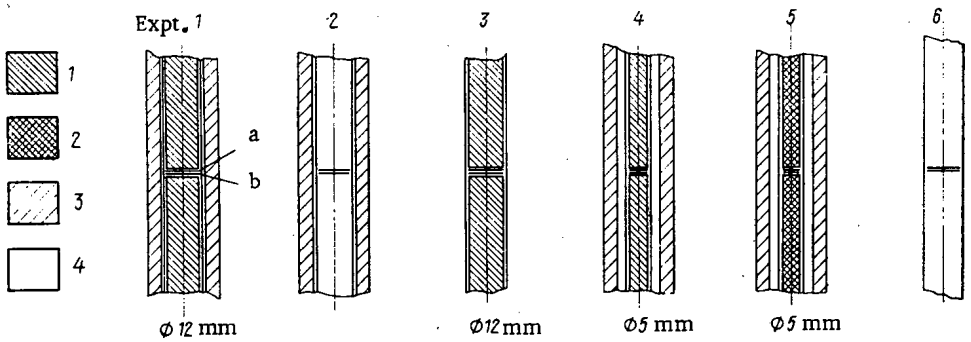

Fig. 1. Diagram of experiments for determination of effect of irradiation conditions on functionals: a) foil of natural uranium; b) foil of uranium enriched 36%; 1) natural UO_2; 2) UO_2 enriched 36%; 3) 1Kh18N9T steel; 4) air.

*All-Union Institute of Scientific-Technical Information.

Translated from Atomnaya Énergiya, Vol. 42, No. 6, pp. 490-493, June, 1977.

TABLE 2. Effect of Mode of Placement of Specimens on Functionals

Functional	Exp. No.					
	1	2	3	4	5	6
$\left(\frac{\bar{\sigma}_f^{238}}{\bar{\sigma}_f^{235}}\right)^i \Big/ \left(\frac{\bar{\sigma}_f^{238}}{\bar{\sigma}_f^{235}}\right)^1$	1	1,04±0,03	1,03±0,03	1,03±0,04	1,62±0,13	1,11±0,03
$\left(\frac{\bar{\sigma}_c^{238}}{\bar{\sigma}_f^{235}}\right)^i \Big/ \left(\frac{\bar{\sigma}_c^{238}}{\bar{\sigma}_f^{235}}\right)^1$	1	1,58±0,05 with $K_{bl}=1,17$	0,96±0,02	1,02±0,02	1,02±0,02	1,37±0,05 with $K_{bl}=1,14$

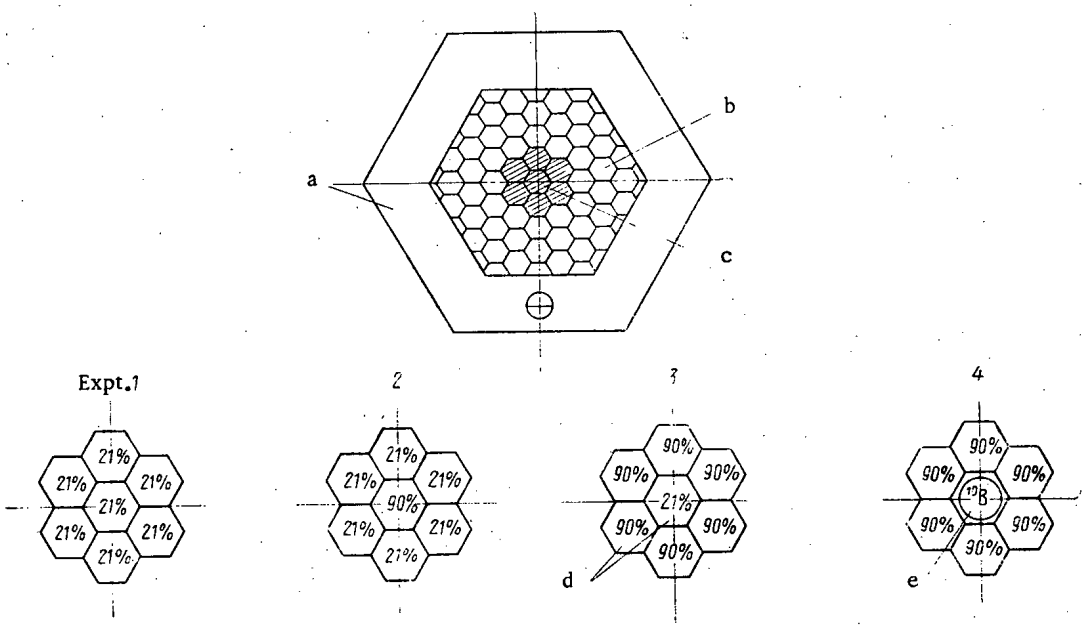

Fig. 2. Diagram of experiments for determination of effect of irregularities of active zone on functionals: a) graphite shield; b) cassette of active zone; c) region for performing experiments; d) enriched cassettes; e) boron-filled rod.

The capsule material was imitated by 1Kh18N9T steel. The experimental results (Table 2) show that the capsule can disturb the neutron spectrum and this effect can be reduced when a dummy fuel element is placed in the capsule. The quantity K_{bl} was determined experimentally through a comparison of the specific activity of the indicators used and indicators with an effective thickness to ^{238}U of about 0.01 mm, for which the self-blocking effect is absent.

The data obtained showed that under the conditions of a hard neutron spectrum the irregularities of the active zone have a weak effect on the functionals $\bar{\sigma}_c^{238}/\bar{\sigma}_f^{235}$ and $\bar{\sigma}_f^{239}/\bar{\sigma}_f^{235}$. The functional $\bar{\sigma}_f^{238}/\bar{\sigma}_f^{235}$ is more sensitive to the composition of the surrounding medium.

In the experiments on the BOR-60 reactor, we used capsules which are employed for prolonged irradiation of specimens in the reactor. The tracers were located inside a fuel element, or in a capsule displacing part of the fuel or directly between fuel tablets. The results showed that the reaction rate in the capsure differs markedly from the reaction rates in the fuel, which necessitates the introduction of the appropriate experimental corrections.

THE POSSIBILITY OF ALLOWANCE FOR THE FINE STRUCTURE OF THE SPECTRUM IN CALCULATIONS OF FAST REACTORS AND INSTALLATIONS

A. G. Morozov, Yu. A. Zverkov,
A. M. Sirotkin, I. S. Slesarev,
and V. V. Khromov

UDC 621.039.51:621.039.526

The problem of the correct description of the spatial–energy distribution of neutrons in fast critical installations is connected, as a rule, with an analysis of the gas-kinetic transfer equation with allowance for the anisotropy of scattering and the detailed energy dependence of the cross sections. The solution of such a problem is achieved through the use of the method of separation of variables with the introduction of a subgroup approach in the resonance region. However, the subgroup representation of the cross sections necessitates a transition to the matrix form of the spectral equations. Consequently, the problem of the search for the simplest numerical schemes possessing an acceptable error in the neutron-flux functionals (about 1-2%) comes to the fore. In the report we propose a new numerical scheme based on the balance equations in a cell of the network with allowance for the discontinuity of the macroscopic cross section at its boundaries. The chosen numerical scheme is realized in the ALGOL program SPEKTR, intended for the calculation of the detailed structure of a spectrum in a multizone plane-parallel system with an arbitrary energy dependence of the cross sections. To test the asymptotic accuracy of the scheme we calculated the spectra and effective resonance integrals in infinite multicomponent mixtures of ^{238}U with different moderators (H, O_2, Fe, Pb) in the vicinity of two strongly interfering resonances (E_{o1} = 189.6 eV and E_{o2} = 208.6 eV). A comparison between the results of calculations by the SPEKTR program with the maximum number of multigroups and analogous results obtained by the precision numerical scheme of [1] showed their full agreement. Further studies were conducted in order to investigate the convergence of the balance scheme in different energy regions and with the different means of describing the neutron cross sections used in practical calculations. It was found that for a correct description of the energy dependence of the neutron flux up to 0.5 keV in multicomponent infinite media using piecewise-constant cross sections (the BNAB-26 system of constants) it is sufficient to introduce 5-10 multigroups per group interval. Calculations in the region of allowed resonances of ^{238}U were conducted in a study of the convergence of the scheme, using models of cross sections with an arbitrary energy dependence. In this case the cross sections were assumed to be constant within a multigroup and were calculated from the equation $\sigma_k = \int_{\Delta E_k} \sigma(E)\, dE/\Delta E_k$, where the integration was performed numerically with an assigned accuracy, while the cross sections were calculated by the URAN program [2].

Effective resonance integrals of ^{238}U in the energy range of 170-220 eV with different numbers of multigroups and the dependence of the error δI_{ef} of the resonance integral on the dilution cross section and the mass number of the moderator, all calculated by the SPEKTR program, are presented in the report. An analysis of the errors δI_{ef} showed that the calculation of the fine structure of the neutron spectrum in the energy range of 1-500 eV, where allowance for the intermediate nature of the resonances of ^{238}U is important, requires the introduction of about 500 multigroups. It is shown in the report that the use of the more correct means of obtaining the multigroup constants σ_k allows one to reduce the error of I_{ef} by about 20 times.

The proposed balance scheme of numerical solution of the integral equation is simple, has a high accuracy and good convergence, and permits the efficient calculation of neutron spectra in multicomponent media with an arbitrary energy dependence of the cross sections, which opens up broad prospects for its use for precision calculations of the neutron-physical characteristics of fast reactors and critical installations.

LITERATURE CITED

1. A. P. Platonov, Candidate's Dissertation, Nauch.-Issled. Inst. Atom. Reakt., Dimitrovgrad (1973).
2. L. P. Abagyan et al., in: Informational Bulletin of the Center on Nuclear Data [in Russian], Part 4, Atomizdat, Moscow (1967), p. 392.

THE CALCULATION OF RESONANCE ABSORPTION IN INFINITE MULTICOMPONENT MEDIA

A. G. Morozov, Yu. A. Zverkov,
A. M. Sirotkin, I. S. Slesarev,
and V. V. Khromov

UDC 621.039.51:621.039.526

The results are presented of the computational investigations of the behavior of the effective resonance integral of ^{238}U (I_{eff}) in the region of intermediate resonance for multicomponent media. The effect of interference of the resonances on I_{eff} — an effect which was not produced until the proper irradiation — is discussed. Thus, although the dependence of I_{eff} on the mass number of the moderator A_{mod}, which reflects the "spacing" of the resonances, has been investigated in [1], the cited curve is of a monotonic nature. Analysis of the detailed energy dependence of the spectrum of the collision density $\Psi(E)$ indicates the presence of fluctuations in the spectrum at the distance of a moderation "step" of the nonresonant component of the mixture q_A from the position of the resonances. It is evident that at some A_{mod}, when q_A is equal to the distance between resonances, a deviation should occur in the monotonic nature of the behavior of the I_{eff} (A_{mod}) curves which is caused by the interference over the spectrum of these resonances. The results of calculations based on the program SPECTRUM have confirmed the interference of intermediate resonances over the spectrum, but they have shown the smallness of its effect on I_{eff}. The latter fact permits us to assume the resonance of ^{238}U to be isolated in the sense of interference over the flux. The possibility was also investigated in this paper of utilizing the results of calculations already performed for two-component media [1] to estimate I_{eff} in multicomponent media. The investigations have demonstrated a breakdown of the law of additivity of the contributions of individual components of the diluent to the variation of I_{eff}. The addition of lead to a uranium—hydrogen mixture cannot only increase I_{eff} (as should be the case with the additive nature of the dependence) but can also reduce the resonance integral. The explanation of this unexpected effect (a decrease in I_{eff} upon an increase of the total σ_0) is caused by the strong sensitivity of the resonance integral to the mass number of the diluent. This example shows convincingly how assumptions which at first glance are natural prove to be untrue upon an estimation of the resonance integral in the region of the low levels of permitted resonances of ^{238}U.

The possibility has also been considered in this paper of the use in the region of permitted resonances of the subgroup approach [2], which has been recommended for the forbidden region of cross sections. A positive solution of this problem would permit changing over to a subgroup catalog prepared beforehand and thus excluding completely the computational efforts associated with the detailed establishment of the cross sections in the region of each resonance. Calculation of the fine structure of the spectrum was carried out in the interval 186-238 eV, which includes the three characteristic resonances of ^{238}U. The results of calculations of the mean cross sections and of I_{eff} are obtained in the case of the establishment of a continuous energy dependence of the cross sections and in the case of use of the subgroup constants. A similar analysis of the different methods of describing the resonance structure of cross sections is given for 14, 15, and 16 energy groups of the BNAB library, where the resonance behavior of the cross sections is observed.

Recommendations are given on the use of various models of cross sections for different energy regions. The universality of the program SPECTRUM, which permits calculating effectively the detailed spectrum both with a continuous and with a subgroup representation of the cross sections, opens up great possibilities for its application in spatial-energy calculations over the entire energy range.

LITERATURE CITED

1. A. P. Platonov, Candidate's Dissertation, NIIAR, Dimitrovgrad (1973).
2. M. N. Nikolaev et al., At. Energ., 29, No. 1, 11 (1970).

THE CALCULATION OF THE ESCAPE OF PHOTONEUTRONS FROM THICK TARGETS IN THE REGION OF GIANT RESONANCE

V. P. Kovalev and V. I. Isaev

UDC 621.384.649:539.125.5.03

A method is expounded in this paper for the calculation of the escape of photoneutrons from thick targets upon their bombardment by electrons. The effective spectrum of the bremsstrahlung in the target was obtained by means of the summation of the spectra of the thin layers into which the target was arbitrarily divided. The site of the production and absorption of the photons was taken into account, and it was assumed that all the photons are directed forward. The Schiff spectrum [1] was taken as the initial elementary spectrum of the bremsstrahlung. The dependence of the electron energy on depth was expressed in terms of the average loss parameters [2].

The expression for the escape of photoneutrons was obtained in the following form:

$$B(E_0, Z, T) = N_0^2 \int_{k_{thr}}^{E_0} \int_{E=k}^{E_0} \frac{\sigma(E, Z, k)\,\sigma_{\gamma n}(Z, k)}{(dE/dx)\,\mu(k)} \left[1 - \left(\frac{dE_0/dx}{dE/dx}\right)^{\mu(k)/\beta} e^{-\mu(k)T}\right] dE\,dk,$$

where E_0 is the initial energy of the electron, E is the energy of the electron at depth x, k is the photon energy, Z is the atomic number of the target material, T is the thickness of the target, N_0 is the number of atoms per gram, k_{thr} is the photoreaction threshold energy, $\sigma(E, Z, k)$ is the Schiff bremsstrahlung spectrum, $\sigma_{\gamma n}(Z, k)$ is the photonuclear reaction cross section, dE/dx and dE_0/dx are the total energy losses per unit thickness by an electron with energy E or E_0 ($k_{thr} \leqslant E \leqslant E_0$) or ($k_T \leqslant E \leqslant E_0$), if the target thickness is less than the value

$$T < t_{thr} = \frac{1}{\beta} \ln \frac{\alpha + \beta E_0}{\alpha + \beta E_{thr}},$$

where $E_{thr} = k_{thr}$, α and β are constants of the total energy losses of the electron, and $\mu(k)$ is the absorption coefficient of photons with energy k.

A comparison of the calculated and experimental data has been carried out for copper and lead [3]. The values of the cross sections $\sigma_{\gamma n}$ are taken from [4], and the values of $\mu(k)$ and the constants α and β are taken from [5]. The calculated and experimental data for lead and copper differ by no more than 15 and 20%, respectively. Calculation of the escape of neutrons by the Monte Carlo method [6] gives the same error.

An expression has also been obtained which has practical value for the target thickness at which the escape of neutrons is similar to the maximum value for the given Z and E_0. For heavy elements the thickness corresponding to maximum escape is equal to 30-40, and for light and medium elements, to 70-100 g/cm^2.

LITERATURE CITED

1. L. Schiff, Phys. Rev., 83, 252 (1951).
2. W. Heitler, Quantum Theory of Radiation, Oxford Univ. Press (1954).
3. W. Barber and W. George, Phys. Rev., 116, 1551 (1959).
4. J. Miller et al., Nucl. Phys., 32, 236 (1962).
5. J. Hubbell, Nat. Standards Data, Vol. NBS-29 (1969).
6. R. Alsmiller and N. Moran, Nucl. Instrum. Methods, 48, 109 (1967).

NEUTRON DISTRIBUTION IN AQUEOUS SOLUTIONS OF α-ACTIVE SUBSTANCES

A. S. Bespyatykh, E. A. Parfent'ev,
V. A. Peregudov, É. M. Tsenter,
and E. V. Chvankin

UDC 539.125.52

The present report is devoted to a method of measuring the content of an α-active substance in an aqueous solution from the neutron yield of the (α, n)-reaction in oxygen and other light elements. The spatial—energy spectrum of neutrons in a cylindrical vessel containing an aqueous solution of the α-active substance is studied. Cases of the uniform and nonuniform distribution of the α-active substance over the height of the vessel are analyzed.

We chose a modified system of Herzel—Selengut equations for the theoretical solution of the problem. The solution is represented in the form of series of orthogonal polynomials by a Bubnov—Galerkin method. The calculating method is realized in the form of a program for a Minsk-22 computer.

In the experiments modeling the distribution of the α-active substance over the height of the vessel we used a commercial Pu—Be source of fast neutrons. The distribution of neutron flux density was measured with a Don-1 radiometer with an SNM-16 type counter. In the calculations we chose a vessel of the same dimensions as in the model experiments for convenience in comparing the theoretical and experimental results.

ERRATA

In the article of É. G. Tertyshnik et al., "^{85}Kr concentration in the atmosphere over the USSR territories in 1971-1975" [Soviet Atomic Energy (At. Energ.), 42, No. 2, 165 (1977)], the following should appear in the literature cited:

7. W. Boeck et al., Bull. Am. Meteorol. Soc., 56, No. 5, 8 (1975).

LETTERS TO THE EDITOR

SPECIFIC SENSITIVITY OF AN NaI(Tl) SCINTILLATOR IN THE RECORDING OF γ RAYS FROM RADIOACTIVE ORES

G. F. Novikov, A. Ya. Sinitsyn,
and Yu. O. Kozynda

UDC 550.835

The mass production of scintillators of various shapes and sizes requires the development of methods for operational comparison of their metric parameters. The comparison of scintillators in measurements of low radioactivity levels has been discussed in a good many studies, in which the quality of the counter was evaluated on the basis of the quantity N_0^2/N_b (where N_0 is the counting rate from the specimen after subtraction of the background N_b) [1], or on the basis of the parameter Q, which is related to N_0^2/N_b [2]. The best scintillator is the one that can be used for most accurately determining a minimal level of radioactivity.

In investigating large masses of radioactive ores, the evaluation of the quality of the scintillator must be based on other principles. A special feature of such measurements is that the magnitude of the characteristic background of the counter is negligibly small in comparison with the γ radiation of the ore. In this case the best scintillator is the one which, under certain conditions, ensures a maximal recordable effect in specific energy intervals of the γ spectrum.

A measure of scintillation detectors in the investigation of high-energy spectra of radioactive ores is the specific volumetric sensitivity of the scintillator, n_{ij} [3], which is the pulse counting rate measured in the i-th energy interval normalized per unit scintillator volume and unit concentration of the j-th radioactive element:

$$n_{ij} = \frac{1}{Vq_j} \int_{E_1}^{E_2} N_j(E)\, dE,$$

where $N_j(E)$ is the scintillation spectrum of γ radiation of the radioactive element with index j, measured by a scintillator volume V, in pulses/sec; E_1 and E_2 are the end points of the energy interval, MeV; q_j is the concentration of the j-th radioactive element in the ore, %.

Knowing the value of n_{ij}, we can easily evaluate the measurable effect for an actual detector, and on the basis of this we can select the optimal dimensions of the phosphor crystal.

Experiments have shown that the value of n_{ij} depends on the volume of the scintillator. We studied the variation of n_{ij} as a function of V experimentally by using NaI(Tl) crystals of different volumes for measuring the hard region of the γ spectrum of large masses of equilibrium ores of uranium and thorium. The reason we chose only the hard region was that the soft region, being unusable under conditions of radiation saturation for quantitative measurements of U(Ra) and Th in ores, is usually eliminated by schematic methods [4]. The experiment was carried out on ore models having the shape of cubes with an edge measuring ~1 m and a density of $\rho = 1.8$ g/cm^3. The U and Th concentration values were 0.128 and 0.037%, respectively. The measurements were made in 4π geometry at the center of the models, and therefore the radioactive background from the surrounding rocks was taken to be zero. In the experiments we investigated nine scintillators whose volumes ranged from 1 to 90 cm^3; six scintillators were almost isometrically shaped ($l \approx d$, where l is the length and d is the diameter of the scintillator), while three were elongated up to a value of $l/d = 5$. The spectra were obtained with a multichannel pulse amplitude analyzer, with a statistical error of no more than 1%.

Translated from Atomnaya Énergiya, Vol. 42, No. 6, pp. 495-496, June, 1977. Original article submitted March 29, 1976.

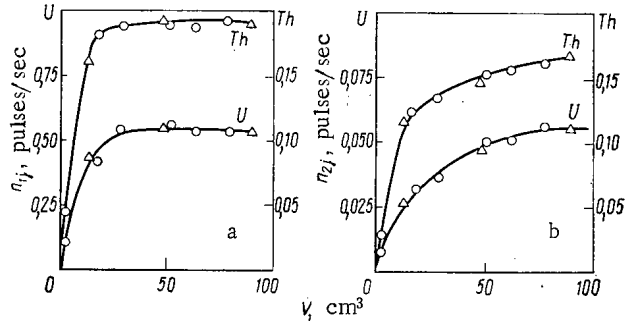

Fig. 1. Variation of n(V) in the energy intervals 1.05-1.35 MeV (a) and 2.05-2.65 MeV (b) for the γ spectra of U(Ra) and Th, based on measurements with isometric (○) and elongated (△) NaI(Tl) scintillators.

TABLE 1. Values of $n_{0,ij}$ and D_{ij} for Different Energy Intervals of the γ Spectra of Radioactive Ores

E, MeV	$n_{0,ij}$, pulses/(cm³·sec·0.01%)		D_{ij}, cm⁻³	
	U (Ra)	Th	U (Ra)	Th
1,05—1,35	0,540	1,192	0,120	0,143
1,00—1,60	0,860	0,320	0,118	0,146
1,00—1,90	1,050	0,440	0,113	0,134
2,05—2,65	0,057	0,168	0,047	0,070

The results of the experiments for the energy ranges 1.05-1.35 MeV and 2.05-2.65 MeV, which are most widely used in spectrometric measurements of U(Ra) and Th in ores [5], are shown in Fig. 1. In the 1.05-1.35 MeV interval, for scintillators with volumes of $V \leqslant 15$ cm³ the values of n increase sharply as the volume increases. When $V > 25$ cm³, the growth stops and n becomes practically independent of V; consequently, for such scintillators the recordable effect is proportional to their volume. In the 2.05-2.65 MeV interval, where the efficiency of γ-ray recording is lower than in the preceding case, the growth of n with increasing V does not stop until the very largest scintillator sizes used in the experiment and is slowed down only slightly for $V > 25$ cm³. Thus, in measurements of the γ spectra of radioactive ores in the aforementioned energy intervals, it is advisable to use scintillators with a volume $V < 25$ cm³. It is also inefficient to replace one single crystal having a volume $V > 25$ cm³ with a number of scintillators having the same total volume if each of these has $V < 25$ cm³.

In both energy intervals the experimental data for the elongated and isometric scintillators are governed by the same law, which proves that such detectors are equivalent for measurements in 4π geometry. Therefore, if the technical conditions of the measurements limit the diameter d of the scintillator (e.g., in investigating boreholes drilled to search for radioactive ores), the volume of the phosphor crystal may be increased by increasing the length l until the value of $l/d = 5$ is reached.

The variation of $n_{ij}(V)$ is approximated, with an error of no more than ±10%, by the expression

$$n_{ij} = n_{0,ij}[1 - \exp(-D_{ij}V)],$$

where $n_{0,ij}$ is the specific sensitivity of a scintillator with a volume of 90 cm³; D_{ij} is a constant coefficient for the i-th energy interval and the j-th radioactive element, cm⁻³.

The values of these parameters for the γ spectra of U(Ra) and Th in the energy intervals recommended for quantitative determination of these elements in radioactive ores at the deposition site are shown in Table 1. Using the data in Table 1, we can easily determine the value of n for a particular scintillator, and on the basis of this we can calculate the

expected effect this scintillator is capable of measuring in saturated volumes of ores of natural radioactive elements.

Obviously, the method of comparing scintillators on the basis of their specific sensitivity can be widely used with the γ spectra not only of radioactive ores but also of any other sufficiently intense γ ray sources.

LITERATURE CITED

1. G. G. Ménov, in: Metrology of Ionizing Radiation [in Russian], Gosatomizdat, Moscow (1962), p. 192.
2. V. M. Malykhin, G. L. Moroz, and N. I. Istratova, in: Spectrometric Methods for the Analysis of Radioactive Contamination in Soils and Aerosols [in Russian], Gidrometeoizdat, Moscow (1974), p. 8.
3. G. F. Novikov et al., At. Energ., 32, No. 3, 238 (1972).
4. A. Ya. Sinitsyn, Prib. Tekh. Eksp., No. 3, 100 (1971).
5. G. F. Novikov, A. Ya. Sinitsyn, and Yu. O. Kozynda, Zap. Leningr. Gornogo Inst. 56, No. 2, 98 (1969).

THERMODYNAMIC PROPERTIES OF LIQUID Pu + In ALLOYS

V. A. Lebedev, V. I. Kober,
V. G. Serebryakov, G. N. Kazantsev,
I. F. Nichkov, S. P. Raspopin,
and O. V. Skiba

UDC 669.8725'824

In the alloy system Pu + In there exists a compound $PuIn_3$ which melts congruently at 1225°C [1]. For the purposes of investigation of the thermodynamic properties of liquid indium-rich alloys in the 660-979°K range, we measured the emf of a galvanic element:

$$\text{Pu—In (liq)} \mid \text{KCl—LiCl} + 3 \text{ mass\% } PuCl_3 \mid \text{Pu—Bi (liq)}. \quad (1)$$

The electrolyte was prepared from dehydrated salts of "chemically pure" quality. The compound $PuCl_3$ was obtained by chlorination of PuO_2. The plutonium content of the bismuth (20-25% by mass) exceeded its solubility at the highest experimental temperature and corresponded to the two-phase region liq + $PuBi_2$. By using as a comparison electrode an alloy with known thermodynamic characteristics, we can expand the interval of temperatures investigated, avoid the complications due to the presence in the plutonium of a number of polymorphic transformations, and exclude the effect of an energic interaction of the plutonium with the salt melt. In our work we used IN-00 indium, VI-00 bismuth, and 99% pure plutonium. The alloys and the electrolyte were in small beryllium oxide crucibles. The current leads were made of molybdenum. The tests were carried out in a helium atmosphere from which we had removed all traces of moisture and oxygen by passing it over uranium metal shavings heated to 800°C. The setup of the measurement cell, the experimental procedure, and the processing of the experimental data are similar to those described earlier [2].

The galvanic-element emf values (Table 1) for Pu + In alloys containing 5-20% plutonium by mass were independent of the alloy composition, were repeatable to within 0.001 V when the temperature was raised or lowered, were repeatable within ±0.003 V in successive experiments, and lay along a straight line on the E—T graph, with the equation

$$E, \text{V} = 0.0869 + 0.0438 \cdot 10^{-3} T. \quad (2)$$

The parameters of the compact form of representation of the experimental data (CFRED) [3] are the following: n = 41, B = 385044.5 K^2; $\overline{T}$ = 801.1°K; S_0^2 = 17.3 mV^2. On the basis of

Translated from Atomnaya Énergiya, Vol. 42, No. 6, pp. 496-498, June, 1977. Original article submitted May 10, 1976.

TABLE 1. Experimental Values of emf of Galvanic Element

T, °K	E_1, mV	T, °K	E_2, mV	T, °K	E_3, mV	T, °K	E_4, mV
979	123,0	995	130,3	765	130,3	700	121,5
935	125,0	959	130,3	716	126,7	751	125,2
922	122,1	878	125,9	671	124,1	854	131,5
899	119,0	843	123,7	768	127,6	758	123,7
808	116,3	810	122,4	794	128,0	661	119,5
788	114,1	765	119,4	758	124,5	677	122,9
844	118,4	716	119,0	661	121,0	756	125,1
977	125,0	671	118,5	756	125,3	813	127,9
934	118,0	768	122,0	813	125,0	860	131,1
918	123,0	794	122,4	689	123,7	689	126,4

TABLE 2. Activity Coefficient of Plutonium in Liquid Indium

T, °K	$x_{Pu} \cdot 10^5$	E, mV		γ_{Pu}	
		galvanic element	rel. to ε–Pu	expt.	according to [5]
683	1,84	80	521,4	$1,6 \cdot 10^{-7}$	$1,1 \cdot 10^{-7}$
683	3,13	93	508,4	$1,8 \cdot 10^{-7}$	$1,1 \cdot 10^{-7}$
794	4,94	80	493,5	$8,3 \cdot 10^{-6}$	$3,8 \cdot 10^{-6}$
828	11,3	84	481,0	$1,5 \cdot 10^{-6}$	$6,6 \cdot 10^{-6}$

TABLE 3. Thermodynamic Characteristics of Liquid Alloys of Indium with Uranium, Thorium, and Plutonium

Compound	$-\Delta\bar{H}$, kcal/g-atom	$-\Delta\bar{S}$, e.u./g-atom	$-\Delta\bar{H}^*$, kcal/g-atom	$-\Delta\bar{S}^*$, e.u./g-atom	$\lg \gamma = A + B \cdot T^{-1}$		$\lg X = C + D \cdot T^{-1}$	
					A	$-B$	C	$-D$
UIn_3 [9]	29,8	17,7	9,3	10,8	2,36	2033	1,52	4480
$ThIn_3$ [10]	42,1	15,2	17,6	3,5	0,77	3850	2,57	5350
$PuIn_3$	47,5	20,1	31,9	14,9	3,26	6970	1,20	3430

Eq. (2) and these parameters, we calculated the variation of the partial thermodynamic quantities when the plutonium passed from the liq + $PuBi_2$ alloy to the liq + $PuIn_3$ alloy:

$$\Delta\bar{H}_{Pu} + 6.01 \pm 0.74 \text{ kcal/g-atom};$$

$$\Delta\bar{S}_{Pu} = 3.03 \pm 0.93 \text{ entropy units/g-atom.}$$

On the basis of the well-known thermodynamic characteristics of liq+ $PuBi_2$ alloys,

$$(\Delta\bar{H}_{Pu} = 53.5 \pm 1.0 \text{ kcal/g-atom};$$

$$\Delta\bar{S}_{Pu} = -17.4 \pm 1.5 \text{ entropy units/g-atom [4]}).$$

we determined the increments $\overline{\Delta H}_{Pu}$ and $\overline{\Delta S}_{Pu}$ for the reaction $\varepsilon - Pu_{(solid)} + 3In_{(liq)} \rightarrow PuIn_3$ (solid):

$$\Delta\bar{H}_{Pu} + -47.5 \pm 1.7 \text{ kcal/g-atom};$$

$$\Delta\bar{S}_{Pu} = -20.4 \pm 2.4 \text{ entropy units/g-atom; } \lg a = 4.46 - 10400 T^{-1}. \quad (3)$$

The formation of the compound $PuIn_3$ is accompanied by the generation of a considerable amount of heat, a decrease in entropy, and a substantial decrease in plutonium activity, which is characteristic of intermetallides. It should be noted that a more exact determination of the characteristics of the Pu–Bi system may change the thermodynamic properties of the Pu + In alloys. If in Eq. (4), which generalizes all the known thermodynamic characteristics of compounds of actinoids and lanthanoids with p-elements [5]:

$$\Delta\bar{H} = -135.6 + 94.3r_2 - 105\Delta\varkappa \pm 5.0 \text{ kcal/g-atom} \quad (4)$$

we substitute the atomic radius of indium (1.50 Å [6]) and the difference in electronegativity between indium (1.7 [7]) and plutonium (1.2 [8]), we obtain $\Delta\bar{H}_{PuIn_3} = -46.4$ kcal/g-atom, which agrees with the value given above within the limits of computational and experimental error.

The characteristics of homogeneous solutions ($\Delta\bar{H}^*$, $\Delta\bar{S}^*$, lg γ) were calculated from the characteristics of the compound $PuIn_3$ ($\Delta\bar{H}$, $\Delta\bar{S}$), using the relation established in [5] between these values for indium-based alloys:

$$\Delta\bar{H}^* = 30.9 + 1.303\Delta\bar{H} = -31.9 \pm 3.1 \text{ kcal/g-atom}$$
$$\Delta\bar{S}^* = 11.3 + 1.286\,\Delta\bar{S} = -14.9 \pm 3.7 \text{ entropy units/g-atom} \quad (5)$$
$$\lg\gamma_{Pu} = \frac{\Delta\bar{H}^* - \Delta\bar{S}^* \cdot T}{4.575T} = 3.26 - \frac{6970}{T}.$$

The activity coefficients of plutonium in indium solutions, calculated from Eq. (5), are compared in Table 2 with the experimental values found by measuring the emf of a galvanic element for homogeneous solutions of Pu + In with known plutonium concentrations x_{Pu} (determined by radiometric analysis).

The experimental values of the activity coefficient of plutonium in indium solutions agree acceptably with the values calculated by Eq. (5); the latter are preferable, however, since the emf of a galvanic element for homogeneous solutions did not remain constant but decreased at a rate of 0.01–0.03 V/h, apparently because of corrosion processes.

The equation for the solubility of plutonium in melted indium as a function of temperature is given by the difference of Eqs. (3) and (5):

$$\lg X_{Pu} = \lg a - \lg\gamma = 1.20 - 3430 \cdot T^{-1}. \quad (6)$$

At 680 and 800°K the amounts of plutonium dissolved in the indium are 0.014 and 0.065 at.%. The low solubility of plutonium in indium makes it difficult to investigate homogeneous solutions experimentally. The thermodynamic characteristics of liquid Pu + In alloys differ considerably from the characteristics of U + In alloys and are close to the corresponding values for Th + In alloys (Table 3). This can be seen particularly clearly in the values of $\Delta\bar{G}$. The same rule has also been observed for liquid alloys of uranium, thorium, and plutonium with aluminum [11].

LITERATURE CITED

1. F. Shank, Structure of Bimetallic Alloys [Russian translation], Metallurgiya, Moscow (1973), p. 473.
2. V. A. Lebedev, I. F. Nichkov, and S. P. Raspopin, Elektrokhimiya, 2, No. 2, 160 (1966).
3. A. N. Kornilov, L. B. Stepina, and V. A. Sokolov, Zh. Fiz. Khim., 41, No. 11, 2975 (1972).
4. V. A. Lebedev et al., At. Energ., 27, No. 1, 59 (1969).
5. V. A. Lebedev, At. Energ., 41, No. 1, 33 (1976).
6. V. M. Vozdvizhenskii, Prediction of Bimetallic Diagrams of State [in Russian], Metallurgiya, Moscow (1975), p. 212.
7. L. Pauling, General Chemistry, W. H. Freeman, San Fransisco, California (1970).
8. S. S. Batsanov, Zh. Struk. Khim., 5, 293 (1964).
9. V. A. Lebedev et al., Zh. Fiz. Khim., 48, No. 3, 542 (1974).
10. A. M. Poyarkov et al., Zh. Fiz. Khim., 49, No. 10, 2615 (1975).
11. V. A. Lebedev et al., in: Theses of Reports of the Conference on the Chemistry of Neptunium and Plutonium [in Russian], Nauka, Leningrad (1975), p. 50.

TEMPERATURE DEPENDENCE OF QUASIELASTIC SCATTERING OF SLOW NEUTRONS BY WATER

A. G. Novikov and S. M. Iskenderov

UDC 539.171.015.162.2

In the last 10-15 years many papers have investigated the quasielastic scattering of slow neutrons by water, building up an idea of the mechanism of self-diffusion for this liqui However, most of them considered water at room temperature. Experiments on the temperature dependence of quasielastic scattering (which are precisely the experiments of most interest) have been very few, and have considered temperatures no higher than 100°C [1, 2].

The present work attempts to examine the quasielastic scattering of slow neutrons by water in the temperature range 300-600°K. The neutron spectra in the absence of elastic scattering by water were measured using a DIN-1M double impulse neutron spectrometer [3] (initial energy of monochromatic neutrons E_0 = 8 MeV, resolution $\Delta E_0 \approx 0.57$ MeV). The samples of water were in the form of quartz capillaries filled with water and sealed at both ends. The capillaries were filled to a level such that, over the whole temperature range, the water inside the capillary was under a pressure approximately corresponding to the saturation vapor pressure at the given temperature.

Analysis of the neutron spectra in the absence of elastic scattering gave the absolute experimental double differential cross sections (DDCS) of scattering in Fig. 1. For absolute normalization of the DDCS special measurements with vanadium samples were used, together with data on the differential scattering cross section $d\sigma/d\Omega$ of water from [4]. The DDCS were converted to the scattering law $S(\varkappa, \hbar\omega)$, where $\varkappa$ is the momentum transfer and $\hbar\omega$ the energy transfer. Hence, by substracting the inelastic component, the quasielastic part was isolated. The inelastic component was calculated by the PRASSIV program [5], using a model that takes into account the temperature dependence of the generalized frequency spectrum of water [6]. Examples of the experimental law of quasielastic scattering for different values of the momentum transfer $\varkappa$ and temperature are shown in Fig. 2. In Fig. 3, the natural halfwidth ΔE of the quasielastic scattering law is shown as a function of $\varkappa^2$ for various temperatures; ΔE was obtained from the curves of Fig. 2 on the assumption that the natural law of quasielastic scattering is described by a Lorentz function and the resolution curve of the spectrometer by a Gaussian. The effect of multiple scattering on the value of ΔE obtained is estimated on the basis of results given in [7].

As frequently remarked [8-10], self-diffusion in water is a complex process, as a result of the structural properties of water and the specific features of its intermolecular interactions. There is reason to expect that the self-diffusion of water involves both a step mechanism (as in solids) and also continuous diffusion, the contribution of which increases with temperature.

In our opinion, a model that corresponds to a certain extent to this picture of self-diffusion in water is that proposed in [11], according to which the law of quasielastic scattering is Lorentzian, with halfwidth

$$\Delta E(\varkappa^2, T) = \frac{2\hbar}{\tau_0(T)}\left\{1+\varkappa^2 D_0(T)\,\tau_0(T) - \frac{\exp[-2W(\varkappa^2, T)]}{1+\varkappa^2 D(T)\,\tau_0(T)}\right\}. \quad (1)$$

An attempt was made to interpret the experimental data on the basis of this model, as follows. Curves constructed in accordance with Eq. (1) were drawn through the experimental points of Fig. 3 for each temperature; the unknown parameters τ_0 and D_0 [the factor $W(\varkappa^2, T)$ was found from experimental data on the angular dependence of the integral density of quasielastic scattering] were chosen by the method of least squares so as to obtain the best agreement

Translated from Atomnaya Énergiya, Vol. 42, No. 6, pp. 498-500, June, 1977. Original article submitted August 11, 1976.

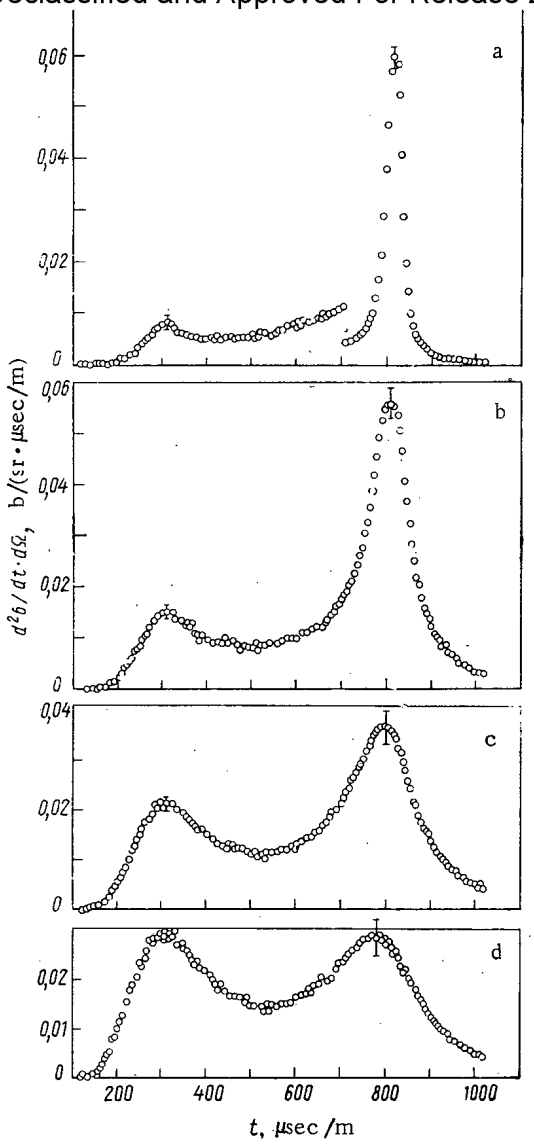

Fig. 1

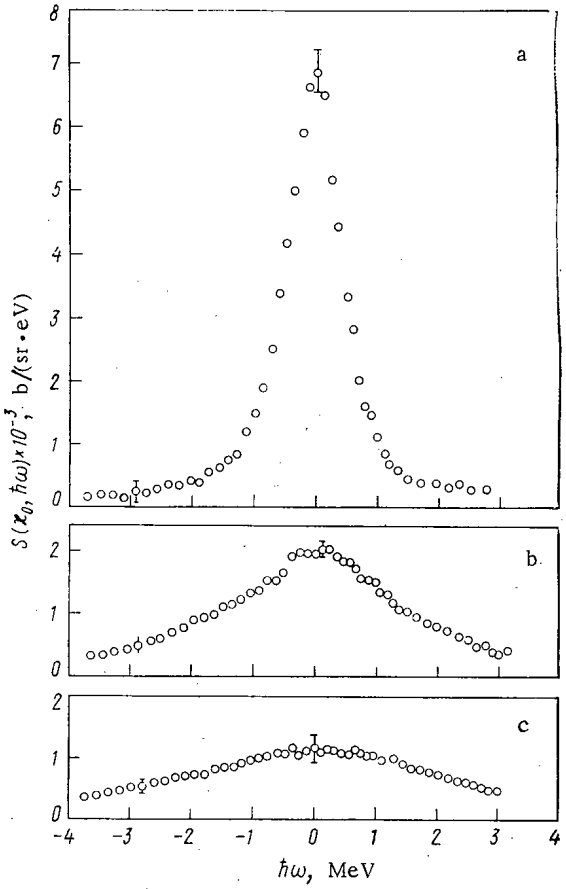

Fig. 2

Fig. 1. Experimental absolute double differential cross section of scattering for water: a) at 300°K; b) 400°; c) 500°; d) 600°; E_0 = 8 MeV; θ = 37°.

Fig. 2. Law of quasielastic scattering of neutrons by water at 600°K: a) $\varkappa_0$ = 0.36 Å^{-1}; b) 0.92 Å^{-1}; c) 1.21 Å^{-1}.

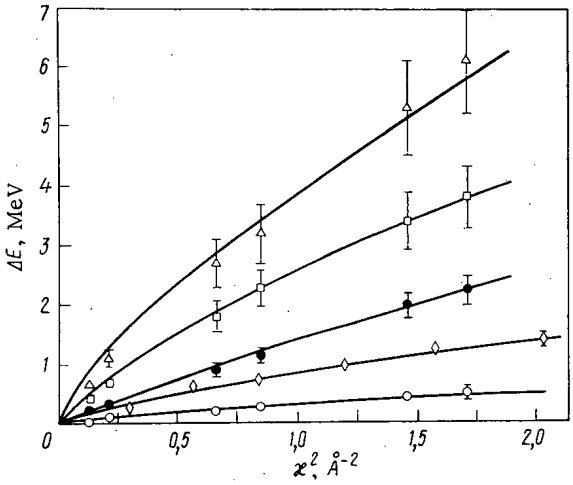

Fig. 3. Halfwidth of law of quasielectric scattering of neutrons by water: ○) at 300°K; ◇) 350°K [2]; ●) 400°K; □) 500°K; △) 600°K.

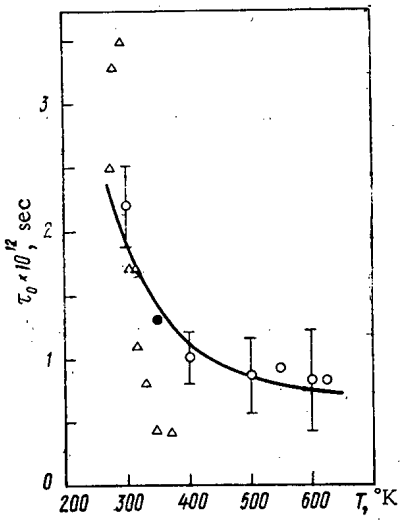

Fig. 4

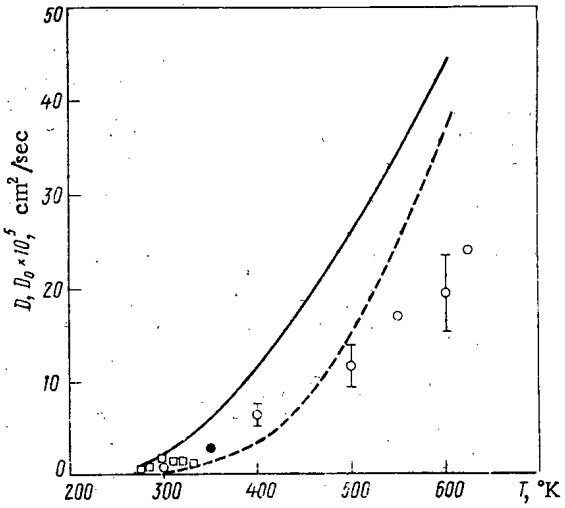

Fig. 5

Fig. 4. Stable lifetime τ_0 of molecule as a function of temperature: ○) results of the present work; △) of [2].

Fig. 5. Coefficient of continuous diffusion D_0 of centers of oscillation of molecules as a function of temperature: ○) results of present work; □) of [2]; the dashed curve shows results of D_0 according to [10], and the continuous curves the total self-diffusion coefficient D of water [12].

between calculation and experiment. The resulting curves are shown by the continuous lines in Fig. 3, the corresponding parameters τ_0 and D_0 are shown as a function of temperature in Figs. 4 and 5, together with analogous data from [2]. It follows from Figs. 4 and 5 that the results of [2] do not agree with those of the present work. The discrepancy arises because of the different methods of evaluating τ_0 and D_0. When treated by our method the experimental data of [2] give values of τ_0 and D_0 consistent with our results (shown by the filled circles in Figs. 4 and 5; T = 348°K).

However, it must be emphasized that at high temperatures the use of Eq. (1), which rests on the assumption that $u \ll d$ (u is the amplitude of the molecule's oscillations around the equilibrium position; d is the internal distance), may not be entirely satisfactory.

An attempt was made to interpret the temperature dependence $\tau_0(T)$ and $D_0(T)$. For $\tau_0(T)$ the following approximate description [13] was used

$$\tau_0(T) = a \exp(W_0/kT) \tag{2}$$

with $a = 0.27 \cdot 10^{-12}$ sec and activation energy $W_0 = 1.15$ kcal/mole, regardless of the temperature (the curve in Fig. 4).

The curve of $D_0(T)$ (dashed in Fig. 5) was calculated by the formula [10]

$$D_0(T) + kT\sqrt{\rho\mu}/16\pi\eta^2, \tag{3}$$

where $\eta(T)$ is the viscosity; $\rho(T)$ is the density. The shear modulus μ is assumed independent of the temperature: $\mu = 3.25 \cdot 10^{10}$ g·cm²/sec² [10]. In fact, μ decreases with rise in temperature, resulting in poorer agreement between calculation and experiment.

The form of the curves of $\Delta E(\varkappa^2, T)$ and the temperature dependences $\tau_0(T)$ and $D_0(T)$ indicate that even at temperatures close to critical the behavior of water is clearly quasi-crystalline. It is to be hoped that experiments at critical and supercritical temperatures with pressure variation will assist our understanding of how the transition to gaslike behavior occurs in water. Such experiments will be carried out in the near future.

LITERATURE CITED

1. G. Safford et al., J. Chem. Phys., 50, 4444 (1969).
2. P. Blanckenhagen, Ber. Bunsenges, Phys. Chem., 76, 891 (1972).
3. V. G. Liforov et al., Preprint FEI-129 [in Russian], Physics and Power Institute, Obninsk (1968).
4. J. Beyster, Nucl. Sci. Eng., 31, 254 (1968).
5. L. V. Maiorov et al., in: Proceedings of Third International Conference, Vol. 2, Geneva (1964), p. 379.
6. K. Esch et al., Nucl. Sci Eng., 46, 223 (1971).
7. M. Johnson, AERE-R7682 (1974).
8. O. Ya. Samoilov, Structure of Aqueous Solutions of Electrolytes and Hydration of Ions [in Russian], Izd. Akad. Nauk SSSR, Moscow (1957).
9. P. Egelstaff, Advances Phys., 11, 203 (1962).
10. N. P. Molomuzh and I. Z. Fisher, Zh. Strukt. Khim., 14, 1105 (1973).
11. V. S. Oskotskii, Fiz. Tverd. Tela, 5, 1410 (1963).
12. R. Hausser et al., Z. Naturforsch., 21a, 1410 (1966).
13. Ya. I. Frenkel', Collected Works. Vol. 2. Kinetic Theory of Liquids [in Russian], Izd. Akad. Nauk SSSR, Moscow (1959).

FINE STRUCTURE OF COMBINATION-SCATTERING LINES AND LASER PLASMA DIAGNOSTICS

A. F. Nastoyashchii

UDC 621.039.665

In laser plasma diagnostics, difficulties arise connected both with the small size of the object under study (~100 μ) and with the short lifetime of the plasma (~1 nsec). A study of the fine structure of the combination-scattering (CS) lines opens up interesting possibilities. For example, the splitting of CS lines [1, 2] can be used to measure the electron temperature and flow velocity of the plasma.

We assume that Langmuir oscillations (LO) are excited in the plasma (as a result of parametric instability [3], for example). Their spectral distribution depends on many factors, and the characteristics of the distribution are still unclear at present. We will assume that the spectral function does not have sharp gaps in the region of wave numbers satisfying condition (2). The question of the intensity of the oscillations is not discussed.

We consider the scattering of a light beam on the LO, i.e., a process of the type

$$\omega=\omega_0+\omega_l;\quad k=k_0+k_l, \tag{1}$$

where ω and k are the frequency and wave vector of the scattered light; quantities pertaining to the incident radiation or the LO are marked by the indices 0 and l, respectively. By using the dispersion equations for a plasma moving with a velocity v [4], we find k_l which satisfies the conservation laws (1):

$$k_l=a_k+\sqrt{a_k^2+(\omega_p^2+2\omega_0\omega_p)\,c^{-2}}, \tag{2}$$

where

$$a_k(\vartheta,\varphi)=-k_0(1+\beta)\cos\vartheta+v(\omega_0+\omega_p)\,c^{-2}\cos\varphi;$$

$$\cos\vartheta=k_0k_l/k_lv;\quad \cos\varphi=k_lv/k_lv;$$

$$\beta=3(1+\omega_0\omega_p^{-1})\,T/(mc^2).$$

Translated from Atomnaya Énergiya, Vol. 42, No. 6, pp. 501-502, June, 1977. Original article submitted September 1, 1976.

By substituting the value obtained into Eq. (1), we obtain an expression for the frequency of the scattered radiation as a function of the angles ϑ and φ. The terms "responsible" for the splitting of the CS lines* are the following:

$$\frac{\Delta\omega}{\omega}=\sqrt{\left(1-2\frac{\omega_p}{\omega}\right)\cos^2\vartheta+\left(1+\frac{\omega_p}{\omega}\right)\frac{\omega_p}{\omega}}\times\left[-6\cdot10^{-3}T\sqrt{\left(\frac{\omega}{\omega_p}-2\right)\frac{\omega}{\omega_p}}\cos\vartheta+\frac{\varphi}{c}\cos\varphi\right]-$$

$$-\left(1-2\frac{\omega_p}{\omega}\right)\frac{v}{c}\cos\vartheta\cos\varphi+6\cdot10^{-3}T\left(\frac{\omega}{\omega_p}-2\right)\cos^2\vartheta. \qquad (3)$$

In the case of a nonuniform plasma, Eq. (3) must be averaged over the spatial density distribution, which must lead to broadening of the line contours.

As an example, let us consider the splitting of the $3/2\omega_0$ line, when the surface of the plane target is oriented perpendicular to the laser beam and the scattered radiation is received in the aperture of a focusing lens. In this case, as seen from (3), when $v = 0$ the receiver of the CS radiation will record two frequencies corresponding to the scattering of the direct and reflected laser beams. Four frequencies can be observed when $v \neq 0$. The splitting of the $2\omega_0$ harmonics does not depend on the temperature and is proportional to v. Thus, with $v \approx 3\cdot10^7$ cm/sec we would have a line shift† $\Delta\lambda \sim 10$ Å, which is accessible to measurement.

Thus, after experimental verification the splitting of CS lines can be used as a method of plasma diagnostics. An advantage of the method is that it does not require absolute measurements of the line intensities. The agreement of the results obtained with different angles of observation can serve as a control on the error of the method.

A difficulty of the observation of double lines consists in the strong attention of one of the components. A transition to active diagnostics using probe beams with a specially selected frequency can therefore be useful. For example, two opposing light beams can be used to equalize the intensities of the two components.

Let us discuss the possibility of measuring the velocity of flow of the plasma. As seen from (3), for this it is convenient to use beams with a frequency $\omega_0' = \omega_p$. The maximum splitting should be observed at an angle $\varphi = 0$ to the hydrodynamic velocity vector. Thus, if $\omega = 2\omega_p$ then $\Delta\lambda/\lambda = \sqrt{3}(v/c)$.

In the case of $v \sim 3\cdot10^7$ cm/sec we have $\Delta\lambda \sim 18$ Å when $n = n_{cr}/4$ and $\Delta\lambda \to 9$ Å when $n = n_{cr}$, where n_{cr} is the critical density for the laser frequency ω_0.

The direction of the probe beam plays no role in the given case (since $k' = 0$). By measuring the angular dependences of the frequency of the scattered light one can find v from the equation

$$\frac{v}{c}=\frac{2}{\sqrt{3}}\frac{\omega_2-\omega_1}{\omega(\cos\varphi_2-\cos\varphi_1)}\equiv\frac{2}{\sqrt{3}}\frac{\omega_3-\omega_2}{\omega(\cos\varphi_3-\cos\varphi_2)}\equiv\ldots, \qquad (4)$$

where the indices 1, 2, and 3 denote quantities pertaining to the angles φ_1, φ_2, φ_3.

The variations of the quantities on the right-hand side of Eq. (4) can serve as a control on the error of the method.

To determine the temperature one can use, e.g., two opposing light beams of frequency $\omega_0' = 2\omega_0$ with recording of the lines $5/2\omega_0$ and $3\omega_0$. The hydrodynamic corrections can be eliminated if one measures the splitting of the lines in the direction of one of the probe beams ($|\cos\vartheta| = 1$, $|\cos\varphi| = 0$):

$$\omega=5/2\omega_0;\quad \Delta\lambda/\lambda=4.1\cdot10^{-2}T; \qquad (5)$$

$$\omega=3\omega_0;\quad \Delta\lambda/\lambda=1.8\cdot10^{-2}T. \qquad (6)$$

*The question of the absolute value of the shift of the CS lines goes beyond the framework of the model adopted.

†Here and later the estimates are made for a laser frequency $\omega_0 = 2\cdot10^{15}$ sec^{-1} (neodymium laser).

When T ∿ 1 keV the splitting comprises ∿50-150 Å and is easily found.

Probing of the plasma with a light beam having a variable frequency can also give information on the spectrum of the Langmuir oscillations.

In experiments on the heating of a plasma by a laser pulse the choice of diagnostic methods is very limited (direct methods of measurement of the velocity of dispersion of the plasma, e.g., are entirely absent). Therefore, the study of the fine structure of CS lines can be an important source for obtaining data on the parameters of the plasma and the mechanism of its interaction with the laser radiation. At the same time, there is no doubt that the arguments presented are in serious need of experimental verification.

I thank N. G. Koval'skii and M. I. Pergament for a discussion.

LITERATURE CITED

1. J. Bobin et al., Phys. Rev. Lett., 30, 594 (1973).
2. H. Pant et al., Opt. Communs, 16, No. 3, 396 (1976).
3. V. P. Silin, The Parametric Interaction of Powerful Laser Radiation with a Plasma [in Russian], Nauka, Moscow (1974).
4. V. D. Shafranov, in: Problems of Plasma Theory [in Russian], Part 3, Gosatomizdat, Moscow (1963), p. 3.

USE OF THE CALORIMETRIC METHOD TO MEASURE THE ENERGY RELEASE IN A COMPENSATING ROD

A. S. Zhilkin, V. P. Koroleva,
N. P. Kurakov, L. A. Chernov,
and E. V. Shestopalov

UDC 621.039.517

The development and refinement of experimental methods of determining the energy release in the compensating rods of a reactor are urgent for the practical work of reactor construction and for the development of calculating methods. To obtain greater reliability it is desirable to measure the energy release by several independent methods. Along with the relative physical method described in [1], in the present report a highly sensitive calorimeter is proposed and used for the measurement of the energy release in a boron-containing rod of a critical installation. Despite the wide reputation of the calorimetric method, it is used mainly for dosimetric purposes [2] and for the determination of heat release in specmens under the conditions of power reactors [3] because of its relatively low sensitivity.

Sensitive calorimeters (10^{-4} W/g) have recently been created which have made it possible to measure the energy release in fissionable materials in a critical installation [4]. And only the appearance of such sensitive temperature detectors as microthermistors has made it possible to increase still more the sensitivity of the calorimetric method (up to 10^{-6} W/g).

The aim of the present report is the creation of a highly sensitive calorimeter, the measurement of the energy release in an absorbing rod of a critical installation, and the comparison of the measurement results of the calorimetric and physical methods.

Calorimetric Method. The proposed highly sensitive calorimeter belongs to the quasi-adiabatic type. The principle of its operation is based on the measurement of the rate of change of the temperature of a specimen isolated from the external medium. The temperature of the specimen varies by an linear law during a certain time, which depends on the thermal insulation of the specimen, its geometrical dimensions, and other factors. The cylindrical specimen of boron carbide 19.2 mm in diameter and 30 mm high was insulated from the other parts of the rod by foam plastic and by an air gap 1 mm thick, and from the lateral walls

Translated from Atomnaya Énergiya, Vol. 42, No. 6, pp. 502-503, June, 1977. Original article submitted September 20, 1976.

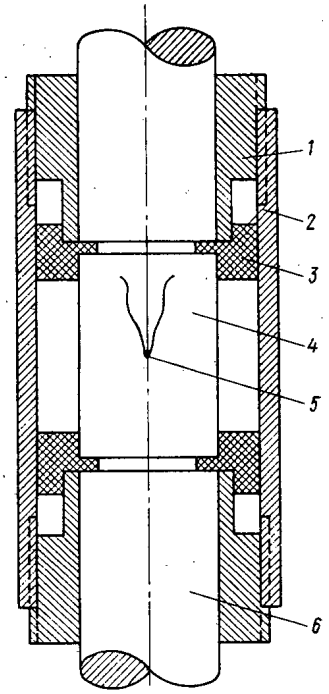

Fig. 1. Diagram of calorimeter for measuring radiation energy release in a boron carbide rod: 1) holder (aluminum); 2) outer shield (aluminium); 3) insulator (foam plastic); 4) cylindrical specimen of boron carbide; 5) MT-64 thermistor; 6) remaining part of absorbing rod.

of the reactor channel by an air gap of 5-7 mm. During heating of the specimen in the reactor through radiation energy release the length of the linear temperature rise was 150-200°C. This is also confirmed by calculations. With more prolonged heating the heat exchange between the specimen and the surrounding medium shows up, which disturbs the linear rise of the specimen temperature. For a linear temperature rise with time the specific energy release in the specimen per unit time owing to the (n, α) reaction in boron and the absorption of the γ and β radiation of the reactor is determined from the equation

$$Q = C_p \, dT/W \text{ dt } W/(g \cdot W), \tag{1}$$

where C_p is the specific heat capacity of the specimen; dT/dt is the rate of change of the specimen temperature; W is the reactor power. Thus, to determine Q one has to measure dT/dt, C_p, and W.

A diagram of a colorimeter for measuring the radiation energy release in a boron carbide rod placed at the center of a PF-4F8 critical installation [5] is presented in Fig. 1. The temperature detector, and MT-64 thermistor (R = 64.5 kΩ at 20°C), was fastened to the lateral surface of the thermally insulated specimen. The sensitivity threshold of the calorimeter was $(1\text{-}2) \cdot 10^{-6}$ W/g, and a power of 10 W liberated in the active zone of the installation was enough to perform the measurements.

In order to allow for the effect of heat exchange between the surrounding medium and the specimen on the rate of temperature change, the quantity dT/dt was measured during three time periods with the same duration of 150-200 sec, corresponding to different reactor states:

$$dT/\text{dt} = (dT/dt)_m - 1/2\,[(dT/dt)_i + (dT/dt)_f], \tag{2}$$

where $(dT/dt)_i$ is the rate of change of the temperature of a specimen placed in the reactor in the initial period; $(dT/dt)_m$ is the rate of temperature change in the main period, when dynamic equilibrium is established in the heat exchange between the specimen and the surround-

ing medium; $(dT/dt)_f$ is the rate of temperature change in the final period after the power drop.

The specific heat capacity of the boron carbide was determined with the help of an electric heater of constantan wire ∿0.19 mm in diameter wound on the surface of the boron carbide specimen. The mass of the heater and the thermistor comprised ∿2% of the mass of the specimen. The correctness of such a method of determination of C_p was verified experimentally on aluminum.

It was shown through calculation that when the boron carbide specimen was heated by a surface heater the temperature at the center of the specimen becomes equal to the temperature at the surface 5-10 sec after the start of heating. During the heating time of 150-200 sec the heat losses from the specimen to the external medium do not exceed 5%. The power W of the installation was determined by measuring the specific energy release in the reactor fuel with the calorimeter and subsequent integration over the volume of the active zone.

Knowing all the quantities in Eq. (1), one can calculate the radiation energy release in the boron carbide: $Q = (1.05 \pm 0.1) \cdot 10^{-6}$ W/(g·W). The standard error for several series of measurements is presented here. To compare the results of the calorimetric and physical methods, in which we measured the energy release in natural boron and only that due to the (n, α) reaction, we made a recalculation in which we allowed for the boron content in B_4C (0.737) and through calculation obtained the contribution of the (n, α) reaction to the total energy release of $(1.29 \pm 0.13) \cdot 10^{-6}$ W/(g·W).

Physical Method. In this case the ratio of the cross section for ^{10}B capture and ^{235}U fission, averaged over the reactor spectrum at the monitoring point, was determined with a semiconducting gold–silicon detector. The coefficient of nonuniformity of the energy distribution was measured at the same point using a KNT-5 ionization chamber. The ratio of the numbers of neutron captures at the monitoring point and in the boron-containing rod (averaged over the cross section of the rod) was obtained by the method of track detectors (nitrocellulose with a layer of boron). All the experiments were conducted at the middle of the height of the active zone. In contrast with [1], we additionally studied and introduced a correction for the effect of the empty channel on the cited ratio of captures in boron. The value of the specific energy release has the form

$$Q = (1.34 \pm 0.03)\, 10^{-6}\ \text{W/(g·W)}.$$

Thus, the results obtained by the two independent methods agree well within the limits of the experimental errors, which confirms their correctness and the possibility of using such calorimeters in physical installations.

The authors express deep gratitude to A. A. Kutuzov, Yu. G. Pashkin, and Yu. E. Shvetsov for helpful advice and some calculations.

LITERATURE CITED

1. V. A. Kuznetsov et al., At. Energ., 33, No. 5, 926 (1972).
2. V. M. Kolyada et al., ibid., 21, No. 6, 520 (1966).
3. B. Lewis, Nucl. Sci. Eng., 18, 76 (1964).
4. O. A. Gerashchenko, V. B. Klimentov, and A. V. Nikonov, At. Energ., 33, No. 3, 232 (1972).
5. A. I. Mogil'ner et al., ibid., 24, No. 1, 42 (1968).
6. S. Genna et al., At. Energ. Rev., 1, No. 4, 239 (1963).

BEHAVIOR OF CHROMEL–ALUMEL THERMOCOUPLES DURING AN EMERGENCY SHUTDOWN OF THE BR-10 REACTOR

A. S. Kruglov, P. V. Vyrodov,
and M. I. Redchenko

UDC 621.039.531

In measuring the temperature, with thermocouples, in the zone of action of the intense radiation of a reactor, the allowance for the influence of radiation effects, which can distort the thermocouple readings, acquires importance. Despite the considerable number of published reports on this question, there is no single opinion concerning the existence of an instantaneous effect of the action of the radiation field on the thermo-emf. For example, some authors have not observed instantaneous deflections in the reading of Chromel–Alumel (CA) thermocouples during a sharp drop in reactor power, with the initial flux density of fast neutrons reaching $\sim 10^{13}$ neutrons/(cm^2•sec). In other cases instantaneous deflections in the readings of CA thermocouples reaching −5.6 and −10°C were observed during the shutdown of a reactor with a flux density of fast neutrons of $\sim 10^{13}$ and $\sim 6.5 \cdot 10^{12}$ neutrons/(cm^2•sec), respectively [1]. For the SM-2 reactor with a flux density of fast neutrons of $\sim 4 \cdot 10^{14}$ neutrons/(cm^2•sec) the instantaneous deflection for CA thermocouples reached +26°C [2]. Such disagreement of the experimental results casts doubt on the reliability of thermometry using thermocouples under the conditions of the active zones of reactors.

In order to clarify the behavior of CA thermocouples during sharp variations in the power of a fast-neutron reactor we conducted tests on thermometry during a shutdown of the BR-10 reactor. The thermodynamic assembly, for which a massive specimen of stainless steel with two thermocouples of KTMS (CA) cable with a cross section of 2 × 0.06 mm mounted inside served as the basis, was placed in a vertical channel of the BR-10 reactor located in a nickel shield at a distance of ~40 cm from the axis of the central zone. In addition, five more analogous thermocouples were built into different elements of the assembly. The hot junctions of the thermocouples had thermal and electrical contact with the thermocouple cover and with elements of the assembly. The cold junctions were located outside the reactor and the connecting lines were made of CA conductors. During the operation of the reactor the specimen was heated to a temperature of 215°C, which exceeded by 50–70°C the temperature of the channel wall, separated from the assembly by an air gap. The thermo-emf was measured with an FZO digital ampere voltmeter with a sensitivity of 10 μV. The measuring instrument was connected with the thermocouples through an automatic commutator device allowing measurements to be made with an interval of 1 sec. The FZO readings were recorded on an MP-16 digital printer. Up to the time of the test all the thermocouples were irradiated by a neutron flux of from $\sim 1.2 \cdot 10^{20}$ to $\sim 1.2 \cdot 10^{21}$ neutrons/cm^2 distributed along a length of ~0.5 m (in the zone of the hot junction). A temperature drop reaching ~100°C was observed over the same length, with the maximum of the heating falling in the region of the hot junction.

The thermo-emf of the CA thermocouples was measured during a planned shutdown of the reactor through the actuation of the quick-acting accident protection (QAP). Before the actuation of the QAP the reactor power was 3 MW, the neutron flux density in the zone where the specimen was located was $\sim 4 \cdot 10^{13}$ (for $E \geq 0.1$ MeV) and $\sim 7 \cdot 10^{13}$ neutrons/(cm^2•sec) (for all energies) at this power, and the dose rate of γ radiation was 10^3 R/sec. The sharp drop in reactor power is not equivalent to the complete "turning off" of the radiation field, since γ radiation from the radioactive fission products of the fuel and activation products in the construction materials of the active zone, the shield, and the coolant remains after the reaction ceases. According to the calculated and experimental data the dose rate of γ radiation is reduced by more than an order of magnitude as a consequence of the cessation of the fission reaction.

Translated from Atomnaya Énergiya, Vol. 42, No. 6, pp. 504-505, June, 1977. Original article submitted October 4, 1976.

TABLE 1. Variation of Thermo-emf during and after Activation of QAP (τ = 0)

τ, sec	E, mV	τ, sec	E, mV	τ, sec	E, mV	τ, sec	E, mV
—120	8,06	8	8,05	18	8,05	28	8,04
—60	8,05	9	8,07	19	8,06	29	8,04
0	8,07	10	8,06	20	8,06	30	8,04
1	8,05	11	8,05	21	8,05	40	8,03
2	8,06	12	8,06	22	8,04	50	8,03
3	8,06	13	8,05	23	8,06	60	8,00
4	8,05	14	8,05	24	8,05	120	7,98
5	8,07	15	8,06	25	8,04	180	7,87
6	8,06	16	8,06	26	8,04	240	7,74
7	8,06	17	8,05	27	8,05	300	7,58

The data obtained showed that after the activation of the QAP none of the seven thermocouples changed their readings within the limits of the experimental accuracy. The character of the variation of the thermo-emf of one of the thermocouples mounted in the specimen is presented in Table 1. The instability of the thermo-emf does not exceed 20 μV, and the relatively smooth decrease in the thermo-emf only begins 60 sec after the activation of the QAP and is obviously connected with the natural cooling of the specimen.

On the basis of these data, one can conclude that a fast shutdown of the BR-10 reactor does not cause instantaneous deflections in the readings of cable CA thermocouples exceeding 30 μV (less than a degree). Possible distortions in the readings connected with the uneven buildup of radiation defects in the thermocouple materials and with the presence of a temperature gradient along the irradiated section can obviously affect the values of the measured thermo-emf only upon a change in the temperature gradient and cannot have a significant effect on the character of its variation at the moment of a discontinuity in the intensity of the radiation field.

Thus, the results of the experiment show that instantaneous effects of variation in the thermo-emf of CA thermocouples, the theoretical possibility of which may be connected with a change in the Fermi level of electrons in metals under the effect of a radiation field [3], are not detected under the conditions of irradiation in the BR-10 reactor.

LITERATURE CITED

1. B. V. Lysikov et al., Temperature Measurements in Nuclear Reactors [in Russian], Atomizdat, Moscow (1975), p. 81.
2. N. V. Markina, B. V. Samsonov, and V. A. Tsykanov, Fiz. Met. Metallov., 32, No. 4, 747 (1971).
3. G. Dau, R. Bourassa, and S. Keeton, Nucl. Appl., 5, No. 5, 322 (1968).

TOTAL NEUTRON CROSS SECTIONS OF ^{230}Th IN THE THERMAL ENERGY REGION AND ^{226}Ra UP TO 1 keV

R. N. Ivanov, S. M. Kalebin,
V. S. Artamonov, G. V. Rukolaine,
N. G. Kocherygin, S. I. Babich,
S. N. Nikol'skii, T. S. Belanova,
and A. G. Kolesov

UDC 621.039.556

The results of measurements of the total neutron cross sections σ_t for ^{230}Th and ^{226}Ra by the transit-time method are presented in the report. The measurements were carried out on the reactors of the Institute of Theoretical and Experimental Physics and the Scientific-Research Institute of Atomic Reactors using a selector with synchronously rotating rotors suspended in a magnetic field [1, 2]. Counters filled with ^{3}He served as the neutron detectors. The best resolution of the spectrometer was 35 nsec/m and the background did not exceed 4%.

Thorium 230. The specimen was prepared from ThO_2 powder in which the ratio of the amount of ^{232}Th to ^{230}Th was equal to 1.463 ± 0.03. The impurities in % were: Nd < $1\cdot10^{-5}$, La < $1\cdot10^{-5}$, Ce < $1\cdot10^{-5}$, Pr < $1\cdot10^{-5}$, Sm < $1\cdot10^{-5}$, Eu < $1\cdot10^{-5}$, Gd < $2\cdot10^{-4}$, Zr < $5\cdot10^{-3}$.

The measurements were made in the thermal region of neutron energies on a specimen with a ^{230}Th content of $(4.23 \pm 0.05)\cdot10^{21}$ atoms/cm^2. The transmission was measured relative to a specimen in which the amount of $^{232}ThO_2$ was equal to its content in the thorium specimen being studied. The data were corrected for the cross section of the oxygen [3] which was directly bound with the ^{230}Th.

The results of the measurement of the total cross section for ^{230}Th are presented in Fig. 1. The values of σ_t calculated from the parameters of the positive resonance taken from [4] are also presented here. At the thermal point the experimental value is σ_t = 54 ± 3 b while the calculated value is 31.8 b. A value of σ_t = 71.8 b was obtained at the thermal point in [4], where the scattering of slow neutrons through small angles was not taken into account. In a calculation of the 1.431 eV resonance by the shape method from the Breit–Wigner one-level equation for ^{230}Th we obtained a value of 16 ± 4 b for the potential scattering cross section. If one assumes that neutron capture is the main reaction for ^{230}Th in the thermal energy region then from the data obtained one can determine the value of this cross section at an energy of 0.025 eV, σ_α = (38 ± 5) b, which is considerably greater than the value of σ_α = 23.2 ± 0.6 b recommended in the atlas [3].

The data published on the cross section σ_α at the thermal point have a scatter of from 21.5 to 61 b [5-9].

Radium 226. We studied $RaSO_4$ powder which contained the following impurities: Na_2SO_4 1% and $BaSO_4$ 4.75%. The measurements were made in the energy region of 30-1400 eV on specimens with a ^{226}Ra content of $(5.56 \pm 0.53)\cdot10^{21}$ and $(8.12 \pm 0.78)\cdot10^{20}$ atoms/cm^2.

We found 38 resonances. For 31 of the resonances we determined the values of the neutron widths Γ_n by the area method and for five of them we determined the values of the radiation widths Γ_γ. The average value of Γ_γ = 25 ± 2 meV was used in analyzing the other resonances. The resonance parameters of the levels and the measured resonance [10, 11] with an energy of 0.539 eV, the parameters of which are taken from [10], are presented in Table 1.

A diagram of the distribution of the number of neutron levels as a function of the energy is presented in Fig. 2. It follows from the diagram that the omission of levels begins with 950 eV. Up to this energy we calculated the following: $\overline{D}$ = 32 ± 3 eV; $\overline{\Gamma_n^0}$ = 3.2 ± 0.8

Translated from Atomnaya Énergiya, Vol. 42, No. 6, pp. 505-506, June, 1977. Original article submitted October 4, 1976.

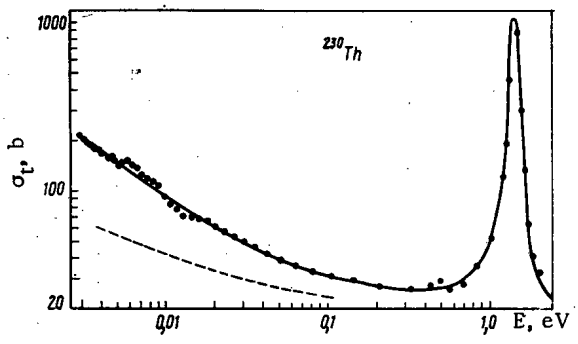

Fig. 1

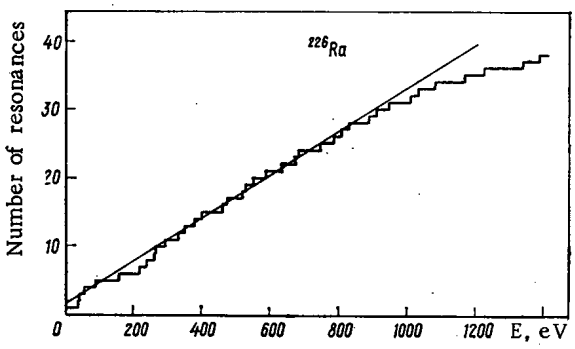

Fig. 2

Fig. 1. Total neutron cross section for ^{230}Th: ---) calculated dependence of σ_t with allowance for positive resonances; ●) experiment.

Fig. 2. Diagram of distribution of number of neutron resonances as a function of energy for ^{226}Ra.

TABLE 1. Parameters of Neutron Resonances of ^{226}Ra

E_0, eV	Γ_γ, meV	Γ_n, meV	E_0, eV	Γ_n, meV	E_0, eV	Γ_n, meV
0,539±0,003	26,5±3,0	0,015±0,001	377,3±1,6	88±24	809±6	13±8
35,84±0,15		0,05±0,01	398,6±1,8	187±41	828±6	57±31
39,95±0,15	26,4±2,6	0,36±0,04	459±2	24±11	887±7	68±37
55,80±0,18	22,4±5,9	6,0±0,9	471±3	23±11	907±7	280±100
88,5±0,3	19,2±7,0	21,2±2,4	516±3	26±11	945±7	47±22
155,3±0,7		2,0±0,4	526±3	40±17	1007±8	
217,8±0,9		1,4±0,4	548±3	5±3	1029±8	
237,7±1,0	31,2±7,6	138±17	585±4	11±4	1078±8	
259,8±1,1		2,4±0,8	630±4	422±33	1166±10	
263,0±1,1		15,2±5,4	669±4	33±17	1222±10	
292,3±1,4		53±14	681±5	21±11	1336±13	
329,4±1,4		153±45	745±5	98±60	1385±13	
348,2±1,5		243±61	785±6	67±29		

meV; $S_0 = (1.0 \pm 0.3) \cdot 10^{-4}$, and I = 236 ± 16 b.

A statistical analysis of the data obtained for the neutron resonances below 950 eV shows that the distribution of distances between levels coincides with a Wigner distribution while the reduced neutron widths follow a Porter–Thomas distribution for one degree of freedom. The experimental value of $\Delta_3 = 0.48$ (Dyson–Mehta statistics [12]) agrees with its theoretical value of 0.35 ± 0.11.

LITERATURE CITED

1. S. M. Kalebin et al., Prib. Tekh. Eksp., 3, 79 (1970).
2. S. M. Kalebin et al., in: Proceedings of Conference on Neutron Physics [in Russian], Vol. 2, Naukova Dumka, Kiev (1972), p. 267.
3. Brookhaven Nat. Lab.-325, 3rd ed., New York (1973).
4. S. M. Kalebin et al., At. Energ., 26, No. 6, 507 (1969).
5. A. Jaffey and E. Hyde, Argonne Nat. Lab.-4249 (1949).
6. E. Hyde, Argonne Nat. Lab.-4183 (1948).
7. H. Pomerance, Oak Ridge Nat. Lab.-1620 (1953).
8. M. Cabell, Canad. Phys., 36, 989 (1958).
9. R. Attre, ibid., 40, 194 (1962).
10. S. M. Kalebin et al., Yad. Fiz., 14, 22 (1971).
11. M. I. Pevzner et al., At. Energ., 1, No. 4, 67 (1956).
12. E. Dyson and M. Mehta, Mat. Phys., 4, 701 (1963).

TOTAL NEUTRON CROSS SECTIONS AND RESONANCE PARAMETERS OF ^{175,176}Lu UP TO 200 eV

S. M. Kalebin, V. S. Artamonov,
R. N. Ivanov, G. V. Rukolaine,
T. S. Belanova, A. G. Kolesov, and
V. A. Poruchikov

UDC 621.039.556

The results of measurements of the total neutron cross section σ_t for ^{175,176}Lu by the transit-time method are given in the report. The measurements were carried out on the reactors of the Institute of Theoretical and Experimental Physics and the Scientific-Research Institute of Atomic Reactors using neutron choppers with magnetic suspension of the rotors [1, 2]. Counters filled with ^{3}He served as the neutron detector. The best resolution was 35 nsec/m, the statistical accuracy was kept within the limits of 0.5-1.5%, and the neutron background did not exceed 4%.

Lutetium 175. We studied Lu_2O_3 powder which contained the following impurities by %: ^{176}Lu 0.23; Yb < 0.1; Fe, Cu, Pb < 0.01; Si < 0.02; Al, Ca < 0.05. The measurements were conducted in the region of energies up to 200 eV for two thicknesses of specimens containing $0.14 \cdot 10^{22}$ and $0.76 \cdot 10^{22}$ atoms/cm^2 of ^{175}Lu.* The total neutron cross section in the thermal energy region was corrected for the contribution made by the 0.14-eV resonance of the impurity isotope ^{176}Lu. The calculated curve of the total neutron cross section determined by the positive resonances of ^{175}Lu is presented in Fig. 1. The total neutron cross section of ^{175}Lu at the energy of 0.025 eV is equal to 30 ± 1 b. The parameters of the neutron resonances up to an energy of 57 eV are found by the shape method; the parameters above this energy are found by the area method.

The positions of the resonances (E_0) and the values of the neutron width ($2g\Gamma_n$) and the total width (Γ) are presented in Table 1. Analogous data are contained in [3, 4].

Simultaneously with the calculation of the parameters of the resonances by the shape method we found σ_p = 7.5 ± 1.0 b for ^{175}Lu. If one assumes that neutron capture is the main reaction in the narrow energy region then from the values of σ_t and σ_p obtained the cross section for this reaction at the energy of 0.025 eV is σ_γ = 22.5 ± 1.5 b. It agrees well with σ_γ = 23.4 ± 2 b recommended in the atlas [3].

From the data presented in Fig. 1 we determined the parameters of the negative resonance (see Table 1). A detailed analysis of the transmission curves in the region of 14 eV is interesting. A resonance is cited in the published reports for E_0 = 13.83 eV with the parameters $2g\Gamma_n$ = 20 ± 2 meV [3, 4] and a spin I = 3 [5]. In the determination of the parameters of this resonance for a specimen with a thickness of $0.14 \cdot 10^{22}$ atoms/cm^2 the trend of the theoretical curve (Fig. 2a, dashed curve) clearly indicated that the resonance with an energy of 14 eV should be considered as double, consisting of two levels which have merged because of the great thickness of the specimen. With such an assumption the subsequent calculations revealed two resonances at E_0 = 13.93 and 14.17 eV with the parameters $2g\Gamma_n$ = 7.61 and 6.8 meV, respectively, which described the experimental data well (see Fig. 2a). In order to conclusively ascertain the existence of two levels in the region of 14 eV, we measured the transmission with a thinner specimen with a thickness of $0.608 \cdot 10^{21}$ atoms/cm^2. Both resonances are well seen on the transmission curve of the thin specimen (dots on Fig. 2b). The

*The measurements were conducted under conditions for which the effect of neutron scattering through small angles was excluded.

Translated from Atomnaya Énergiya, Vol. 42, No. 6, pp. 506-509, June, 1977. Original article submitted October 4, 1976.

TABLE 1. Parameters of Neutron Resonances of ^{176}Lu

E_0, eV	Γ, meV	$2g\Gamma_n$, meV	E_0, eV	$2g\Gamma_n$, meV
−1,65		$2g\Gamma_n^0 = 0{,}14$	96,7±0,3	54±5
2,621±0,007	63±2	0,229±0,006	99,8±0,4	18,0±0,3
4,78±0,01	65±3	0,318±0,086	101,2±0,4	5,5±1,4
5,22±0,01	80±9	1,14±0,18	103,1±0,4	9,3±0,8
11,27±0,06	88±8	3,13±0,50	107,1±0,4	41,6±3,2
13,93±0,07	74±4	7,83±0,36	*109,5±0,4	0,5±0,3
14,16±0,07	82±6	8,12±0,37	113,0±0,5	4,1±0,4
15,38±0,07	73±4	1,75±0,06	115,3±0,5	35,1±2,5
20,54±0,08	87±6	2,22±0,26	118,2±0,5	8±5
23,52±0,09	96±6	6,1±0,7	127,5±0,5	38,3±5,0
28,02±0,12	89±5	1,80±0,12	129,8±0,5	53,3±5,2
30,20±0,13	103±9	7,19±1,20	138,0±0,6	41,4±3,1
31,10±0,13	94±9	3,05±0,28	143,0±0,7	2,2±0,7
36,58±0,15	126±8	6,22±1,20	146,3±0,7	3,4±0,8
40,65±0,17	150±5	13,2±3,1	148,7±0,7	1,2±0,3
41,16±0,17	148±12	3,50±0,21	151,1±0,7	3,2±0,7
49,48±0,18	156±30	11,6±1,6	155,5±0,7	4,2±1,4
50,35±0,18	136±16	7,95±1,15	158,4±0,7	10,1±3,5
53,58±0,18		0,47±0,07	163,9±0,7	9,5±2,6
56,88±0,18		4,22±0,63	169,2±0,8	8,4±2,9
61,15±0,19		0,43±0,07	171,2±0,8	3,3±1,0
69,44±0,19		0,24±0,12		
69,97±0,19		3,2±0,9	175,3±0,9	24±9
74,0±0,2		0,25±0,07	180,8±0,9	12,4±4,8
81,1±0,2		0,15±0,05	185,1±0,9	42±15
85,2±0,3		5,85±1,20	192,8±0,9	54±16
88,2±0,3		4,3±0,5	195,8±0,9	5,4±1,5

* Doubtful resonances.

TABLE 2. Parameters of Neutron Resonances of ^{175}Lu

E_0, eV	Γ, meV	$2g\Gamma_n$, meV	E_0, eV	$2g\Gamma_n$, meV
0,141±0,003	73±4	0,0864±0,0047	55,98±0,18	28,9±3,4
1,568±0,005	61±2	0,480±0,005		
4,370±0,010	68±4	0,419±0,022	58,54±0,18	0,49±0,11
6,130±0,014	58±7	1,438±0,160	59,63±0,18	0,27±0,08
8,14±0,02	177±17	0,0287±0,0016	60,68±0,18	6,7±0,8
9,73±0,03	68±2	1,365±0,012	64,02±0,19	3,4±0,5
10,79±0,04	73±2	1,697±0,017	64,96±0,19	4,6±0,6
11,44±0,04	69±8	1,072±0,073	65,84±0,19	0,13±0,06
11,88±0,05	69±8	0,442±0,015	67,81±0,19	12,0±1,6
16,90±0,07	277±17	0,052±0,007	70,6±0,2	19,1±2,1
19,06±0,07	129±14	0,139±0,006	71,6±0,2	8,3±1,3
19,94±0,07	86±7	0,409±0,008	75,6±0,2	13,7±1,6
21,76±0,08	75±5	1,364±0,042	78,3±0,2	8,7±1,5
24,49±0,10	85±7	3,514±0,069	79,7±0,2	1,9±0,5
27,15±0,11	98±15	11,04±0,16	82,7±0,2	16,4±1,9
* 28,80±0,12			84,2±0,2	0,53±0,25
29,34±0,12	59±32	2,25±1,38	85,4±0,2	39,5±4,0
29,53±0,12	188±47	3,28±1,15	89,4±0,3	13,4±2,5
31,83±0,14	136±15	2,55±0,10	92,4±0,3	19,2±2,1
32,66±0,14	46±22	0,35±0,04	95,6±0,3	5,0±1,3
33,25±0,14	86±10	2,70±0 17	98,9±0,3	10±3
36,97±0,15		5,31±1,13	104,7±0,4	11±4
38,30±0,15		1,76±0,60	105,1±0,4	
42,06±0,16	62±12	5,66±0,54	108,6±0,4	21±7
42,55±0,16	42±22	1,46±0,12	112,6±0,5	7±3
45,13±0,17	117±27	1,49±0,05	122,2±0,5	2,3±1,0
46,22±0,17	90±22	3,66±0,26	124,1±0,5	9,4±4,3
47,80±0,17		0,08±0,04	126,4±0,5	10,5±4,5
49,02±0,18		11,2±5,0	133,5±0,6	135±15
50,13±0,18		3,0±1,6	135,4±0,6	59±10
* 51,35±0,18		0,15±0,06		
52,13±0,18	150±31	4,57±0,25		

* Doubtful resonances.

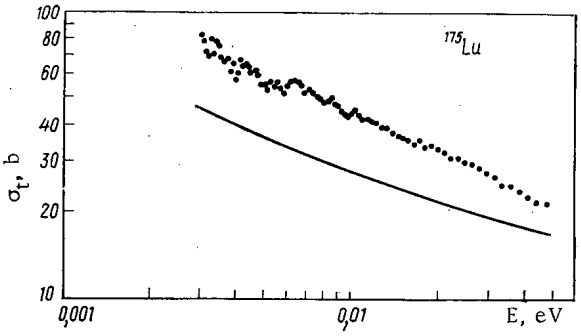

Fig. 1. Total neutron cross section for ^{175}Lu: ——) calculated dependence of σ_t with allowance for positive resonances; ...) experiment.

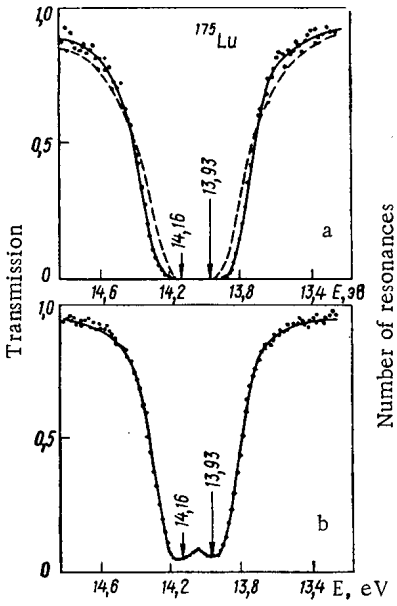

Fig. 2

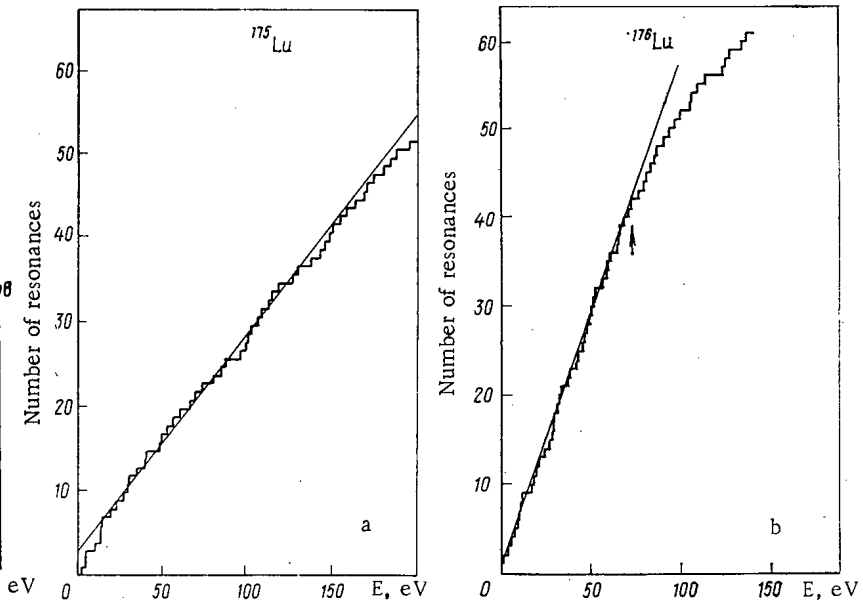

Fig. 3

Fig. 2. Transmission curves for ^{175}Lu specimens of different thicknesses of $0.14 \cdot 10^{22}$ (a) and $0.608 \cdot 10^{21}$ atoms/cm^2 (b) near 14 eV.

Fig. 3. Diagram of energy distribution of number of neutron resonances of ^{175}Lu (a) and ^{176}Lu (b).

parameters of these resonances are presented in Table 1 and the theoretical curve corresponding to them is given in Fig. 2b. An identification of the spins of the ^{175}Lu resonances in the region of 14 eV requires additional study. Analogous measurements at E $\sim$ 41 eV revealed two resonances at 40.65 and 41.16 eV, which agrees well with the data of [4].

Resonances with energies of 119.45 eV ($2g\Gamma_n$ = 1.240 meV) and 124.45 eV ($2g\Gamma_n$ = 0.246 meV) are cited in [4]. From the transmission curve obtained for ^{175}Lu in this region in our work it is hard to draw a conclusion concerning the existence of these levels.

In Fig. 3a we present a diagram of the energy distribution of the number of neutron levels, from which it follows that an appreciable omission of levels is not observed below 195.8 eV. For this energy region we calculated the following: D = 3.78 ± 0.26 eV; $2g\overline{\Gamma_n^0}$ = 1.18 ± 0.23 meV; $S_0 = (1.56 \pm 0.34) \cdot 10^{-4}$.

Lutetium 176. The specimen was prepared from Lu_2O_3 powder which had the following isotopic composition: ^{176}Lu 64.3% ^{175}Lu 35.7%. The measurements were made in the region of energies up to 135 eV for two thicknesses which corresponded to a ^{176}Lu content of $1.09 \cdot 10^{21}$ and $9.25 \cdot 10^{21}$ atoms/cm^2. We found 61 resonances below the energy of 135 eV, of which 41 were detected for the first time. The parameters of the neutron resonances up to an energy of

52 eV were calculated by the shape method and those above 52 eV by the area method (Table 2). Analogous data are contained in [3, 6].

A diagram of the energy distribution of the number of neutron resonances for ^{176}Lu is presented in Fig. 3b. It follows from the diagram that the omission of levels begins above 70 eV. Up to an energy of 72 eV we calculated the following: $\overline{D}$ = 1.74 ± 0.17 eV; $2g\overline{\Gamma}_n^o$ = 0.58 ± 0.14 meV; $S_o = (1.70 \pm 0.43) \cdot 10^{-4}$.

LITERATURE CITED

1. S. M. Kalebin et al., Prib. Tekh. Eksp., 3, 79 (1970).
2. S. M. Kalebin et al., in: Proceedings of Conference on Neutron Physics [in Russian], Vol. 2, Naukova Dumka, Kiev (1972), p. 267.
3. Brookhaven Nat. Lab.-325, 3rd ed., New York (1973).
4. H. Lion et al., Phys. Rev., 11, 1231 (1975).
5. A. Namenson et al., Nucl. Phys., A237, 45 (1975).
6. Block, Oak Ridge Nat. Lab.-2718 (1959), p. 28.

ALL-UNION CONFERENCE ON THE PREPARATION OF OPERATING PERSONNEL FOR ATOMIC POWER PLANTS

L. M. Voronin, G. N. Ushakov,
and V. M. Gordina

High-quality trained personnel who have undergone special theoretical and practical preparation are needed to assure the start-up and the reliable and safe exploitation of newly introduced atomic power plants (APP) in the USSR and member countries of the Council of Mutual Economic Aid (CMEA). This was the topic at the All-Union Scientific-Technical Conference organized by the Atomic Energy Bureau on February 9-11, 1977, at the Novovoronezh APP. Taking part in it were more than 150 specialists from 38 organizations, including the Novovoronezh, Beloyarsk, Kolsk, Leningrad, Armyansk, and Kursk APP, the Bilibinsk atomic thermoelectric power plant, representatives of the West-Ukraine, Kalinin, and Smolensk APP under construction, the Kurchatov Institute of Atomic Energy, the Moscow Power Institute, and others. A total of 39 reports were heard and discussed. They included review reports of the Atomic Energy Bureau and the Kiev Institute of Automation devoted to the preparation of operating personnel for APP in the USSR and abroad and to the principles of construction of educational-training centers; reports on the preparation of exploitational and operating personnel in the educational-training center of the Novovoronezh APP and at the Kolsk APP, and on methodological problems.

In the reports of the Kiev Institute of Automation the principles required by the developers were formulated, based on the results of studies of the educational-training center for operators of power units with a power of 300 MW, including a study of operating activity, the programming approach to training, the selection of simulators, the algorithmic approach to training, and the universality of preparation programs.

The creation of training centers equipped with simulators — imitators of operating APP — was recognized as effective. At the Novovoronezh APP there is already an educational center for the preparation of qualified specialists. During the years of its existence of preparation of over 1000 foreign specialists, mainly from member countries of the CMEA, has taken place at it. At the end of 1976 a new building was placed in use, equipped with specialized auditoriums in which provision is made for the use of the latest technical means of training. The training branch intended for the training of operators of water-cooled-water moderated VVER-440 power units closes in 1977.

Great interest was aroused by reports on the principles and results of the development of psychophysiological criteria for the selection for training by the leading specialists of nuclear power engineering and on the principal psychophysiological aspects of the professional preparation of operators, presented by the Institute of Biophysics of the Academy of Medical Sciences (AMS) of the USSR and by the Institute of Labor Hygiene and Professional Illness of the AMS of the USSR.

However, as shown by an analysis of the principal problems in the organization of the preparation of operating personnel for APP, the simulators presently being used in the USSR and abroad are distinguished by great variety both in the circuit design and mathematical provision and in their functions and capacities and in the completeness and accuracy of the duplication of the corresponding stage. This occurs because they are still in the development stage and unified principles for their construction and criteria and standards for equipping them and training on them have not been defined. Insufficient work has been done on the generalization of experience on operation in emergency situations and during equipment failures with the analysis of the actions of the operating personnel, and no criteria have been developed for the selection of personnel from the point of view of psychological

Translated from Atomnaya Énergiya, Vol. 42, No. 6, p. 510, June, 1977.

compatibility, etc.

The conference yielded many interesting results, which permits a considerable degree of expansion of the research being conducted in this direction. It developed the appropriate recommendations for organizations occupied with the preparation of personnel for APP.

The reports presented at the conference will be published.

FIFTH INTERNATIONAL CONFERENCE ON THE PEACEFUL USE OF UNDERGROUND NUCLEAR EXPLOSIONS

I. D. Morokhov, M. P. Grechushkina,
and V. N. Rodionov

There were 56 people from 26 countries present at the conference of experts under the aegis of the Technical Committee on the Technology of Peaceful Nuclear Explosions, which took place at Vienna (Austria) on November 22-24, 1976. The nine reports presented for discussion can be divided into the following three groups.

Scientific Reports. F. Prieto (Mexico) noted in his report that the equation of state for solids at high pressures, when the dependence between the velocities of shock waves and particles is linear, can be represented in a dimensionless form such that it will also be valid for certain liquids and, under certain conditions, even for gases.

The report of S. Reagan (USA) was devoted to the results of research on the equation of state of molybdenum in which a wave of record intensity (20 Mbar) was recorded by direct measurements. The shock wave, produced by the rapid heating of a plate of ^{235}U owing to fission during irradiation by neutrons of a nuclear explosion, acted on a specimen of molybdenum located next to it. Its velocity of displacement was found during the passage of a plane wave between two points in the specimen. The velocity of particle motion was determined from the doppler shift of six neutron resonances in the neutron energy range 200-800 eV.

Experimental—Industrial Peaceful Nuclear Explosions and Projects. Calculations of the thermal cycle in the burial of highly active wastes in the cavity of an underground nuclear explosion showed the possibility of accomplishing their storage so that the melting and subsequent solidification of the rock takes place owing to the liberation of heat (L. Schwarz et al., USA). As a result of the low rate of heat removal the hot center will be retained for hundreds of years and contact with water will thereby be eliminated. As an example, the author calculated that the wastes from the operation for 10 years of 100 GW power stations can be placed in the cavity created by a nuclear explosion with a power of 5 kton which occurs at a depth of 2000 m in dry silicate rock with a low porosity.

The results of recent studies in the region of the Rio Blanco triple explosion for the purpose of gas stimulation were presented by L. Ballou (USA). In the first report on this subject made at the Fourth Conference, it was noted that a zone uniformly permeable to gas could not be obtained as a result of the three explosions of 30 kton each at depths of 1780, 1900, and 2040 m. To clarify the reasons for the isolation of the fragmentation zones, additional studies were made both of the initial characteristics of the collector and of the state of the rock near the deepest explosion. Very interesting data, although incomplete, were obtained. Nevertheless, the absence of the expected considerable increase in gas output and the weak permeability between the upper and lower plates, explained by the incorrect original estimate of the initial state of the collector, made the financing of the experiment difficult and unfortunately led to the cessation of the studies of this unique explosion.

The report of V. N. Rodionov et al. (USSR) was devoted to a study of the filtration properties of a rock massif. The permeability of the massif was found through a determination of the flow rate of air forced under different pressures into specially drilled holes.

Translated from Atomnaya Énergiya, Vol. 42, No. 6, pp. 510-511, June, 1977.

The results of measurement at different distances from the center of an explosion with a power of 1 kton showed that the permeability increases toward the center and hardly changes over a long time (about a year). In the authors' opinion, this method can be applied to the study of the degree of destruction of rock near an explosion.

A report on a project for the construction of a canal from the Mediterranean Sea to the Qattara Depression in the Sahara (E. el-Shasli, Egypt) elicited great interest. The average depth lies at 70 m below sea level and it is proposed to use the flow of water into it from the Mediterranean Sea for the operation of electric power stations. After the depression is filled to a depth of 60 m, which will occur in 10 years according to the calculations, the evaporation of water from the water table of the lake which is formed can compensate for the inflow of water, equal to 650 m^3/sec, and thus provide for the prolonged operation of the hydroelectric stations (HES). The length of the channel over the various planned routes is 70-80 km and the total power of the explosions needed for the construction is estimated at 155 Mton.

It is proposed to reduce the radiation danger to the minimum through the use of charges of small fission power, by choosing days with a suitable wind direction for the explosions, and by evacuation of the local population, which comprises less than 25,000 people within the limits of 80 km from the canal route. After the depression is filled the HES with a power of 1200 MW will operate for the coverage of peak loads.

Safety. Data on ground motion and damage to buildings during the Rulison explosion were taken into account in predicting the consequences of the Rio Blanco experiment on gas stimulation which was conducted in the same sedimentary rock (report of F. Holzer, USA). The results of these and other explosions made it possible to widen the range of application of the prediction method which takes into account both the power of the charge and its depth of placement. It was also noted that the peak accelerations grow with an increase in power and depth and the characteristics of the spectra for deeper explosions are shifted into frequency intervals which are dangerous to buildings.

In a report on assuring the minimum radioactive contamination of the natural environment during the conducting of underground nuclear explosions for peaceful purposes (Yu. A. Izrael' and M. P. Grechushkina, USSR) estimates are given of the composition and distribution of radioactive products among the different contamination zones during underground and excavating nuclear explosions. Experimental data are cited which show that a large portion of the radioactive products formed remains in the central and epicentral zones even in the case of an excavating nuclear explosion.

The main products which spread to great distances are $^{89,90}Sr$, ^{137}Cs, ^{140}Ba, and some isotopes — products of the interaction of neutrons with the construction materials of the charge. The authors suggest approaches to the development of criteria for the possibility of conducting peaceful nuclear explosions under conditions of radiation safety.

In the report of K. Edvarson (Sweden) it is proposed to apply to peaceful nuclear explosions the general conditions and values of the limiting allowable dose (LAD) from the Recommendations of the International Commission on Radiation Protection in the same way as to other radiation sources created by man, such as atomic power plants. In the author's opinion, along with the LAD it is necessary to introduce a general means of estimating radiation loads in order to provide an answer to whether nuclear explosions are justified and advisable from the point of view of future radiation consequences and to compare them with other forms of human activity leading to exposure of the population. For this it is proposed to use the concept of the collective dose commitment, which is the sum of the individual doses produced by events which can be analyzed in practice.

A RADIATION–CHEMICAL INSTALLATION WITH AN EU-0.4 ELECTRON ACCELERATOR FOR OBTAINING ORGANOSILICON MONOMERS

B. I. Vainshtein, D. M. Margolin,
I. A. Ryakhovskaya, and N. G. Ufimtsev

For the development of the radiation–chemical technology of some organosilicon monomers which are important for industry and for the conducting of scientific-research work in this field a factory pilot installation has been created using an EU-0.4 electron accelerator developed at the L. Ya. Karpov Scientific-Research Institute of Physics and Chemistry on the basis of an RUP-400-5 x-ray flaw-detecting apparatus.

The installation 1 (Fig. 1) is placed in a specially equipped room consisting of a chamber 2 and a control room 6. The biological protection 10 is made of brick and the protective metal rolling door 9 is shielded with lead. The protective observational viewing window 3 with a size of 500 × 500 mm is covered with leaded glass. The control panel for the accelerator 5 and for the technological process 4, the auxiliary technological equipment 8, and the physicochemical monitoring instruments 7 were located in the control room. The installation is equipped with the appropriate kinds of interlocks which are connected sequentially and provide for the operation of the accelerator in the case when the protective door is closed, for supply water for cooling and air for the membrane of the beam outlet, etc.

The technological diagram of the installation (Fig. 2) consists of the electron accelerator 4, the reagent supply system 1, an evaporator 2, the radiation–chemical apparatus 3, and a system 5 for condensation of the reaction products. The EU-0.4 electron accelerator includes the high-voltage transformer unit of the RUP-400-5 apparatus, a modified accelerator tube of type 1.5BPV2-400, a vacuum system with a chamber for the emission of the electron beam, a system for forming the electron beam, and a mounting system. The latter provides for the mounting and operation of the installation. The reagent supply system consists of two vessels and a piston batcher with an adjustable supply rate of 5-30 g/min of the reaction mixture. Heating of the reagent mixture to 350-400°C is accomplished with the evaporator. The radiation–chemical apparatus is built in the form of a parallelepiped with a capacity of 70 liters and with a titanium membrane 20 μ thick for the admission of the electron beam. The condensation system consists of air and water heat exchangers connected in series with traps for the absorption of the emerging gases.

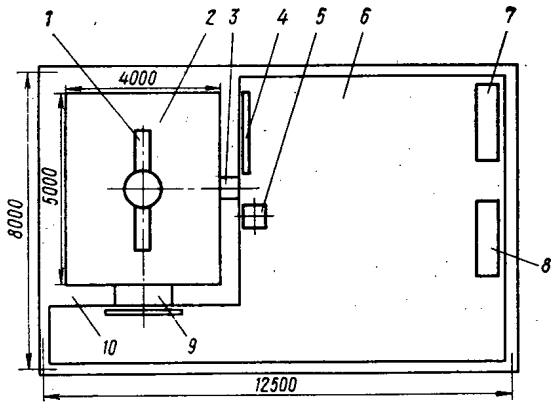

Fig. 1. Arrangement of radiation–chemical installation.

Translated from Atomnaya Énergiya, Vol. 42, No. 6, pp. 512-513, June, 1977.

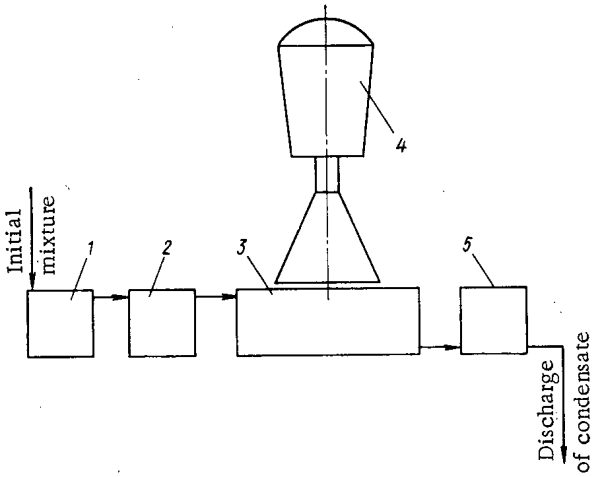

Fig. 2. Technological diagram of radiation-chemical installation.

Principal characteristics of the installation:

Height, m	3
Required power, kW	10-15
Accelerator power supply	from alternating current grid with a frequency of 50 Hz and voltage of 220 V
Electron energy, MeV	0.3-0.35
Current in beam, mA	up to 2
Dimensions of beam cross section at exit from accelerator, mm	40 × 500
Total flow rate, liter/min:	
of cooling water	up to 5
of air	25
Mass, t	1

Principal parameters of the chemical process: temperature of reaction volume up to 350-400°, atmospheric pressure.

The installation operates as follows. The accelerator is turned on and the assigned conditions relative to the energy and current of the electron beam are established. The beam enters the reaction volume through the exit window and the entrance membrane of the radiation-chemical apparatus located below the accelerator, inducing a chemical chain reaction of condensation of the reagents, which are continuously supplied in the vaporized state with the help of the system 1 and the evaporator 2 (see Fig. 2). Form the system 5 with the accelerator turned off samples of the condensate are selected which are analyzed on the LKhM-72 chromatograph and a laboratory fractionating column.

THE RID-41 UNIVERSAL HOSE-TYPE γ-RAY FLAW DETECTOR

V. N. Glebov and V. G. Firstov

The RID-41 γ-ray flaw detector was developed and built at the All-Union Scientific-Research Institute of Radiation Technology for monitoring steel products 60-250 mm thick and products made of light metal and alloys based on them 200-600 mm thick. The instrument consists of a radiation head, an ampule duct inside which the radiation source which is attached to a toothed flexible cable moves, a receiving hose to hold the unused part of the toothed cable, a remote control panel, and an exposure meter. The collimating heads and adapters which fit on the RID-41 form frontal and annular radiation beams, which permits the effective use of the instrument in different systems of radiographic monitoring and in radiometric systems.

The radiation head (Fig. 1) is designed for storing the radiation source in the interval between exposures and for moving it with a velocity of 0.1 and 1 m/sec along the flexible, rigid, or combination ampule duct to the collimating head or adapter at a distance of up to 12 m. The head consists of a cylindrical casing within which are located the biological protection unit, the movement drive, the radiometer pickup for signaling about the radiation environment, and a mechanism for the emergency return of the source. The control of the working cycle and of the process of charging (discharging) of the γ-ray flaw detector takes place remotely from a distance of up to 100 m.

The RID-41 γ-ray flaw detector is the first domestic instrument of such a class which permits the complete automation of the radioscopy process using an exposure meter whose detector is placed at the point where the film is located. The radiation source can be returned to the storage position by hand with the emergency return mechanism in the case of failure of the electromechanical drive, with overexposure of the personnel being eliminated.

The control panel (Fig. 2) consists of the power supply, control, and detector units placed in a common housing.

The electrical signaling system indicates the position of the radiation source by means of signal bulbs: a green color corresponds to the storage position in the radiation head and a red color to the radioscopy position in the collimating head.

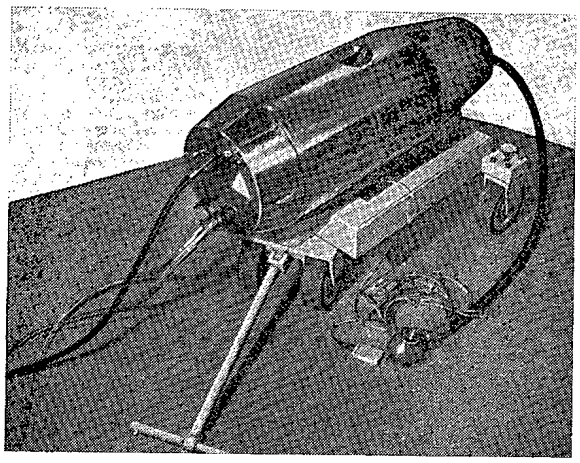

Fig. 1. Radiation head of RID-41 γ-ray flaw detector.

Translated from Atomnaya Énergiya, Vol. 42, No. 6, pp. 513-514, June, 1977.

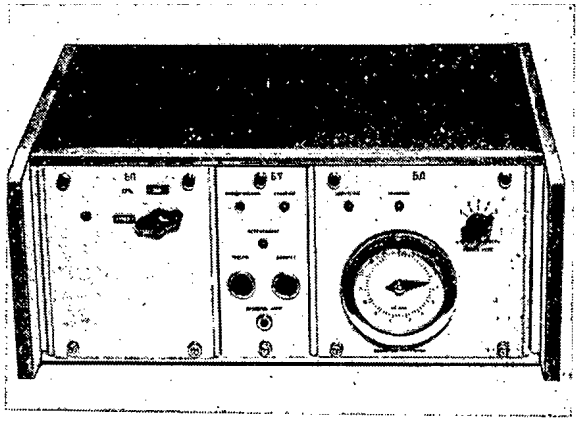

Fig. 2. Control panel.

The electromechanical tracking system indicates the location of the radiation source relative to the storage position at any time with an error of no more than 0.05 m.

The power supply of the apparatus is taken from a three-phase alternating-current line with a voltage of 380 V and a frequency of 50 Hz.

The dimensions of the radiation head on the carriage are 1400 × 800 × 800 mm, those of the control pannel are 490 × 400 × 220 mm, and the masses are 1200 and 45 kg, respectively.

A component part of the instrument is the UKT-D25 packing transportation complex for transporting the recharging container with the radiation source. In assembled form the complex withstands major accidents (fire, a temperature of 800°C, a fall from a height of 9 m onto a concrete base and from 1 m onto a steel spike). Two ^{60}Co sources with a total exposing dose rate of up to $3.6 \cdot 10^{-5}$ A/kg ($1.4 \cdot 10^{-1}$ rd/sec) are stored in the recharging container.

The RID-41 γ-ray flaw detector is designed for work with one of the following sources (MRTU 10-62-68): type II: exposure dose rate $3.1 \cdot 10^{-6}$ A/kg ($1.2 \cdot 10^{-2}$ rd/sec); type IV: $9 \cdot 10^{-6}$ ($3.5 \cdot 10^{-2}$); type V: $3.6 \cdot 10^{-6}$ ($1.4 \cdot 10^{-1}$).

The charging of the source is accomplished with a manipulator in a protective chamber using a special device which makes it possible to reliably fasten the radiation source in the holder; the reloading of the holder from the recharging container into the radiation head is done with the ampule duct.

An experimental model of the γ-ray flaw detector is presently being employed successfully.

A. A. Van'kov, A. I. Voropaev, and L. N. Yurova

THE ANALYSIS OF A REACTOR-PHYSICS EXPERIMENT*

Reviewed by A. D. Zhirnov

The problems of increasing the accuracy of the prediction of the physical characteristics of reactors occupy an important place in the practical work of a reactor physicist. Not only the attainment of the design characteristics but also the determination of the role and the place of one or another reactor in a nuclear power system essentially depend on this.

Two courses have been outlined here: the computational analysis of experimental results in a relatively simple geometry and model experiments. In the first case the constants are refined while in the second case the calculating model is tested. However, the tests answer only a small number of questions, and a considerable portion of the parameters must be determined (predicted) without relying on direct measurements. How can the nuclear constants be refined when one has an integral reactor experiment? The authors of the book under review provide the answer to this question. The statistical method of refining the group constants used in the calculations of fast reactors are presented in considerable detail in the book on the basis of their own work and the work of other authors.

Very roughly the essence of the method consists in the following. Suppose that one knows with a certain accuracy a set of constants (or the region of their determination) and one knows the reaction of a reactor functional to single perturbations of the group constants, i.e., the sensitivity coefficients. Having available a set of critical experiments where this functional is determined with sufficient accuracy one can, having approximated the calculated value of the functional to the experimental value, by the least-squares method, e.g., correct the constants or obtain their shift. In this way one is able to make the calculated and experimental values of K_{eff} converge to 0.3-0.4%. In analyzing in detail the mathematical apparatus used and citing examples the authors dwell on both the advantages and defects of the method. For example, in choosing the matrix of errors of the group constants and justifying their approach they note the subjective character of this choice and do not rule other approaches which might lead to a different set of shifts of the constants. The stability of the shift in the determination of different functionals can serve as a control here. The method is well illustrated with graphs and tables.

The prediction of a characteristic of a fast reactor which is important for nuclear safety, the Doppler and sodium void coefficients, is discussed separately. By refinement of the constants one is able to reduce the error of the calculated prediction of the void coefficients for a number of critical experiments and for the startup of the BN-350. Nevertheless, the authors correctly note that the nature of the temperature and power effects is very complicated and does not yet provide a basis for confident conclusions. The work which has been done pertains mainly to the "startup states" of reactors. A detailed analysis for deep fuel depletions, when higher isotopes of plutonium appear with still greater uncertainties in the constants, still awaits its investigators. The method developed is a good help in this work.

The book contains a large biblography, is written concisely and interestingly, and will undoubtedly find grateful readers.

*Atomizdat, Moscow (1977), 88 pp., 61 kopecks.

Translated from Atomnaya Énergiya, Vol. 42, No. 6, p. 515, June, 1977.

É. A. Stumbur

THE APPLICATION OF PERTURBATION THEORY TO THE PHYSICS OF NUCLEAR REACTORS*

Reviewed by V. N. Artamkin

The book under review is the latest in the series "Physics of Nuclear Reactors" published by Atomizdat and is the first one in the world literature devoted to perturbation theory for nuclear reactors. Although various aspects of perturbation theory are described in numerous periodical publications and textbooks and not one monograph on the general problems of the theory of nuclear reactors has gotten by without the corresponding (usually summary) section, until now nobody has taken the trouble to gather together all the available material. At the same time, the degree of mastery of perturbation theory is now the lodestone by which the qualification of a reactor physicist is determined. Only after many years of work are the capability and skill developed for the extraction of the maximum of information from the minimum of data using sufficiently precise approximate methods, based on perturbation theory in particular. There is no doubt that E. A. Stumbur's book will promote the accelerated preparation of qualified specialists and the general elevation of reactor culture. It is only depressing that there are no more than 1600 of such "lucky ones," which, not suprisingly, is more than the meager press run of the book.

Two of the six sections are essentially devoted to perturbation theory as such: the general propositions are presented in Sec. 4 while several examples of the use of perturbation theory in practical reactor work are presented in Sec. 6. Whereas the first of these sections has a general character and touches upon almost all the main aspects of the theory in one form or another, the choice of illustrations in the latter clearly reflects the author's taste: they all elucidate problems of the interpretation and analysis of experimental data obtained on a reactor. The material presented in Sec. 5 ("Void coefficients and the analysis of their properties") is connected with perturbation theory mostly in a historical way.

A considerable part of the book (40% by size) is by way of an introductory general-educational section. Evidently, the material presented here will not prove to be new to the majority of readers. It is hard to imagine, of course, that such a book would interest a person who did not know how the fields in reactors are described (Sec. 1) or what the importance of neutrons is (Sec. 2), although there might be some difficulties connected with the use of the formalism of functional analysis (Sec. 3). And yet the material of the book would not be complete without these three introductory sections. At the same time, it must be noted that the author was able to demonstrate no little pedagogical mastery, without which it would be impossible to fit such extensive material (even with a considerable lack or rigor) into such a limited space.

Twice in the course of the book, in the foreward and in the last phrase, the author enumerates the problems and tasks which did not find reflection in the book. Unfortunately, there are quite a few. However, this does not hinder the preparation of the book as a finished unified whole, keeping in mind the purpose formulated by the author and its size. All the same, a certain feeling of dissatisfaction remains. First of all, its title gives reason to assume that its contents are broader, and second, several of those aspects of perturbation theory and its applications which make it attractive for a reactor physicist and induce him to adopt the methods of the theory were left outside the limits of the book.

The book under review is distinguished by accuracy and clarity of presentation and by good language, and the individuality of the author is seen in everything. It is pleasant

*Atomizdat, Moscow (1977), 128 pp, 87 kopecks.

Translated from Atomnaya Énergiya, Vol. 42, No. 6, pp. 515-516, June, 1977.

to note that from the very beginning the author has rejected the term "neutron flux density," which is foreign to reactor physics and which has unfortunately so contaminated the language of current publications.

L. S. Tong

BOILING CRISIS AND CRITICAL HEAT FLUX*

Reviewed by N. S. Khlopkin

The book, written by a well-known specialist in the field of heat transfer during boiling in nuclear reactors, a scientist of the Westinghouse Co. (USA), contains data on the effect of various mode parameters and the channel geometry on the boiling crisis, presents calculating equations for critical heat loads, and gives recommendations on their use.

In the introduction, the flow structure and the mechanism of development of the boiling crisis at a heated surface in the four principal cases of heat removal are discussed: during boiling in a large volume; during bubble boiling; in a dispersed–annular mode of motion; at a transversely bathed cylinder.

In the second section, on the basis of the local theory of the crisis according to which its development is caused by a certain set of local conditions, calculating equations for these cases of heat exchange are presented which take into account the effect on the critical heat loads of the various parameters, the structure and prehistory of the flow, the size and location of bubbles, the thickness of the liquid film, the instability of the flow, the channel geometry of the bundle of rods, the spacing grids, and the nonuniformity of the flow distribution along the length and the circumference. Experimental data on the heat-exchange crisis of different liquids are generalized on the basis of similarity theory and similarity criteria are proposed for the crisis of boiling in a large volume and in a stream during dispersed–annular motion. At the end of the section empirical equations for the calculation of critical heat loads are presented with an indication of the source and the regions of applicability. Here it is also noted which of the functions are obsolete.

In a separate table data are given on studies which have been made on bundles of rods with an indication of the nature of the bundle and the range of mode parameters and the number of points obtained, but without giving the equations for the calculation. The sources are indicated so that the information can be looked up when necessary.

It must be noted that the calculating equations based on the allowance for local conditions do not always yield satisfactory results. The method which determines the critical power of the installation and which is based only on the independently controllable parameters is sometimes more successful.

A brief theoretical analysis of the boiling crisis is made in the third section.

The heat-exchange crisis during boiling in a large volume is analyzed using the Helmholtz instability. The equation obtained turned out to be very close to the semiempirical dependence of S. S. Kutateladze which was derived using similarity theory. The heat-exchange crisis in the bubble mode was calculated with allowance for the balance of heat and of the mass of coolant and for the hydrodynamic behavior of the main stream under the assumption that the crisis sets in when the limiting superheating of the liquid sublayer is reached. A calculating equation for estimating the effect of nonuniformity of the specific

*Translated from English [original report available from National Technical Information Service, U.S. Department of Commerce, Springfield, Va. (1972)], Atomizdat, Moscow (1976), 100 pp., 54 kopecks.

Translated from Atomnaya Énergiya, Vol. 42, No. 6, pp. 516-517, June, 1977.

heat flux (the stream form factor) is derived on the basis of these concepts. Adopting the concept of vapor bubbles forcing the liquid boundary layer away from the wall, the author has obtained a semiempirical equation for the critical heat flux which does not differ greatly from the experimental data. The mass exchange of liquid between the liquid film and the vapor core of the stream is taken into account for the dispersed—annular mode of stream motion. However, the analytical estimates of the rate of mass removal and precipitation of the liquid have considerable errors. Empirical values are usually used for them.

The value of the theoretical section consists in the attempts to develop a model for the complex thermophysical and hydrodynamic phenomenon, the crisis, which would make it possible to generalize the cumbersome experimental material with allowance for the physical meaning of the coefficients which enter into the equations. As for the accuracy of the theoretical equations, it is lower than the accuracy of empirical equations.

Recommendations on the selection of the functions presented in the book for calculations of critical heat loads are given in the final section. There are errors in the writing of the equations, however. For example, in Eq. (3.25) and (3.17) it should be "local" instead of "irregular" in accordance with p. 54; in (3.25) it should be q(h) instead of qh and in the equation for F on p. 54 it should be q(z) in the numerator instead of $q_{cr}(z)$; in (3.26) "c" can take on negative values if S is defined as indicated. And this contradicts the physical meaning.

The book introduced is valuable as a reference text for specialists making calculations of critical heat loads — to acquire confidence in the correctness of the equations used; for experimenters making studies of the heat-exchange crisis — for the comparison and analysis of the experimental data obtained; for theoretical heat engineers — for the development of models of the crisis. However, a careful analysis of the applicability of the equations recommended in the book is required for each concrete case of calculation. Where possible it is preferable to use data of direct measurements on full-scale assemblies of heat-releasing elements. Responsible calculations can only be based on data obtained in such a way.

engineering science

continued
from back cover

Title	# of Issues	Subscription Price
Metallurgist *Metallurg*	12	$225.00
Metal Science and Heat Treatment *Metallovedenie i termicheskaya obrabotka metallov*	12	$215.00
Polymer Mechanics *Mekhanika polimerov*	6	$195.00
Problems of Information Transmission *Problemy peredachi informatsii*	4	$175.00
Programming and Computer Software *Programmirovanie*	6	$95.00
Protection of Metals *Zashchita metallov*	6	$195.00
Radiophysics and Quantum Electronics (Formerly Soviet Radiophysics) *Izvestiya VUZ. radiofizika*	12	$225.00
Refractories *Ogneupory*	12	$195.00
Soil Mechanics and Foundation Engineering *Osnovaniya, fundamenty i mekhanika gruntov*	6	$195.00
Soviet Applied Mechanics *Prikladnaya mekhanika*	12	$225.00
Soviet Atomic Energy *Atomnaya energiya*	12 (2 vols./yr. 6 issues ea.)	$235.00
Soviet Journal of Glass Physics and Chemistry *Fizika i khimiya stekla*	6	$ 95.00
Soviet Journal of Nondestructive Testing (Formerly Defectoscopy) *Defektoskopiya*	6	$225.00
Soviet Materials Science *Fiziko-khimicheskaya mekhanika materialov*	6	$195.00
Soviet Microelectronics *Mikroélektronika*	6	$135.00
Soviet Mining Science *Fiziko-tekhnicheskie problemy razrabotki poleznykh iskopaemykh*	6	$225.00
Soviet Powder Metallurgy and Metal Ceramics *Poroshkovaya metallurgiya*	12	$245.00
Strength of Materials *Problemy prochnosti*	12	$295.00
Theoretical Foundations of Chemical Engineering *Teoreticheskie osnovy khimicheskoi tekhnologii*	6	$195.00
Water Resources *Vodnye Resursy*	6	$190.00

Back volumes are available. For further information, please contact the Publishers.

SEND FOR YOUR
FREE EXAMINATION COPIES

Plenum Publishing Corporation

Plenum Press • Consultants Bureau
• IFI/Plenum Data Corporation
227 WEST 17th STREET
NEW YORK, N. Y. 10011

United Kingdom: Black Arrow House
2 Chandos Road, London NW10 6NR England

Declassified and Approved For Release 2013/04/01 : CIA-RDP10-02196R000700090006-3

breaking the language barrier

WITH COVER-TO-COVER ENGLISH TRANSLATIONS OF SOVIET JOURNALS

in engineering science

Title	# of Issues	Subscription Price
Automation and Remote Control *Avtomatika i telemekhanika*	24	$260.00
Biomedical Engineering *Meditsinskaya tekhnika*	6	$195.00
Chemical and Petroleum Engineering *Khimicheskoe i neftyanoe mashinostroenie*	12	$275.00
Chemistry and Technology of Fuels and Oils *Khimiya i tekhnologiya topliv i masel*	12	$275.00
Combustion, Explosion, and Shock Waves *Fizika goreniya i vzryva*	6	$195.00
Cosmic Research (Formerly Artificial Earth Satellites) *Kosmicheskie issledovaniya*	6	$215.00
Cybernetics *Kibernetika*	6	$195.00
Doklady Chemical Technology *Doklady Akademii Nauk SSSR*	2	$65.00
Fibre Chemistry *Khimicheskie volokna*	6	$175.00
Fluid Dynamics *Izvestiya Akademii Nauk SSSR mekhanika zhidkosti i gaza*	6	$225.00
Functional Analysis and Its Applications *Funktsional'nyi analiz i ego prilozheniya*	4	$150.00
Glass and Ceramics *Steklo i keramika*	12	$245.00
High Temperature *Teplofizika vysokikh temperatur*	6	$195.00
Industrial Laboratory *Zavodskaya laboratoriya*	12	$215.00
Inorganic Materials *Izvestiya Akademii Nauk SSSR, Seriya neorganicheskie materialy*	12	$275.00
Instruments and Experimental Techniques *Pribory i tekhnika eksperimenta*	12	$265.00
Journal of Applied Mechanics and Technical Physics *Zhurnal prikladnoi mekhaniki i tekhnicheskoi fiziki*	6	$225.00
Journal of Engineering Physics *Inzhenerno-fizicheskii zhurnal*	12 (2 vols./yr. 6 issues ea.)	$225.00
Magnetohydrodynamics *Magnitnaya gidrodinamika*	4	$175.00
Measurement Techniques *Izmeritel'naya tekhnika*	12	$195.00

SEND FOR YOUR FREE EXAMINATION COPIES

Back volumes are available. For further information, please contact the Publishers.

continued on inside back cover

Declassified and Approved For Release 2013/04/01 : CIA-RDP10-02196R000700090006-3